ULB

UNIVERSITÉ LIBRE DE BRUXELLES

Faculty of Applied Sciences

Active Tendon Control
of Cable-Stayed Bridges

Younes ACHKIRE

Thesis submitted in candidature for
the degree of Doctor in Applied Sciences   Academic year 1996-1997

Active Structures Laboratory
Department of Mechanical Engineering and Robotics

ULB

UNIVERSITÉ LIBRE DE BRUXELLES

Faculty of Applied Sciences

Active Tendon Control of Cable-Stayed Bridges

Younes ACHKIRE

UNIVERSITÉ LIBRE DE BRUXELLES

The analog position sensing photodetector can be used to measure the real time transverse displacement of string and cable vibration

Younes ACHKIRE

In memory of
Sidi Mohamed Achkire,
Jean Roseeuw, and Ahmed Chajaï ...

Acknowledgements

Summary

In this work, we investigate the active damping of vibrations of the cable-stayed structures. The control strategy involves an active tendon consisting of an actuator controlling the displacement of the cable anchor point collocated with a force transducer sensing the dynamic tension in the cable. We have developed a control law (*Integral Force Feedback*) which guarantees stability and damping, even for nonlinear systems. The efficiency and the robustness of this control law have been experimentally confirmed on several laboratory cable structure mock-ups; the structure is nicely damped, even at the parametric resonance. The control strategy has been implemented in a decentralized manner for cable structures with several cables. For demonstration purposes, a laboratory scale-model has been designed with two dominant degrees of freedom (representing the torsion and the bending modes of the bridge deck) and provided with two cables equipped with active tendons. Experiments have been performed on this test article, and the properties of the Integral Force Feedback have been demonstrated.

Simple and powerful criteria have also been established, which allow one to predict the closed-loop poles of the system; these criteria are likely to be useful for the design of active cable-stayed structures. All the theoretical results have been confirmed experimentally on the test articles.

The torsion flutter of a cable-stayed bridge, has been simulated on a laboratory mock-up using a specially designed control system involving a shaker and an accelerometer. It has been demonstrated that the flutter speed can be significantly increased when the decentralized active tendon is applied to the cable-stayed structure.

We have also established an efficient modelling technique of cable structures; the nonlinear analytical model combines a finite element model of the structure and the nonlinear dynamics of the stay cables. This technique is very efficient and especially adapted for control system design purposes.

Contents

iv

Chapter 1

Introduction

Over the past 30 years , the center span of cable-stayed bridges with two plane stay cables has increased considerably, as we can see in Fig.1.1.a for Japanese bridges. In Europe, the main span of the largest existing cable-stayed bridge is 850 m (Normandy bridge in France (Fig.1.1.b)), and future projects are expected to exceed 1000 m. These structures are very flexible, because the strength of high performance materials increases faster than their stiffness. Consequently, the damping of cable-stayed bridges has become a major issue in civil engineering, because their high flexibility makes them more sensitive to wind and traffic induced vibrations as well as to flutter instability which can lead to the complete destruction of the structure. The most famous example is the Tacoma Narrows suspended bridge, which collapsed under torsion flutter at a wind speed of 42 mph, on November 7th, 1940 (Fig.1.3).

Cables have been widely used as structural member in many fields of engineering, including transmission overhead lines, guyed trusses and towers, roofs in large public building as the olympic stadium in Australia, tension trusses for large deployable antennas in space, high speed transportation, suspended and cable-stayed bridges. The current design of the space station is largely based on trusses, but it is quite likely that the future large space structures (LSS) will use large trusses connected by tension cables, to increase their global stiffness, in a way similar to that used to stiffen the airplanes in the early days of aeronautics. This concept of tension truss structure has already been used for large mesh antennas (a 10 m deployable mesh antenna was flown by the Russian in 1979). The cable dynamics is essentially nonlinear; it is responsible of a strong interaction with the structure to which they are anchored; the best known of these interactions is the parametric excitation, which can sometimes lead to serious damages. Under special weather conditions combining ice and wind, transmission lines can experience large amplitude vibrations known as *galloping*; these oscillations are responsible of failures. During, the passage of a high speed train, the overhead equipment and the pantograph is another example of coupled dy-

1
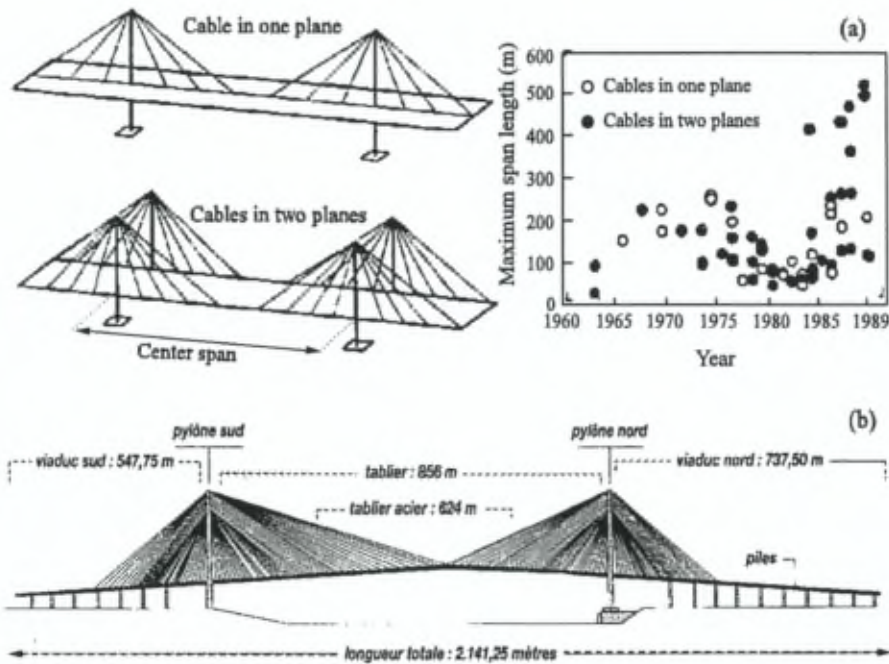
Figure 1.1: Cable stayed bridges : (a) Evolution of the center span in Japan, (b) Schematic view of the Normandy bridge in France.

namic system involving cables. The varying elasticity of the catenary (along the track) and the dynamic response of the overhead structure to the moving contact force induces vibrations of the pantograph. As a result, contact loss arises and leads to a disturbance of the power transmission as well as abrasion and erosion of the contact wire.

All the above examples where the vibrations are detrimental to the structure show the need for damping devices to reduce the amplitude of the oscillations.

1.1 Sources of excitation

As the span of cable-stayed bridges increases, the stay cables become more and more important, because their light weight, their high flexibility and low inherent damping makes them more sensitive to wind and rain-wind induced vibration as well as deck and pylon vibration.
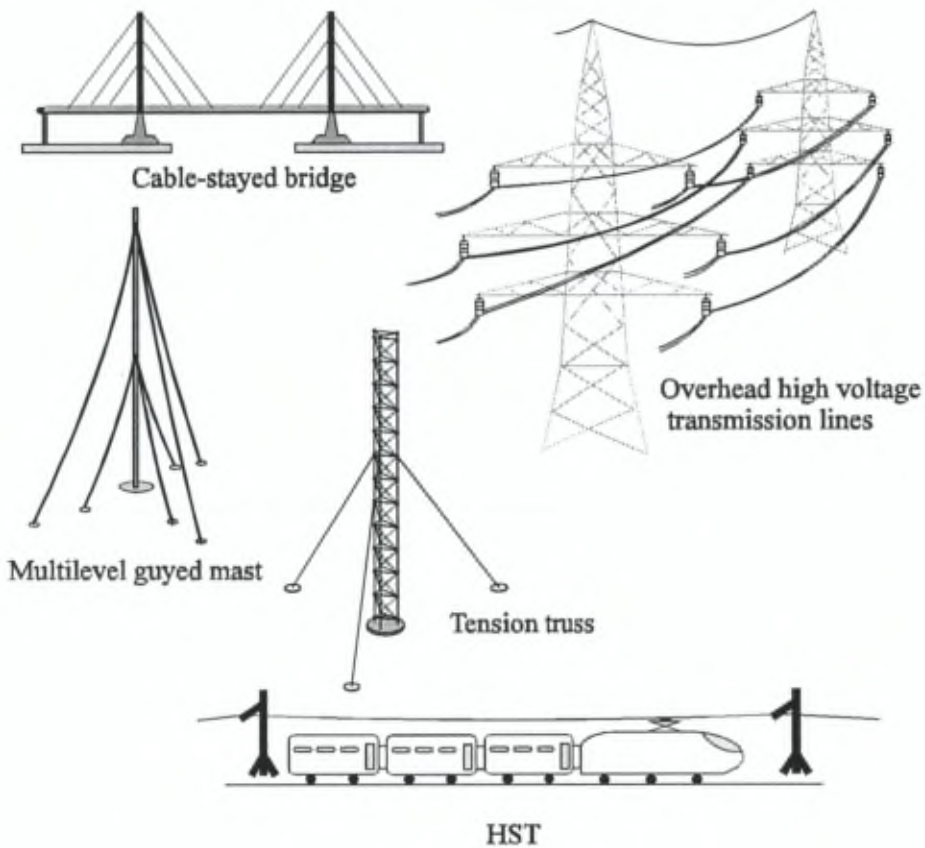
Figure 1.2: Cable structures.

1.1.1 Wind induced vibration

Wind induced vibrations of the stay cables are well known as one of the important design issue in the aeroelastic design of the recent cable-stayed bridges, because of their low damping structural characteristics and basically circular cross-section. Wind induced vibration of a single stay cable with circular profile is due to a vortex-induced vibration. As steady wind blows across a cable, small vortices of air are shed alternately above and below the cable, inducing a periodic excitation force with a frequency depending mainly on the cable diameter and the wind speed. Wind induced vibrations can lead to significant oscillations and a strong coupling between in-plane and out-of-plane motion arises when internal resonance conditions are met. With the increased size of

the main span, the cross-section of the stay cables increases; however, the cost performance of cables with larger cross-section is not good from the point of view of the fabrication and the erection of the cables; therefore, bundle cables formed by two or three cables with smaller cross-section are used instead. Referring to many experimental works and field observations [75], the bundle cables are recognized to be susceptible to wind induced vibration, especially to the so-called "wake galloping". This aeroelastic phenomenon is due to the turbulent air flows in the wake of the upstream cables which causes a varying wind load on the downstream cable when the latter oscillates in and out the wake of the upstream cable. The galloping of a single conductor is due to the modification of the cross-section of the cable due to the deposit of an ice accretion on the conductor line. The resulting movement is mainly vertical and its amplitude may sometimes be comparable the cable sag. The consequence of this kind of flutter instability often leads to the damages or breakages at conductors.

1.1.2   Rain-wind induced vibration

Another type of stay cable source of excitation is the rain-wind induced vibration which is responsible of large oscillation amplitudes of the cables as recorded on the Aratsu Bridge in southern Japan [75]. This self-excited oscillation tends to occur in rainy and windy conditions; it is due to the formation of rainwater rivulets on the upper side of the cable cross section, which change the cross-section, making it more susceptible to aerodynamic excitation. The rain-wind induced vibration can occur at low wind velocity (of the order of 10-15 m/s), accompanied with rainfall; besides it frequently shows rather large amplitudes, sometimes more than seven times the cable diameter.

1.1.3   Parametric excitation

The stay cables are also prone to parametric excitation; the vibrations of the deck and the pylon excite the cables through the axial motion of their support and large oscillations of the cables arise when some tuning conditions are met. Reasonably small amplitudes of an anchorage oscillation may lead to important steady-state cable response when the frequency of the anchorage motion is close to twice the first natural frequency of the cable. The parametric excitation of stay cables has been the origin of minor cracks near the cable anchorages on several bridge decks; thus, this nonlinear phenomenon is of considerable importance and needs to be taken into account in the design of cable-stayed bridges. The parametric excitation of cables is mostly induced by the bridge deck oscillation rather than the pylon. Bridge deck vibration comes from traffic induced vibration as well as wind induced vibration. The former source of excitation is responsible of lower amplitudes than the one induced by the buffeting due to turbulence around the bridge deck; wind is also responsible of an aeroelastic instability known as *flutter*.

Figure 1.3: Failure of the Tacoma Narrows bridge by torsion flutter at a wind speed of 42 *mph* in 1940.

1.1.4 Flutter of the bridge deck

On several occasions, suspended bridges have suffered damages, or even complete destruction under wind excitation. Large bridges are more sensitive to flutter which, in most cases, is associated with the aeroelastic damping coefficient in torsion becoming negative above a critical velocity. Aside from a careful aerodynamic design of the bridge deck aiming at achieving proper flutter derivatives, the traditional way of increasing the critical flutter speed consists of increasing the torsional stiffness by the use of a two plane stay cables and deck of stiffened cross-section. However, this solution is limited by the stiffness and the inherent damping characteristics of materials used in civil engineering.

1.2 Passive damping

As the span of cable-stayed bridges increases, the wind loading induced by the drag force on the stay cables becomes as important as for the deck. Therefore, in addition to aerodynamically stable cross-sections of bridge deck, there is a need for low drag stay cables, for future long span bridge. It is well known that the drag characteristics of circular cylinders change drastically around the critical Reynolds number (1-5 10^5), and their behaviour highly depends on the surface roughness. This fundamental idea has become a major issue in the design of stay cables, to establish low drag cables by surface modification.

To minimize cable vibrations, passive damping devices for stay cables have already been developed and used. The standard solution for long span bridges is
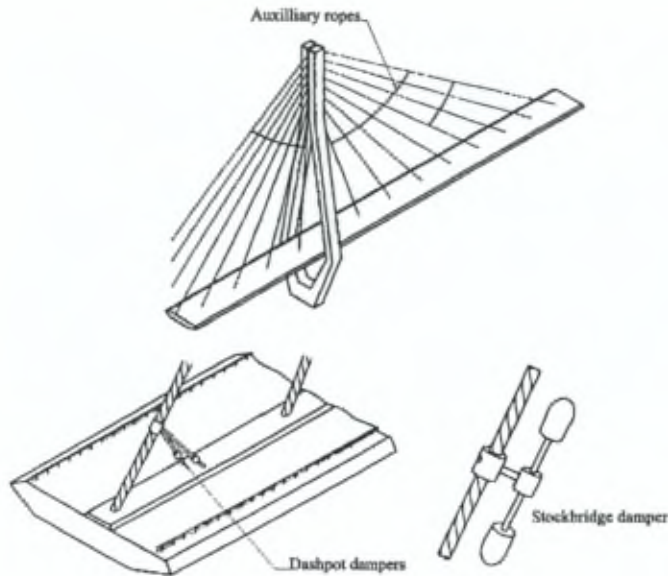
Figure 1.4: Design measures for passive damping of cable vibration.

to insert dampers between the cables and the deck (Fig.1.4). For example, a pair
of oil dampers are installed in the Aratsu Bridge [75]. The dashpot dampers de-
lay the appearance of vibration, but only until a certain level of the excitation,
and their efficiency is limited by the geometrical constraints of the deck cross-
section, and also by aesthetic considerations. As mentioned before, large cable
vibrations can be initiated by the deck and pylon movements. Adjusting cable
tension to certain values, which will change the natural frequency of the cables,
may alleviate parametric resonance; however, this solution on a cable-stayed
bridge is impossible because the static tension in the stay cables are imposed.
Nowadays, the solution often used to prevent cables from the parametric exci-
tation consists in interconnecting the stay cables with auxiliary ropes (Fig.1.4).
The cable ties are often criss-crossed from either side of the plane of stays; thus,
this prevention is twofold : the cable ties force a node in the stays which raises
frequencies of vibration and they introduce some damping by the presence of
some frictional forces at the crossover points. This solution has been applied
on many bridges and recently on the Normandy Bridge in France. The cable
ties have also been installed on the Aratsu Bridge to prevent the cables from
rain-wind induced vibration. The key issue to prevent the formation of rain
rivulets is to carefully design the roughness of the stay cables [40]. The short
fins of the Higashi-Kobe cables are an example of this aerodynamic solution
[48]. However, there is an evident drawback : the diameter of the cables is

increased and consequently also the drag forces. To prevent bundle cables from wake galloping, interconnecting the stay cables with cable ties is one solution, however, not effective. Another method consists in improving the aerodynamic performance by so closely and rigidly connecting bundle cables as not to give influence of the upstream cable wake to the downstream cable [29]. Another damping system for the control of aeolian vibration is the use "stockbridge dampers" clamped on the cable; however, this tuned mass damper has to be tuned on the frequency of the cable and the application to cable-stayed bridges is not practical and not effective for low frequencies. The anti-galloping devices in transmission overhead lines are based on the frequency tuning between the torsion and vertical movement. A proposed solution for bundle conductors [33] consists in a combination of torsional damping and increased torsional stiffness. The current approach to flutter alleviation consists of a careful aerodynamic design of the deck cross-section and an increase of its torsional stiffness. An alternative approach which may be more promising for future very long span bridges consists of applying active control techniques.

1.3 Active damping of cable-stayed bridges

One solution for flutter alleviation, widely studied, is based on the idea of constantly monitoring movements of the deck and use a control surface movements to generate stabilizing aerodynamic forces (lift) which damps the movement of the deck. The flutter control of cable-stayed bridges can be also based on the use of a gyrostabilizer or active tendons. The former solution consists in placing a gyrostabilizer on the bridge deck in order to control the torque of the deck. This concept is the object of a separate investigation at ULB.
The application of active tendons to flutter control has been considered theoretically by Yang [73]. The active tendon methodology consists in providing the cable anchorage with an actuator which controls the axial force in the cable or the displacement of the cable support. The strategies differ from each other by the localisation of the sensor measuring the structural vibration.

1.4 The proposed active damping strategy

We propose an alternative control strategy based on an active tendon consisting of an actuator collocated with a force sensor, as indicated on Fig.1.5. The active damping is based on the control of the displacement of the cable anchor point. The proposed active tendon control can be extended to other cable structures. We have developed a control algorithm which guarantees stability and damping in the cable structure. The proposed active damping methodology consists in providing some stay cables with an active tendon. We have established simple and powerful criteria useful for the first step design process of an active
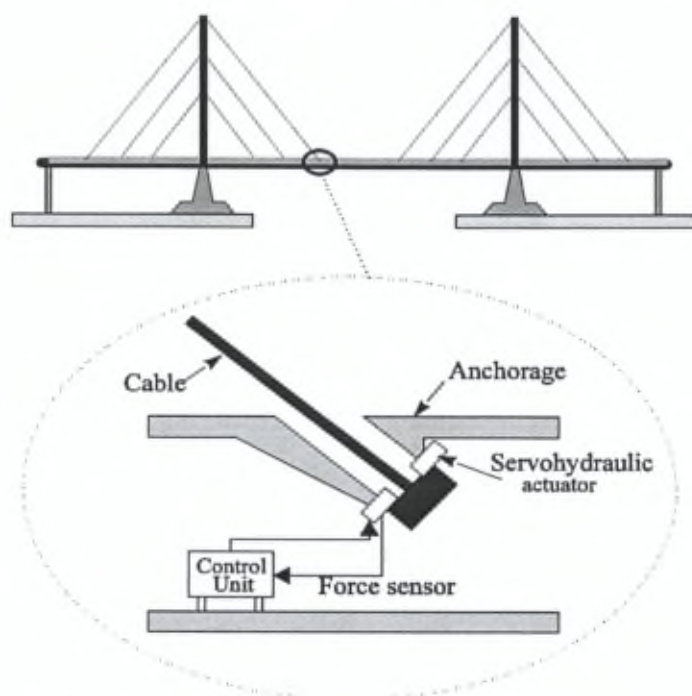
Figure 1.5: Active tendon control of cable-stayed bridges.

cable structure : the criteria allow the designer to choose the number and the location of the active cables with respect to an effective damping of the cable structure modes to be controlled. For flutter prevention, the active damping design should mainly focus on the first torsion and bending modes. The properties of this control strategy and the results are experimentally demonstrated on several laboratory test articles. We also propose a modelling technique for cable structure dynamics, including the nonlinear dynamics of small sag cables.

1.5   Organization of this work

This thesis is organized in 7 chapters. Chapter 2 describes the analytical nonlinear model of a cable subjected to an axially movable support where the active tendon is located. In chapter 3, the cable nonlinearities are experimentally demonstrated on a laboratory mock-up, and compared with the numerical simulations, for model validation purposes. Chapter 4 deals with the active damping of a cable alone, including a review of the existing control strategies and the experimental verification of our proposed control law. A modelling technique of

cable structures is presented in chapter 5. The decentralized active tendon control is applied to several cable structures in chapter 6, including a single-degree of freedom structure, a guyed truss and a simple representative scale model of a cable-stayed bridge. In chapter 7, the decentralized active tendon strategy is proposed to control the purely torsion flutter of cable-stayed bridges. Finally, the conclusions and the perspectives of industrial applications are discussed in chapter 8.

Chapter 2

Vibration of a cable with small sag

2.1 Linear theory

A linear theory has been developed by Irvine [24, 26] for the free vibration of a uniform suspended cable (see Fig.2.1) in which the sag to span ratio is about 1:8 or less. He showed that the symmetric in-plane modes depend heavily on a parameter (λ^2) which allows for the effects of cable geometry and elasticity. The theory has been confirmed by experiments. The governing equations are as follows.

2.1.1 Static equilibrium

Consider the static equilibrium of a uniform cable (see Fig.2.2) hanging from supports located at the same level.
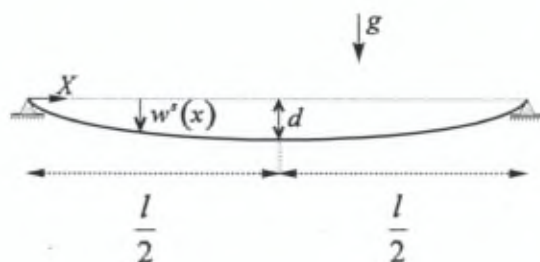
Figure 2.1: Model of the cable.
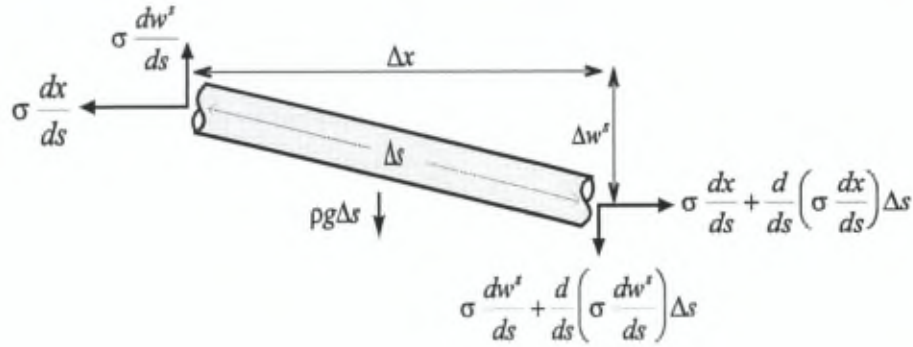
Figure 2.2: Equilibrium of a cable element.

The equations of static equilibrium of an element of the cable are :

$$\frac{d}{ds}\left(\sigma\frac{dx}{ds}\right) = 0$$
$$\frac{d}{ds}\left(\sigma\frac{dw^s}{ds}\right) = -\rho g \tag{2.1}$$

where σ is the stress in the cable, ρ is the specific mass of the cable, x is the position measured along the cable span and g is the acceleration due to gravity. If the slope of the cable is small (i.e. cable with small sag, $ds \approx dx$), the profile of the cable can be taken as a parabola :

$$w^s = \frac{\rho g l^2}{2\sigma^s}\left(\frac{x}{l} - \left(\frac{x}{l}\right)^2\right) \tag{2.2}$$

where l is the span and σ^s is the static stress in the cable. The relation between the sag d at mid span (see Fig.2.1) and the static stress σ^s is given by,

$$d = \frac{\rho g l^2}{8\sigma^s} \tag{2.3}$$

2.1.2 Dynamic equilibrium

Consider the small displacements of the cable about its static equilibrium position; if one denotes by the superscript (s) the static equilibrium, the equations of motion read,

$$\frac{\partial}{\partial s}\left[(\sigma^s + \sigma)\left(\frac{dx}{ds} + \frac{\partial u}{\partial s}\right)\right] = \rho\frac{\partial^2 u}{\partial t^2}$$
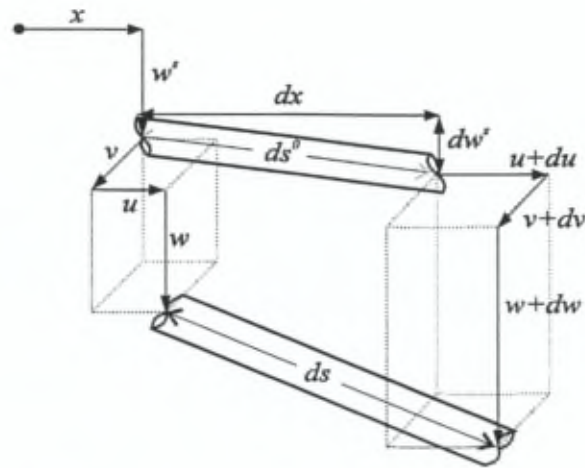
Figure 2.3: Displacement of a cable element.

$$\frac{\partial}{\partial s}\left[(\sigma^s + \sigma)\left(\frac{\partial v}{\partial s}\right)\right] = \rho\frac{\partial^2 v}{\partial t^2} \tag{2.4}$$

$$\frac{\partial}{\partial s}\left[(\sigma^s + \sigma)\left(\frac{dw^s}{ds} + \frac{\partial w}{\partial s}\right)\right] = \rho\frac{\partial^2 w}{\partial t^2} - \rho g$$

where u and w are the longitudinal and vertical components of the in-plane motion respectively; v is the transverse horizontal component (perpendicular to the vertical plane through the supports) and σ is the additional stress caused by the motion. The components of the motion are functions of both position and time. In order to linearize the previous equations, we assume that the sag is small ($\frac{d}{l} < \frac{1}{8}$), that the second order terms can be neglected, and that the stress σ induced by the motion is constant along the cable and negligible compared to the static stress ($\sigma \ll \sigma^s$). It follows that $ds \simeq dx$ and $u(x,t) \simeq 0$. Expanding the equations, ignoring the longitudinal component, and using the static equilibrium equation (2.1), Equ.(2.4) becomes

$$\sigma^s\frac{\partial^2 v}{\partial x^2} = \rho\frac{\partial^2 v}{\partial t^2} \tag{2.5}$$

$$\sigma^s\frac{\partial^2 w}{\partial x^2} + \sigma\frac{d^2 w^s}{dx^2} = \rho\frac{\partial^2 w}{\partial t^2} \tag{2.6}$$

2.1.3 Stress-strain relation

Consider a cable element subjected to a displacement from its static equilibrium profile as indicated in Fig.2.3. If ds^0 denotes the initial length of the element,

and ds is its new length, then we have

$$ds^0 = (dx)^2 + (dv^s)^2 + (dw^s)^2$$
$$ds^2 = (dx + du)^2 + (dv^s + dv)^2 + (dw^s + dw)^2 \tag{2.7}$$

where u, v and w represent the three components of the dynamic displacement; the axial strain in the cable reads

$$\varepsilon = \frac{ds - ds^0}{ds} \tag{2.8}$$

Substituting Equ.(2.7) in Equ.(2.8) and expanding ε to the second order of finite displacements, we obtain,

$$\varepsilon = \frac{dx}{ds}\frac{\partial u}{\partial s} + \frac{dv^s}{ds}\frac{\partial v}{\partial s} + \frac{dw^s}{ds}\frac{\partial w}{\partial s} + \frac{1}{2}\left[\left(\frac{\partial u}{\partial s}\right)^2 + \left(\frac{\partial v}{\partial s}\right)^2 + \left(\frac{\partial w}{\partial s}\right)^2\right] \tag{2.9}$$

The axial stress in the cable is given by the Hooke law

$$\sigma = E\varepsilon \tag{2.10}$$

where E represents the Young modulus of the cable.
For small sag cable $(ds \approx dx)$ we have

$$\varepsilon = \frac{\partial u}{\partial x} + \frac{dv^s}{dx}\frac{\partial v}{\partial x} + \frac{dw^s}{dx}\frac{\partial w}{\partial x} + \frac{1}{2}\left[\left(\frac{\partial u}{\partial x}\right)^2 + \left(\frac{\partial v}{\partial x}\right)^2 + \left(\frac{\partial w}{\partial x}\right)^2\right] \tag{2.11}$$

Assuming that the cable stress is constant over the span, we rewrite Equ.(2.10) in the integrated form,

$$\sigma(t) = E\varepsilon(t) = E\frac{\int_0^l \varepsilon(x,t)dx}{\int_0^l ds} \tag{2.12}$$

If we assume that the quadratic contribution of the cable strain is negligible, the axial strain becomes

$$\varepsilon = \frac{\partial u}{\partial x} + \frac{dw^s}{dx}\frac{\partial w}{\partial x} \tag{2.13}$$

Equations (2.5), (2.6), (2.12) and (2.13) are the linearized equations governing the problem. Note that the transverse horizontal motion is uncoupled from the in-plane motion, because the transverse horizontal motion involves no additional cable stress (to the first order).

Figure 2.4: Mode shapes of the out-of-plane modes.

2.1.4 Transverse horizontal motion

A solution of Equ.(2.5) can be obtained by assuming,

$$v(x, t) = \sum_n \phi_n(x) e^{i\omega_{y_n} t} \tag{2.14}$$

where ω_{y_n} is the natural circular frequency of the transverse vibration. In this way, Equ.(2.5) is reduced to,

$$\sigma^s \frac{d^2 \phi_n}{dx^2} + \rho \omega_{y_n}^2 \phi_n = 0 \tag{2.15}$$

with the boundary conditions $\phi_n(0) = \phi_n(l) = 0$. The transverse horizontal mode of order n is given by

$$\phi_n(x) = A_n \sin(\frac{n\pi x}{l}) \tag{2.16}$$

associated with the natural frequency,

$$\omega_{y_n} = \frac{n\pi}{l} \sqrt{\frac{\sigma^s}{\rho}} \tag{2.17}$$

The shapes of the first out-of-plane modes are represented in Fig.2.4.

2.1.5 In-plane motion

The in-plane (vertical) motion contains two types of modes : symmetric and antisymmetric modes. A solution of Equ.(2.6), can be obtained assuming

$$w(x,t) = \sum_n \psi_n(x) e^{i\omega_{z_n} t} \tag{2.18}$$

Substituting the expression Equ.(2.18) and (2.2) into (2.13), integrating over the cable span, we get the dynamic strain in the cable :

$$\varepsilon(t) = \frac{\int_0^l \varepsilon(x,t) dx}{\int_0^l ds} = \frac{1}{l_c} \left(u(l,t) - u(0,t) + \frac{8d}{l^2} \sum_n e^{i\omega_{z_n} t} \int_0^l \psi_n(x) dx \right) \tag{2.19}$$

where $l_c = \int_0^l ds \approx l \left[1 + 8 \left(\frac{d}{l} \right)^2 \right]$ represents the approximate length of the cable. For small sag, we have $\frac{d}{l} \ll 1$ and $l_c \approx l$. Assuming no displacements at the anchorages, we have $u(0,t) = u(l,t) = 0$. Substituting Equ.(2.19) in the stress-strain relation Equ.(2.12), we obtain the dynamic stress in the cable as a function of time only

$$\sigma(t) = \sum_n \Gamma_n e^{i\omega_{z_n} t} \tag{2.20}$$

with

$$\Gamma_n = \frac{\lambda^2}{8} \frac{\sigma^s}{dl} \int_0^l \psi_n(x) dx \tag{2.21}$$

and

$$\lambda^2 = \left(\frac{\rho g l}{\sigma^s} \right)^2 \frac{E}{\sigma^s} = \left(\frac{8d}{l} \right)^2 \frac{E}{\sigma^s} \tag{2.22}$$

The dimensionless parameter λ^2 introduced by Irvine [24] is of fundamental importance in the static and dynamic response of cables; it accounts for geometric and elastic effects.

Substituting the equations Equ.(2.18), (2.2) and (2.20) into Equ.(2.6), we get the equation governing the nth vertical mode shape,

$$\sigma^s \frac{d^2 \psi_n}{dx^2} + \rho \omega_{z_n}^2 \psi_n = \frac{8d}{l^2} \Gamma_n \tag{2.23}$$

The right hand side of Equ.(2.23) is responsible for the existence of two types of modes :

Antisymmetric modes

The antisymmetric in-plane modes consist of antisymmetric vertical components and symmetric longitudinal components. In this case, $\Gamma_n = 0$ which indicates that no additional cable stress is induced by the motion and Equ.(2.23) becomes

$$\sigma^s \frac{d^2\psi_{2n}}{dx^2} + \rho\omega^2_{z_{2n}}\psi_{2n} = 0 \tag{2.24}$$

With the boundary conditions $\psi_n(0) = \psi_n(l) = 0$ the solution of Equ.(2.24) yields the expression of antisymmetric in-plane mode shape,

$$\psi_{2n}(x) = A_{2n}\sin\left(\frac{2n\pi x}{l}\right) \tag{2.25}$$

associated with the natural frequency,

$$\omega_{z_{2n}} = \frac{2n\pi}{l}\sqrt{\frac{\sigma^s}{\rho}} \tag{2.26}$$

Symmetric in-plane modes

Symmetric in-plane modes consist of symmetric vertical components and antisymmetric longitudinal components. In this case, an additional cable tension is induced by the motion. Irvine has established the solution of Equ.(2.23) for the nth symmetric vertical mode [26],

$$\psi_{2n-1}(x) = A_{2n-1}\left[1 - \tan\left(\frac{\beta_n l}{2}\right)\sin\left(\beta_n x\right) - \cos\left(\beta_n x\right)\right] \tag{2.27}$$

where

$$\beta_n = \sqrt{\frac{\rho}{\sigma^s}}\omega_{z_{2n-1}} \tag{2.28}$$

Substituting the expression of ψ_{2n-1} into Equ.(2.21) and (2.23), we obtain the transcendental equation governing the natural frequencies of symmetric modes:

$$\tan\left(\frac{\beta_n l}{2}\right) = \frac{\beta_n l}{2} - \frac{4}{\lambda^2}\left(\frac{\beta_n l}{2}\right)^3 \tag{2.29}$$

We observe that the parameter involving cable elasticity and geometry (λ^2) plays an important role for the in-plane symmetric modes, affecting both the shape and the frequency.

Figure 2.5 compares the first two symmetric and antisymmetric in-plane modes of a suspended cable with that of a taut string as a function of the parameter λ^2 [24]. We recall that the frequencies of a taut string are given by,

$$\omega_n = n\frac{\pi}{l}\sqrt{\frac{\sigma^s}{\rho}} \tag{2.30}$$

One notices that, for small values of λ^2, the cable profile approaches that of a taut string.
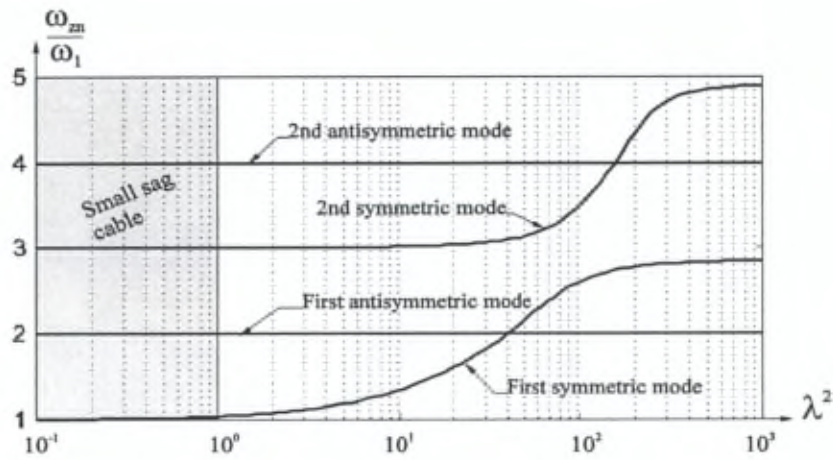
Figure 2.5: Evolution of the natural frequencies of the in-plane modes of a suspended cable as a function of λ^2.
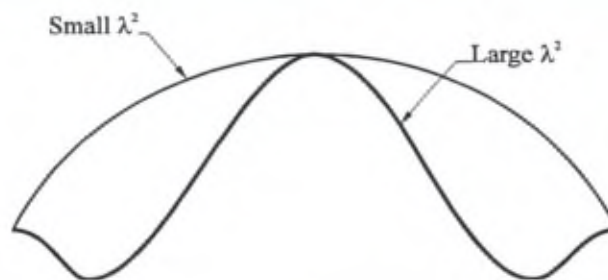
Figure 2.6: Possible forms for the first symmetric vertical mode shape.
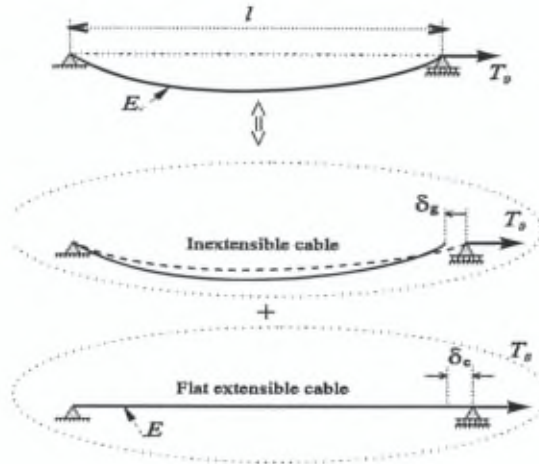
Figure 2.7: Physical interpretation of the effective axial modulus.

Figure 2.6 shows possible forms for the vertical component of the first symmetric in-plane mode. We note the presence of internal nodes for large values of λ^2. For small λ^2, the analytical expression of the symmetric vertical mode shapes and natural frequencies are reduced to the same form as the antisymmetric modes :

$$\psi_{2n-1} = A_{2n-1} \sin\left(\frac{(2n-1)\pi x}{l}\right) \quad \text{and} \quad \omega_{z_{2n-1}} = \frac{(2n-1)\pi}{l}\sqrt{\frac{\sigma^s}{\rho}} \quad (2.31)$$

Thus, for small sag cables characterized by small λ^2, we note that no distinction can be made between out-of-plane and in-plane frequencies and mode shapes.

2.1.6   The effective axial modulus

Consider a sagged cable in which the ends are being stretched apart (see Fig.2.7). The total displacement results from the contribution of an elastic displacement δ_e due to the cable stretching and a "geometric" displacement δ_g due to the sag reduction. The length of the cable is,

$$
\begin{aligned}
l_c &= \int_0^l ds = \int_0^l \sqrt{1 + \left(\frac{dw^s}{dx}\right)^2}\, dx \\
&\approx \int_0^l \left\{1 + \frac{1}{2}\left(\frac{dw^s}{dx}\right)^2\right\} dx \approx l + \frac{l}{24}\left(\frac{\rho g l}{\sigma^s}\right)^2
\end{aligned} \quad (2.32)
$$

Note that the cable length l_c is a function of the static stress σ^s. Since, the length of an inextensible cable is constant we can write

$$\frac{dl_c}{d\sigma^s} = 0 \tag{2.33}$$

and using Equ.(2.32) the condition Equ.(2.33) becomes for small sag cable

$$\frac{dl}{d\sigma^s} = \frac{\frac{1}{12}\left(\frac{\rho g l}{\sigma^s}\right)^2 \frac{1}{\sigma^s}}{1 + \frac{1}{8}\left(\frac{\rho g l}{\sigma^s}\right)^2} \approx \frac{l}{12}\frac{\lambda^2}{E}$$

$$\Rightarrow \frac{dl}{dT_0} = \frac{l}{12}\frac{\lambda^2}{EA} \tag{2.34}$$

where A denotes the cable cross-section and $T_0 = A\sigma^s$ represents the static tension in the cable. Thus we introduce the "geometric" stiffness,

$$K_g = \frac{dT_0}{dl} = \frac{EA}{l}\frac{12}{\lambda^2} = \frac{T_0}{\delta_g} \tag{2.35}$$

Note that this "geometric" stiffness is a function of the parameter λ^2. However, the axial stiffness of a flat extensible cable is,

$$K_e = \frac{EA}{l} = \frac{T_0}{\delta_e} \tag{2.36}$$

Hence, the equivalent stiffness of an extensible sagged cable is obtained by considering the arrangement of two springs in series (see Fig.2.7) :

$$h_u = \left(\frac{1}{K_g} + \frac{1}{K_e}\right)^{-1} = \frac{E_q A}{l} \tag{2.37}$$

where we have introduced the effective axial modulus

$$E_q = \frac{1}{1 + \frac{\lambda^2}{12}}E \tag{2.38}$$

2.2   Nonlinear model of small sag cables

As seen in the previous section, the linear theory applied to a cable with small sag shows that the in-plane and out-of-plane behaviours of the cable are essentially uncoupled; the out-of-plane modes and the in-plane antisymmetric modes are the same as those of a taut string, while the in-plane symmetric modes are controlled by λ^2. This model is inaccurate, because second order terms which have been ignored turn out to be significant and introduce some coupling between the in-plane and out-of-plane motions.
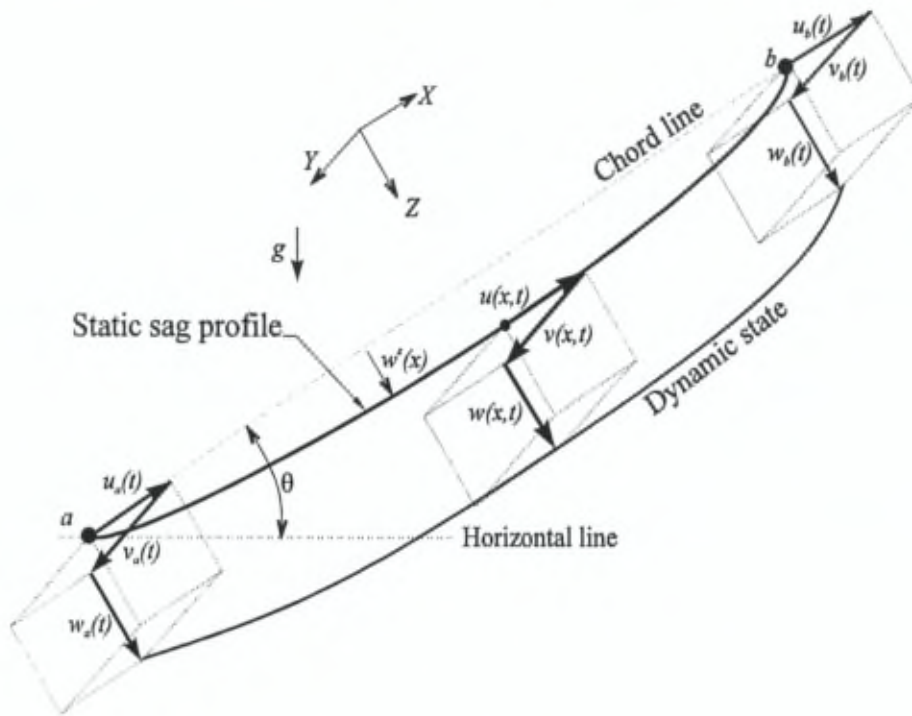
Figure 2.8: 3D-model of a cable with small support motion (a and b).

Next, we propose a non-linear model of the inclined cable which accounts for coupling between the in-plane and out-of-plane motions, and also for the displacement of the support points (see Fig.2.8); this problem has been considered in [19, 24, 41, 50]. The cable motion is separated into two parts : the quasi-static and the dynamic contributions. The model of the cable is written in a local coordinate system as indicated in Fig.(2.8); the local x axis is taken along the chord line while the z axis is in the gravity plane and perpendicular to the chord line.

2.2.1   Static configuration

The equations governing the static equilibrium of an element of an inclined cable are :

$$\frac{d}{ds}\left(\sigma\frac{dx}{ds}\right) = -\rho g \sin\theta$$

$$\frac{d}{ds}\left(\sigma\frac{dw^s}{ds}\right) = -\rho g \cos\theta \tag{2.39}$$

where w^s is the z component of the cable static profile expressed in the local coordinate system (xyz) and θ is the angle of the chord line with respect to the horizontal plane. For small sag $(ds \approx dx)$, we assume that the stress in the cable is constant along the span and is equal to σ^s; this assumption is valid only for small sag cable because $\gamma = \rho g \cos\theta \ll \sigma^s$. In this context the static profile of an inclined cable can be approximated by a parabola,

$$w^s = \frac{\gamma l^2}{2\sigma^s}\left[\frac{x}{l} - \left(\frac{x}{l}\right)^2\right] \tag{2.40}$$

where σ^s is the static stress, l is the cable chord length, x is the position measured along the cable span, γ is the component of distributed weight along z. We note that for an inclined cable, the parameter (2.22) involving cable elasticity and geometry is changed into,

$$\lambda^2 = \left(\frac{\gamma l}{\sigma^s}\right)^2 \frac{E}{\sigma^s} \tag{2.41}$$

2.2.2 Governing equations

For an inclined cable element subjected to external distributed forces $\mathcal{X}, \mathcal{Y}, \mathcal{Z}$, the dynamic equilibrium equations (2.4) become

$$\begin{aligned}
\frac{\partial}{\partial s}\left[(\sigma^s+\sigma)\left(\frac{dx}{ds}+\frac{\partial u}{\partial s}\right)\right] + \mathcal{X} &= \rho\frac{\partial^2 u}{\partial t^2} - \rho g \sin\theta \\
\frac{\partial}{\partial s}\left[(\sigma^s+\sigma)\left(\frac{\partial v}{\partial s}\right)\right] + \mathcal{Y} &= \rho\frac{\partial^2 v}{\partial t^2} \\
\frac{\partial}{\partial s}\left[(\sigma^s+\sigma)\left(\frac{dw^s}{ds}+\frac{\partial w}{\partial s}\right)\right] + \mathcal{Z} &= \rho\frac{\partial^2 w}{\partial t^2} - \rho g \cos\theta
\end{aligned} \tag{2.42}$$

where σ^s is the static stress, σ is the dynamic stress and u, v, w are the components of the cable dynamic motion expressed in the local coordinate system (xyz). If we denote the two supports by the subscripts a and b, the boundary conditions are expressed as,

$$\begin{aligned}
u(0,t) &= u_a(t) &,& \quad u(l,t) = u_b(t) \\
v(0,t) &= v_a(t) &,& \quad v(l,t) = v_b(t) \\
w(0,t) &= w_a(t) &,& \quad w(l,t) = w_b(t)
\end{aligned} \tag{2.43}$$

Using Equ.(2.39) governing the static equilibrium of a small sag cable, Equ.(2.42) is simplified as follows,

$$\frac{\partial \sigma}{\partial x} + \sigma^s \left(1 + \frac{\sigma}{\sigma^s}\right) \frac{\partial^2 u}{\partial x^2} + \mathcal{X} = \rho \frac{\partial^2 u}{\partial t^2}$$

$$\frac{\partial \sigma}{\partial x} \frac{\partial v}{\partial x} + \sigma^s \left(1 + \frac{\sigma}{\sigma^s}\right) \frac{\partial^2 v}{\partial x^2} + \mathcal{Y} = \rho \frac{\partial^2 v}{\partial t^2} \qquad (2.44)$$

$$\frac{\partial \sigma}{\partial x} \left[\frac{dw^s}{dx} + \frac{\partial w}{\partial x}\right] + \sigma^s \left(1 + \frac{\sigma}{\sigma^s}\right) \frac{\partial^2 w}{\partial x^2} + \sigma \frac{d^2 w^s}{dx^2} + \mathcal{Z} = \rho \frac{\partial^2 w}{\partial t^2}$$

Assuming the longitudinal inertia force $\rho \frac{\partial^2 u}{\partial t^2}$, the longitudinal external force $\mathcal{X}$ and the term $\frac{\partial^2 u}{\partial x^2}$ to be negligible, the first of equations (2.44) shows that the dynamical stress in the cable can be assumed constant along the cable span. Thus, introducing this result in the two other equations (2.44), we get

$$\frac{\partial \sigma}{\partial x} = 0$$

$$(\sigma^s + \sigma) \frac{\partial^2 v}{\partial x^2} + \mathcal{Y} = \rho \frac{\partial^2 v}{\partial t^2} \qquad (2.45)$$

$$(\sigma^s + \sigma) \frac{\partial^2 w}{\partial x^2} + \sigma \frac{d^2 w^s}{dx^2} + \mathcal{Z} = \rho \frac{\partial^2 w}{\partial t^2}$$

2.2.3   Quasi-static motion

The quasi-static motion (denoted by the subscript q) is the displacement of the cable which moves as an elastic tendon due to the support movements; it satisfies the time-dependent boundary conditions statically. In the case of small displacements of the cable supports, the following assumptions are made in Equ.(2.45).

- The stress induced by the quasi-static motion is negligible compared to the static stress ($\sigma^q \ll \sigma^s$).

- The inertia forces $\rho \frac{\partial^2 v}{\partial t^2}$ and $\rho \frac{\partial^2 w}{\partial t^2}$ induced by the transverse movements of the cable supports are neglected.

- The second order components of the axial strain in the cable equation (2.11) are neglected,

$$\left(\frac{\partial u^q}{\partial x}\right)^2 \approx 0 \,, \ \left(\frac{\partial v^q}{\partial x}\right)^2 \approx 0 \text{ and } \left(\frac{\partial w^q}{\partial x}\right)^2 \approx 0 \qquad (2.46)$$

As a result of the first two assumptions the quasi-static motion becomes

$$\frac{\partial \sigma^q}{\partial x} = 0$$

$$\sigma^s \frac{\partial^2 v^q}{\partial x^2} = 0 \tag{2.47}$$

$$\sigma^s \frac{\partial^2 w^q}{\partial x^2} + \sigma^q \frac{d^2 w^s}{dx^2} = 0$$

with the following boundary conditions,

$$
\begin{aligned}
u^q(0,t) &= u_a(t) &,& & u^q(l,t) &= u_b(t)\\
v^q(0,t) &= v_a(t) &,& & v^q(l,t) &= v_b(t)\\
w^q(0,t) &= w_a(t) &,& & w^q(l,t) &= w_b(t)
\end{aligned} \tag{2.48}
$$

Introducing the third assumption (2.46) into the nonlinear strain-displacement relation Equ.(2.11), the strain induced by the quasi-static motion of the cable is reduced to its linear part :

$$\varepsilon^q(x,t) = \frac{\partial u^q}{\partial x} + \frac{dw^s}{dx}\frac{\partial w^q}{\partial x} \tag{2.49}$$

and the quasi-static stress reads

$$\sigma^q = E\varepsilon^q \tag{2.50}$$

Expanding the partial differential equations (2.47) and introducing some constants of integration (see section A.1) and assuming small displacements of the cable anchorages,

$$\left(\frac{u_b - u_a}{l}\right)^2 \quad,\quad \left(\frac{v_b - v_a}{l}\right)^2 \quad,\quad \left(\frac{w_b - w_a}{l}\right)^2 \ll 1 \tag{2.51}$$

the quasi-static displacements are finally expressed in the form,

$$
\begin{aligned}
u^q(x,t) &= u_a - \frac{w_b - w_a}{l}w^s(x)\\
&\quad + \frac{E_q}{E}(u_b - u_a)\left[\frac{x}{l} + \frac{\lambda^2}{4}\left(\frac{x}{l} - 2\left(\frac{x}{l}\right)^2 + \frac{4}{3}\left(\frac{x}{l}\right)^3\right)\right]\\
v^q(x,t) &= v_a + (v_b - v_a)\frac{x}{l}\\
w^q(x,t) &= w_a + (w_b - w_a)\frac{x}{l} - \frac{E_q}{\sigma^s}\frac{u_b - u_a}{l}w^s(x)
\end{aligned} \tag{2.52}
$$

with the quasi-static stress,

$$\sigma^q = E_q \frac{u_b - u_a}{l} \tag{2.53}$$

where E_q denotes the effective modulus defined by Equ.(2.38).

2.2.4 Dynamic motion

The purely dynamic motion (denoted by the superscript d) is expanded into the linear undamped modes of a cable with fixed ends. For small sag, the axial dynamic component can be neglected :

$$u^d(x,t) \approx 0 \tag{2.54}$$

We expand the transverse motion into the linear undamped modes according to,

$$v^d(x,t) = \sum_n y_n(t)\phi_n(x)$$
$$w^d(x,t) = \sum_n z_n(t)\psi_n(x) \tag{2.55}$$

where the generalized coordinates, y_n and z_n are the amplitudes of out-of plane and in-plane modes respectively. The out-of-plane modes are independent of λ^2 and given by,

$$\phi_n(x) = \sin(\frac{n\pi x}{l}) \tag{2.56}$$

For small λ^2, the in-plane mode shapes, can be approximated by,

$$\psi_n(x) \approx \sin(\frac{n\pi x}{l}) \tag{2.57}$$

The global motion of the cable is obtained from the superposition of the quasi-static and modal motion as,

$$u(x,t) = u^q(x,t)$$
$$v(x,t) = v^q(x,t) + v^d(x,t) \tag{2.58}$$
$$w(x,t) = w^q(x,t) + w^d(x,t)$$

2.2.5 Lagrange equations

In order to establish the analytical model of the cable, we use the Lagrange equations which, in this case, read

$$\frac{d}{dt}\left(\frac{\partial \mathcal{T}}{\partial \dot{y}}\right) + \frac{\partial \mathcal{V}_c}{\partial y_n} = 0$$
$$\frac{d}{dt}\left(\frac{\partial \mathcal{T}}{\partial \dot{z}}\right) + \frac{\partial \mathcal{V}_c}{\partial z_n} = 0 \tag{2.59}$$

Thus, the kinetic energy $\mathcal{T}_c$ and potential energy $\mathcal{V}_c$ should be expressed as functions of the generalized Lagrange coordinates y_n and z_n; the full development, is given in appendix A.

Kinetic Energy

The kinetic energy of the cable is,

$$\mathcal{T} = \frac{1}{2}\rho A \int_0 \left[\dot{u}^2 + \dot{v}^2 + \dot{w}^2\right] dx \qquad (2.60)$$

Strain-stress relation

The variable part of the axial strain in the cable ε is composed of a purely quasi-static strain ε_q and a dynamical one ε_d. Substituting the global components of motion Equ.(2.58) into the nonlinear strain-displacement relation Equ.(2.11), and using the assumptions Equ.(2.46), we obtain the axial strain

$$\varepsilon(x,t) = \varepsilon_q(x,t) + \varepsilon_d(x,t) \qquad (2.61)$$

where the dynamical component of the axial strain involves a linear and a non-linear term as follows

$$\varepsilon_d(x,t) = \varepsilon_d^{(1)}(x,t) + \varepsilon_d^{(2)}(x,t) \qquad (2.62)$$

where the linear contribution is caused by the static profile

$$\varepsilon_d^{(1)}(x,t) = \frac{dw^s}{dx}\frac{\partial w^d}{\partial x} \qquad (2.63)$$

and the nonlinear contribution is due to the cable stretching which is induced by both the quasi-static and the modal transverse motion of the cable,

$$\varepsilon_d^{(2)}(x,t) = \frac{\partial w^q}{\partial x}\frac{\partial w^d}{\partial x} + \frac{1}{2}\left[\left(\frac{\partial v^d}{\partial x}\right)^2 + \left(\frac{\partial w^d}{\partial x}\right)^2\right] \qquad (2.64)$$

The axial stress in the cable contains a quasi-static contribution σ^q and a dynamic one σ^d as follows

$$\sigma = E\varepsilon = E\varepsilon_q + E\varepsilon_d = \sigma^q + \sigma^d \qquad (2.65)$$

Since the first equation of Equ.(2.45) shows that the dynamical axial stress is constant along the cable span, the dynamical strain is a function of time only; averaging $\varepsilon(x,t)$ over the cable span, we get

$$\varepsilon(t) = \frac{1}{l}\int_0^l \varepsilon(x,t)dx = \varepsilon_q(t) + \varepsilon_d^{(1)}(t) + \varepsilon_d^{(2)}(t) \qquad (2.66)$$

The time-varying contribution of the axial tension in the cable is given by

$$T(t) = T_q + T_d = EA \left[\varepsilon_q + \varepsilon_d^{(1)} + \varepsilon_d^{(2)} \right] \qquad (2.67)$$

Potential Energy

The potential energy [22] of the cable is given by,

$$\mathcal{V}_c = \mathcal{V}^* + \mathcal{V}^o + \mathcal{V}_{ext} \qquad (2.68)$$

which contains the contribution of,

- the strain energy due to elastic elongation of the cable

$$\mathcal{V}^* = \frac{l}{2} EA \left(\varepsilon_o + \varepsilon \right)^2 \qquad (2.69)$$

  where $\varepsilon_0 = \frac{\sigma^s}{E}$ denotes the static strain.

- the gravitational potential energy

$$\mathcal{V}^o = - \int_o^l A\rho g \left[(w^s + w^q + w^d) \cos\theta + x \sin\theta \right] dx \qquad (2.70)$$

- the potential due to external distributed forces

$$\mathcal{V}_{ext} = \int_0^l A\mathcal{Y}(v^s + v^q + v^d)dx + \int_0^l A\mathcal{Z}(w^s + w^q + w^d)dx \qquad (2.71)$$

  in which we have assumed that the longitudinal external distributed force $\mathcal{X}$ is negligible.

2.2.6   Analytical model of cable dynamics

The Lagrange equations (2.59) may now be used to derive the equations of motion of the small sag cable. Substituting the expressions of the kinetic energy and the potential energy in the Lagrange equations (see section A.2) and assuming no transversal motion of the cable supports,

$$v_a(t) = v_b(t) = 0$$
$$w_a(t) = w_b(t) = 0 \qquad (2.72)$$

we obtain the differential equations governing the generalized coordinates y_n and z_n for the cable mode n :

$$\mu_{cn}\left(\ddot{y}_n + 2\xi_{yn}\omega_n\dot{y}_n + \omega_n^2 y_n\right) + S_n y_n(T_q + T_d) = F_{yn} \qquad (2.73)$$

$$\mu_{cn}\left(\ddot{z}_n + 2\xi_{zn}\omega_n\dot{z}_n + \omega_n^2 z_n\right) + S_n z_n(T_q + T_d)$$
$$+ \Lambda_n T_d - \alpha_{cn}(\ddot{u}_b - \ddot{u}_a) = F_{zn} \qquad (2.74)$$

$$T = T_q + T_d = h_u(u_b - u_a) + \sum_n \left[h_{1n}z_n + h_{2n}\left(y_n^2 + z_n^2\right)\right] \qquad (2.75)$$

where F_{yn} and F_{zn} represent the modal forces applied to the cable. In Equ.(2.75) $h_u = \frac{E_q A}{l}$ is the static stiffness of the cable. The dynamical tension T_d has a linear and a quadratic contribution; the former is due to the presence of cable sag and includes the in-plane symmetric modes only, because $h_{1n} = 0$ if n is even; the latter is due to cable stretching.

As compared to Equ.(2.73), Equ.(2.74) has two additional terms due to the sag:

- the **sag induced stiffness** $\Lambda_n T_d$ has a linear and a quadratic contribution; the linear one is responsible for the increase of the natural frequency of the cable in the vertical plane ($\omega_{zn} = \sqrt{\omega_n^2 + \Lambda_n h_{1n}} > \omega_n$).

- the **sag induced inertia** $-\alpha_{cn}(\ddot{u}_b - \ddot{u}_a)$ is the inertia force induced by the axial acceleration of the supports. It affects the in-plane symmetric modes only because $\alpha_{cn} = 0$ if n is even.

Moreover, the differential motion of the cable supports is also responsible of the *parametric excitation* through the terms $S_n y_n T_q$ and $S_n z_n T_q$, which exist for both in-plane and out-of-plane modes.

If we expand the expressions of T_d [see Equ.(2.75)] in Equ.(2.73) and (2.74), we notice that the nonlinearities of the cable dynamics appear through the quadratic and cubic couplings between modes and through the parametric excitation [18, 41]. Figure 2.9 summarizes the various types of interactions between the modes.
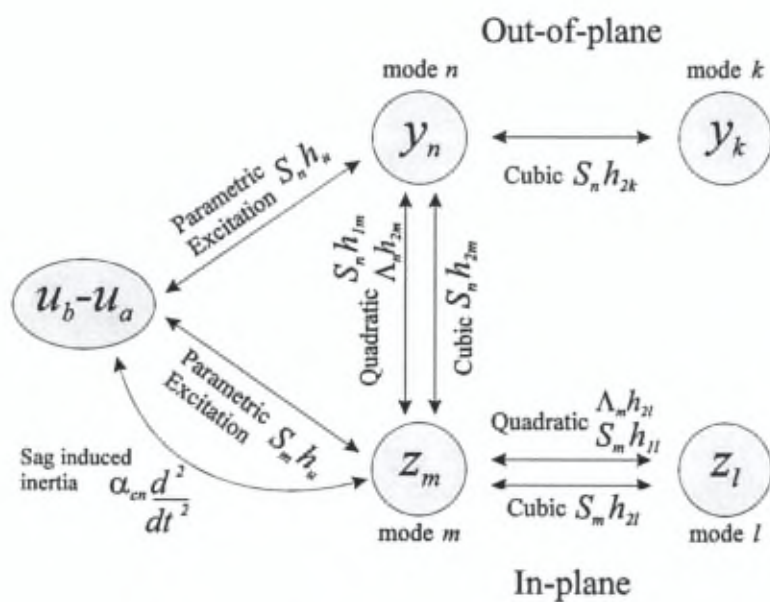
Figure 2.9: Coupling between cable modes.

Chapter 3

Experimental validation of the cable model

3.1 Introduction

The aim of this chapter is to validate the analytical nonlinear model of a small sag cable with movable supports. For this purpose, a laboratory mock-up has been built; the vertical cable modes are excited through the axial motion of the anchor and through a vertical external force applied directly to the cable. The experimental results are compared with the numerical predictions.

The effect of the support displacement on the vertical motion is twofold : it is responsible for inertia forces exciting the cable, and it also produces a variable stiffness which is known as *parametric excitation* [41].

This chapter also discusses the properties of the control system with respect to the controllability and observability.

3.2 Experimental set-up

Figure 3.1 shows the experimental model of the cable. It is similar to that used by Fujino and coworkers [18, 19]; it consists of a stainless steel wire of 2.0 m long with a cross-section area of 0.196 mm^2, provided with some additional lumped masses attached at regular intervals in order to achieve a representative value of the cable mass to tension ratio ($\frac{\rho g A}{\sigma^*}$). The chord line is horizontal; the mass per unit length is 0.057 kg/m; the Young modulus of the cable, measured from the stress-strain relation of the model, is $1.8\,10^5$ MN/m. One end of the cable is fixed to a lever system in order to amplify the motion of the active element which consists of a linear piezoelectric actuator collocated with a force sensor (see Fig.3.2). The amplification ratio of the lever arm is 3.4, corresponding to
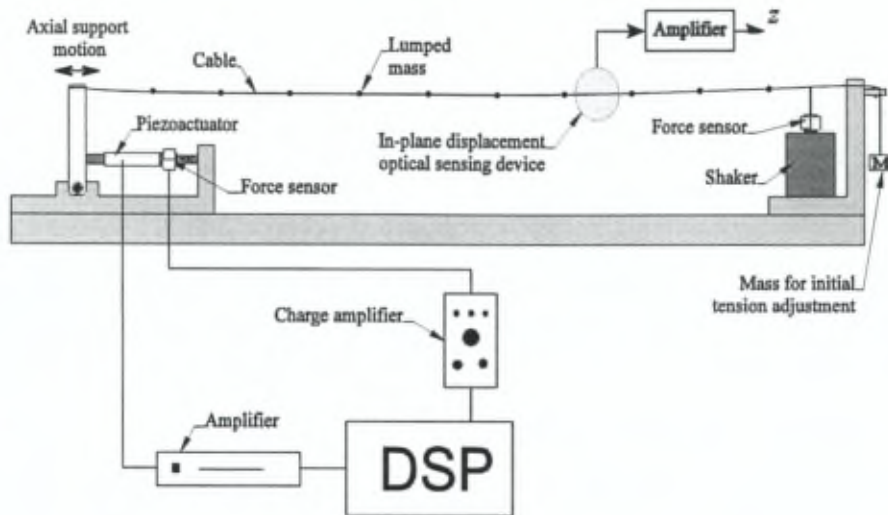
Figure 3.1: Experimental model of the cable.

a maximum axial displacement of 150 μm for the moving support. A flexible tip is used to avoid bending moments in the piezoactuator. A picture of the actual device is shown in Fig.3.3. The axial motion is measured by a strain gauge included in the actuator. An electrodynamic shaker equipped with a force sensor is placed near the other end of the cable, to generate the in-plane excitation, and an optical system described later is installed as indicated in Fig.3.1, in order to measure the in-plane cable vibrations. The model was carefully designed to simulate the dynamic properties of typical cable stayed-bridges as shown in

Parameter	Symbol	Model	Typical bridges
Cable static strain	$\epsilon^s = \frac{\sigma^s}{E}$	0.2 %	0.2-0.4 %
cable weight / tension	$\frac{\gamma l}{\sigma^s}$	2 %	0.1-1 %
Sag to span ratio	$\frac{d}{l}$	0.5 %	0.01-0.5%

Table 3.1: Dynamic similarity parameters.

Table 3.1. One notices that the first two parameters appearing in table 3.1 can be combined to form the parameter λ^2 defined by Equ.(2.41).
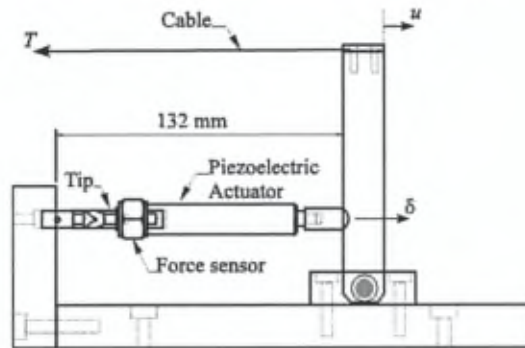
Figure 3.2: Design of the movable cable support mechanism.
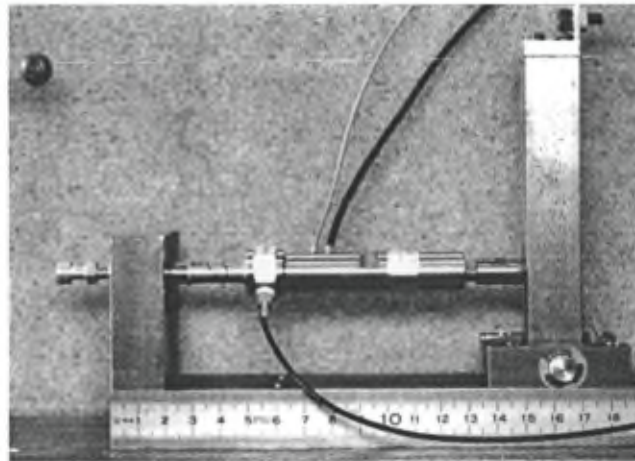
Figure 3.3: Photograph of the movable cable support mechanism.

3.2.1 The active tendon

The actuator used in the experiment is a low voltage piezotranslator *Physik Instrumente* P-843.30 whose extension is a linear function of the applied electric field and of the applied load; this can be expressed by the following equation,
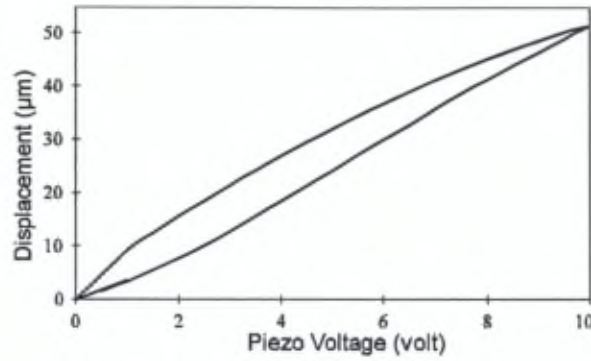
Figure 3.4: Hysteresis curve of the piezotranslator P-843.30.

$$\delta = \delta_d - \frac{F}{K_a} \tag{3.1}$$

where δ and δ_d are the effective and the desired expansion of the piezoactuator respectively, F is the force acting on it and K_a is its stiffness. If k_l is the geometric amplification of the arm, Equ.(3.1) can be written as,

$$u = k_l \left(\delta_d - \frac{k_l}{K_a} T \right) \tag{3.2}$$

where u is the axial support displacement and T is the tension in the cable.
Actually, the expansion of a piezotranslator is not exactly proportional to the electric field strength and the voltage/expansion curve exhibits some hysteresis as shown in Fig.3.4. The natural frequency of the actuator is about 10 kHz which is high enough for not interacting with the cable dynamics. A force sensor is mounted colinear with the piezoactuator; it consists of B & K type 8200 with its charge amplifier B & K type 2635. The charge amplifier includes an adjustable band-pass filter. Note that, because of the high pass behaviour of the piezoelectric force sensor, it measures only the dynamic component of the tension in the cable.

3.2.2   Sensing cable vibrations

As shown on Fig.3.1, a sensor is used to monitor the cable vibrations and to evaluate the performances of the various active tendon control algorithms.
In this context, a non contact optical measurement system for cable and string vibrations has been developed [2]. Cable vibrations can be measured through the variation of the tension in the cable; however, this signal includes a complex mixture of linear and quadratic terms [see Equ.(2.75)]; the former appears at
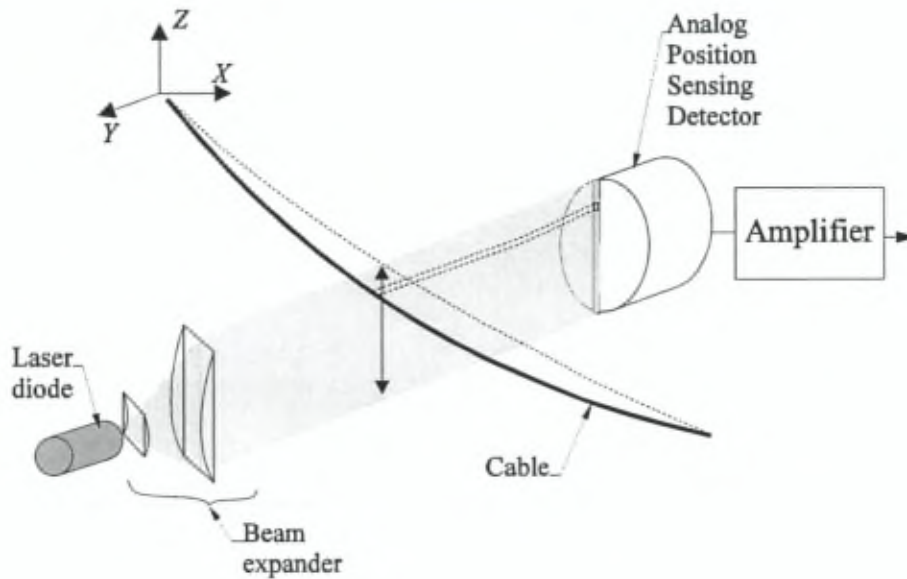
Figure 3.5: Sensing the vibration of a wire.

the natural frequency of the cable while the latter appears at twice the natural frequency; besides, the modes of even number are not linearly observable from the tension in the cable, because the corresponding coefficients h_{1n} vanish in Equ.(2.75). A direct measurement of the cable displacement can be obtained with a CCD camera [19] or with an analog *position sensing detector* (PSD) [31]. We have selected the PSD technology which supplies analog signals proportional to the position of a light spot on the detector. The technology exists in one or two dimensions; it is linear, wide-band, and perfectly adapted to the range of amplitudes of our application (typically cable vibrations of 10 mm).

The principle of the optical measurement system is represented in Fig.3.5; the light source is a 5 mW laser diode ILEE type LDA1015 (670nm); its beam is expanded into a flat parallel beam by two cylindrical lenses with focal length of 25mm and 150mm respectively; the cable is placed in such a way that the chord line is normal to the light plane. The light plane produces a line on the PSD, with a dark spot corresponding to the shade of the cable (Fig.3.5). The analog output of the sensor is proportional to the position of the centroid of the dark spot. In order to improve the sensor signal, the PSD can be supplemented with a bandpass filter centered on the wavelength of the laser diode (670 nm in this case).

3.3   Nonlinear oscillations of a cable

Consider the mass spring system subjected to an external force f. The response of the undamped system is governed by the linear equation

$$M\ddot{x} + Kx = f \tag{3.3}$$

For such a system, a small excitation cannot produce a large response unless the frequency of the excitation is close to the natural frequency of the system (i.e. *primary resonance* : $\omega = \sqrt{K/M}$). If we modify the previous linear system
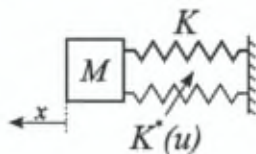
Figure 3.6: The parametric excitation of the mass spring system.

by adding a spring with a variable stiffness $K^*(u)$ controlled by the command u (see Fig.3.6), the equation governing the free response of the modified system becomes nonlinear and is changed into

$$M\ddot{x} + Kx + K^*(u)x = 0 \tag{3.4}$$

We note that, the variable u can be used for exciting the system through the variable stiffness which appears as a time-varying coefficient in the governing differential equation (3.4). This type of excitation is called *parametric excitation* [41]. By contrast with the case of external excitation (e.g. for the linear mass spring system), a small parametric excitation can produce a large response when the frequency of excitation is away from the primary resonance, usually equal to twice the primary resonance (parametric resonance : 2ω). As an example of parametrically excited system, Fig.3.7 describes the nonlinear model of a taut string excited through an axially movable support, and the gravity effect on the dynamics of a cable; the equations governing the dynamics of each system are also shown.

Figure 3.7.a compares the linear and nonlinear one d.o.f. model of a taut string stretched between its fixed supports points with a static tension T_0. In addition to the linear part, we note the presence of a cubic nonlinearity as a result of the stretching. Furthermore, if we consider the same taut string subjected to an axially movable support as shown in Fig.3.7.b, we notice a parametric excitation term (i.e. a variable stiffness) induced by the axial motion of the support, which excites the system when the frequency of the support motion is twice the primary resonance (2ω).

Now, consider the previous system in which the string is replaced by a cable

(a)

$$m\ddot{y} + \frac{\pi^2}{l} T_0\, y = 0 \qquad \text{(Linear)}$$

Stretching

$$m\ddot{y} + \frac{\pi^2}{l}\left[T_0 + h_1 y^2\right] y = 0 \qquad \text{(Nonlinear)}$$

$$\omega = \pi \sqrt{\frac{T_0}{ml}}$$

(b)

$$m\ddot{y} + \frac{\pi^2}{l}\left[T_0 + h_1 y^2 + h_u u\right] y = 0$$

Parametric excitation

(c)

$$\begin{cases} m\ddot{y} + \dfrac{\pi^2}{l}\left[T_0 + h_1\left(y^2 + z^2\right) + h_u u + h_z z\right] y = 0 \\[2mm] m\ddot{z} + \dfrac{\pi^2}{l}\left[T_0 + h_1\left(y^2 + z^2\right) + h_u u + h_z z\right] z \\[2mm] \qquad\qquad + \Lambda\left[h_1\left(y^2 + z^2\right) + h_z z\right] - \alpha_u \ddot{u} = 0 \end{cases}$$

Sag effect   Inertia
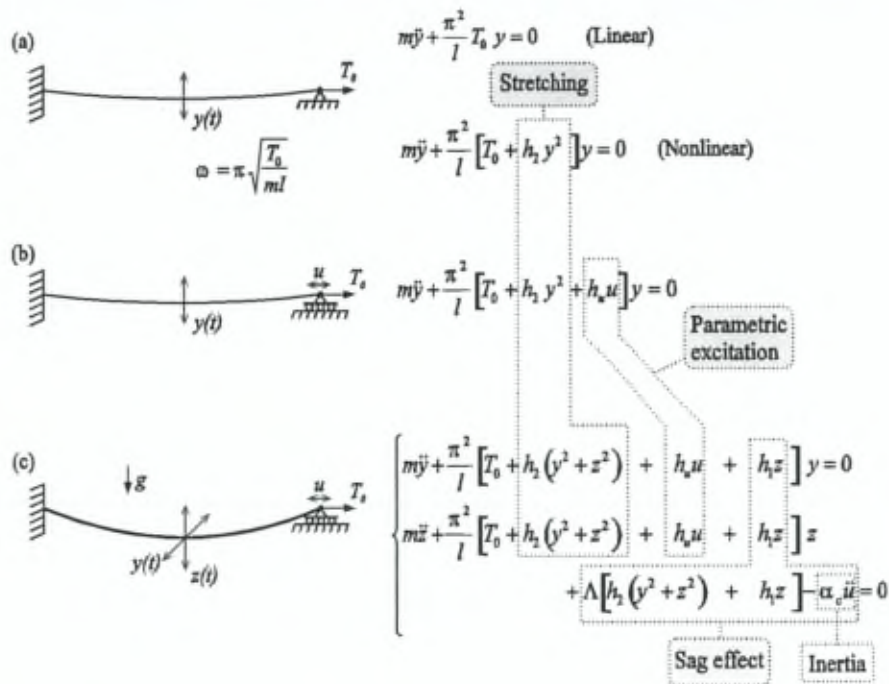
Figure 3.7: Model of a string and a cable with an axially movable support.
(a) String with fixed support.
(b) String with axially moving support.
(c) Cable with small sag and axially moving support.

with small sag, as shown in Fig.3.7.c. The cable vibration is composed of two motions : one lying in the plane defined by the cable equilibrium (i.e. gravity plane) and one normal to this plane; the equation is written for one mode only. The presence of sag introduces two additional contributions : The sag induced inertia corresponds to an external excitation which affects the vertical symmetric modes only; this term becomes dominant in the vicinity of the primary resonance. There are also some additional linear and quadratic coupling terms due to sag; the magnitude of their coefficients depends on the cable sag and they vanish for antisymmetric in-plane modes. Thus, if we consider the excitation of a small sag cable through the axial movement of the cable support, two types of excitation do exist : an external force excitation and a parametric one :

- The symmetric in-plane modes can be excited through the sag induced inertia if the frequency of the support displacement is close to the primary resonance of the considered mode.

- All transverse modes (i.e. in-plane and out-of-plane modes) can be parametrically excited, when the frequency of the support movement is close to the parametric resonance (i.e. twice the primary resonance) of the mode concerned. In this range of frequencies, the sag induced inertia does not modify the frequency response and then can be assumed negligible.

Next, consider the effect of the two foregoing types of excitation on the first vertical symmetric mode of a small sag cable. In this case, neglecting the modal coupling and adding some damping, the equation governing the vertical cable mode Equ.(2.74) becomes

$$\ddot{z}_n + 2\xi_{zn}\omega_{zn}\dot{z}_n + \omega_{zn}^2 z_n + \beta_n z_n{}^2 + \nu_n z_n{}^3 + R_n u z_n - \frac{\alpha_{cn}}{\mu_{cn}}\ddot{u} = 0 \qquad (3.5)$$

with

$$\nu_n = \frac{1}{\mu_{cn}}S_n h_{2n} \quad , \quad \beta_n = \frac{1}{\mu_{cn}}(S_n h_{1n} + \Lambda_n h_{2n})$$

$$\omega_{zn}^2 = \omega_n^2 + \frac{1}{\mu_{cn}}\Lambda_n h_{1n} \quad , \quad R_n = \frac{1}{\mu_{cn}}S_n h_u \qquad (3.6)$$

The equation governing systems with cubic nonlinearities is known as the *Duffing* equation [41]. The main characteristics of such systems are as follows :

- The frequency response may exhibit two different values at the same frequency.

- The bending of the frequency response curve is responsible of a *jump phenomenon* as shown in Fig.3.8 and 3.9. We observe that when the frequency is increased the response follows the upper branch and suddenly jumps down to the lower branch. Conversely, when the frequency is decreased from large values the response follows the lower branch and suddenly jumps up to the upper branch.

- The cubic nonlinearity may induce an internal resonance (i.e. sub-harmonic resonance) which occurs at one third of the primary resonance for large amplitudes of the response. This phenomenon has never been observed in this work.

3.3.1 Cubic and quadratic nonlinearities

The aim of this section is to validate the presence of cubic nonlinearities in the equation governing the cable vibration. For this purpose the sag induced inertia excitation is considered. As previously discussed, for this type of excitation, only

Figure 3.8: Frequency response function between the active tendon displacement and the in-plane vibration, at the primary resonance ω_{z1}.

the symmetric in-plane modes are excited, and the variable stiffness term (i.e parametric excitation component) can be neglected :

$$\ddot{z}_n + 2\xi_{zn}\omega_{zn}\dot{z}_n + \omega_{zn}^2 z_n + \beta_n z_n^2 + \nu_n z_n^3 = \frac{\alpha_{cn}}{\mu_{cn}}\ddot{u} = \frac{F_{un}}{\mu_{cn}} \qquad (3.7)$$

where F_{un} represents the excitation force applied to the in-plane mode z_n induced by the support acceleration $\ddot{u}$. When, a harmonic displacement at frequency Ω is applied to the actuator, the modal excitation force becomes,

$$F_{un} = \alpha_{cn}\Omega^2 u(t) = \alpha_{cn}\Omega^2 a_u \sin \Omega t \qquad (3.8)$$

An analytical prediction of the steady state response of Equ.(3.7) can be made using the method of *multiple scales* [41] (see appendix B.1). The frequency response equation in the vicinity of the primary resonance ω_{zn} reads,

$$\left[\frac{\Omega - \omega_{zn}}{\omega_{zn}} - \left(\frac{3}{8}\nu_n - \frac{5}{12}\frac{\beta_n^2}{\omega_{zn}^2}\right)\frac{a_{zn}^2}{\omega_{zn}^2}\right]^2 = \left(\frac{\alpha_{cn}a_u\Omega^2}{2\mu_{cn}a_{zn}\omega_{zn}^2}\right)^2 - \xi_{zn}^2 \qquad (3.9)$$

where a_{zn} is the response amplitude, a_u is the amplitude of the axial motion and Ω is the excitation frequency.

The resonance curve bends to the right or to the left depending on the relative size of coefficients of quadratic (β_n) and cubic (ν_n) nonlinearities. For small sag cable investigated here, the frequency response curve bends to the right (hardening nonlinearity), because $\nu_n \gg \beta_n$. The bending of the frequency

Parameters		Value
μ_{c1}	(kg)	0.053
T_0	(N)	32.6
$f_{z1} = \omega_{z1}/2\pi$	(Hz)	6.4
ξ_{z1}	(%)	0.12
λ^2		0.8
S_1		2.46
Λ_1		0.02
α_{c1}	(kg)	0.159
h_u	(Nm^{-1})	1.188 10^4
h_{11}	(Nm^{-1})	257.2
h_{21}	(Nm^{-2})	1.56 10^4
β_1	(Nm^{-2})	952
ν_1	(Nm^{-3})	3.86 10^4

Table 3.2: Coefficients used for the analytical predictions.

response curve leads to multivalued amplitudes (i.e. more than one stable steady state response) and hence to a jump phenomenon [41].

Experiments have been performed with the set-up of Fig.3.1. The input excitation is a slow sine sweep and each point corresponds to a steady state harmonic excitation of 3 min. The theoretical coefficients and parameters used for solving the predicted frequency response equation are summarized in Table 3.2. The damping ratio ξ_{z1} has been obtained from an experimental identification and the static tension applied to the cable is known initially; the other coefficients are calculated from their theoretical expression [Equ.(3.6), (A.32) to (A.40)]. The amplitude a_u of the moving support is approximately equal to 4.25 μm. Figure 3.8 shows the good agreement between the experimental frequency response curve and the prediction (3.9) in the vicinity of the primary resonance (ω_{z1}).

3.3.2 Parametric excitation

When the frequency of the cable support is close to the parametric resonance, the sag induced inertia can be neglected and Equ.(3.5) is reduced to the parametrically excited Duffing equation [41]

$$\ddot{z}_n + 2\xi_{zn}\omega_{zn}\dot{z}_n + \omega_{zn}^2 z_n + \beta_n z_n^2 + \nu_n z_n^3 + R_n z_n u = 0 \qquad (3.10)$$

When a harmonic signal at a frequency Ω in the range of $2\omega_{zn}$ is applied to the actuator, the analytical prediction of the steady state response around the parametric resonance is, here again, obtained using the method of multiple scales (see appendix B.1.2); we obtain
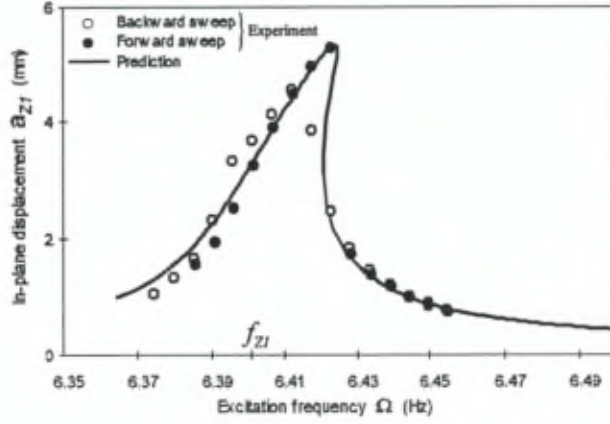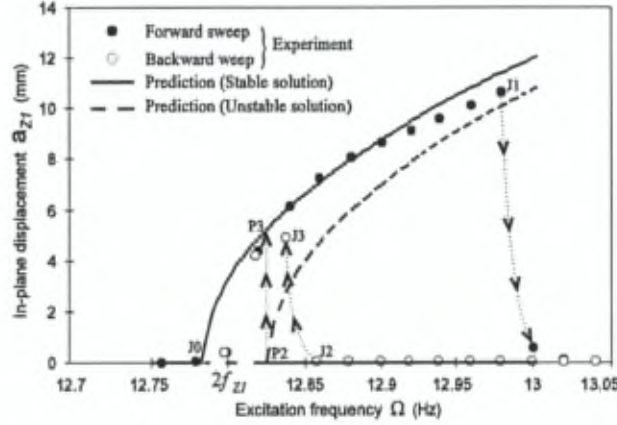
Figure 3.9: Frequency response function between the active tendon displacement and the in-plane vibration at the parametric resonance $2\omega_{z1}$. P2 and P3 indicate the predicted jump points, while J1, J2 and J3 indicate the experimental ones.

$$\left[\frac{\Omega - 2\omega_{zn}}{\omega_{zn}} - \left(\frac{3}{4}\nu_n - \frac{5}{6}\frac{\beta_n^2}{\omega_{zn}^2}\right)\frac{a_{zn}^2}{\omega_{zn}^2}\right]^2 = \left(\frac{R_n a_u}{2\omega_{zn}^2}\right)^2 - 4\xi_{zn}^2 \tag{3.11}$$

where a_{zn} is the response amplitude and a_u is the amplitude of the axial displacement of the support. One notices that the steady state solution exists only if the amplitude a_u of the excitation is greater than a critical value :

$$a_u > \frac{4\xi_{zn}\omega_{zn}^2}{R_n} \tag{3.12}$$

If this condition is satisfied, one or two steady state solutions of Equ.(3.11) are possible; only one of them is stable and can be observed in experiments, as we shall see below.

Experiments have been conducted on the same cable test article. The amplitude of the cable moving support a_u is 7 μm. Figure 3.9 shows the comparison between the experimental frequency response curve and the prediction (3.11) around the parametric resonance $2\omega_{z1}$ ($2f_{z1} = 12.8$ Hz). Note that when the frequency is increased from small values, beyond point J0 the amplitude of vertical motion of the cable rises and a downwards jump occurs at point J1.

The stability of the parametrically excited Duffing equation [41] is addressed in Appendix B.1.2; it is shown that the lower branch of the predicted frequency response (in dashed line on Fig.3.9) is unstable. When the frequency decreases from a large value, we note that upon reaching point P2 the trivial solution becomes unstable and there is a jump up to point P3 which is experimentally observed in Fig.3.9 (jump up from J2 to J3).
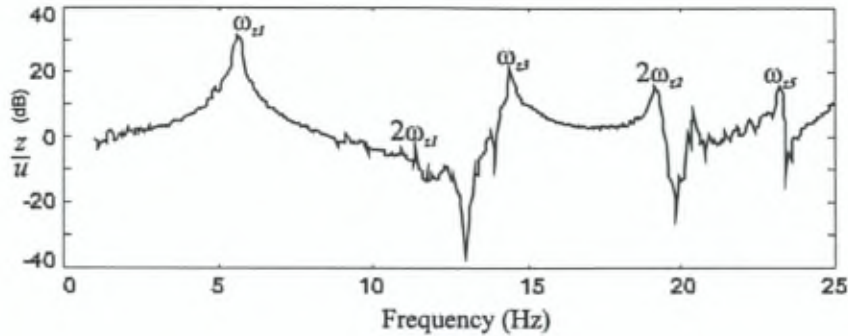
Figure 3.10: Frequency response function between the active tendon displacement u and the amplitude z of the in-plane vibration.

3.4 Open-loop control system

The aim of this section is to assess the open-loop properties of the control system, in particular with respect to the controllability and the observability. To this end, experimental frequency response functions have been measured over the whole frequency range, using a white noise source. The static tension in the cable is in this case $T_0 = 25$ N.

3.4.1 Controllabilty

Figure 3.10 shows the linear frequency response function between the displacement u of the active tendon and the amplitude of the in-plane vibration z of the cable (measured with the optical sensor). All the modes of odd number (symmetric modes) are excited through the induced sag inertia, whereas the modes of even number (antisymmetric modes) are not excited because the corresponding coefficients α_{cn} vanish.

The contributions at $2\omega_{z1}$ and at $2\omega_{z2}$ correspond to the parametric resonance. One observes that the parametric resonance of mode 2 is much more pronounced than that of mode 1; this remark is theoretically predicted by Equ.(3.11).

3.4.2 Observability

In order to verify experimentally the observability properties in the active tendon, a forced excitation is applied to the vertical cable modes, using a shaker as indicated in Fig.3.1. Figure 3.11.a shows the frequency response function between the shaker force F_{in} and the amplitude of the in-plane vibration z. As expected from Equ.(2.74), all in-plane modes z contribute to the response. Figure 3.11.b shows the frequency response function between the shaker force
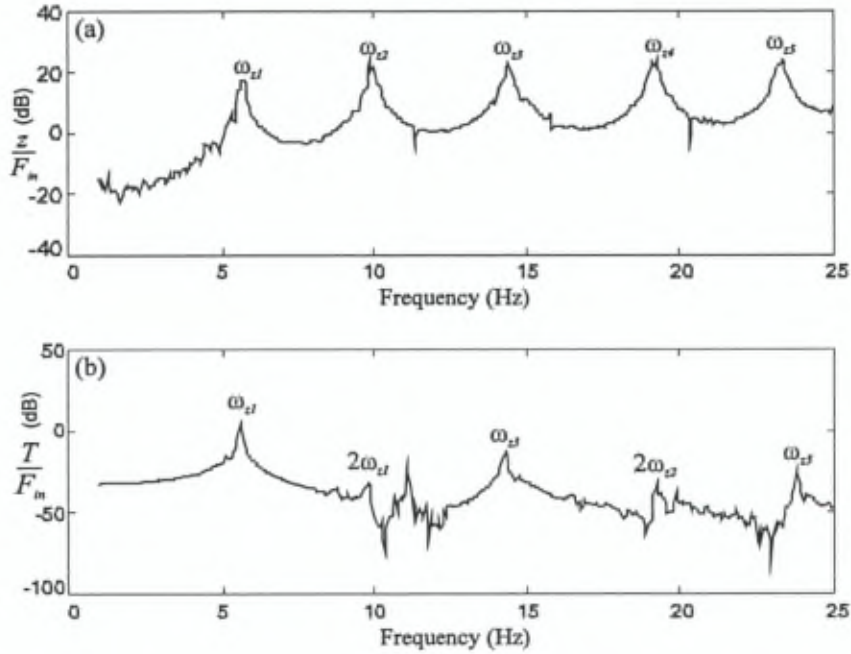
Figure 3.11: Frequency response function between
(a) the shaker force F_{in} and the amplitude z of the in-plane vibration.
(b) the shaker force F_{in} and the tension T in the cable.

and the tension in the cable T. Note that mode 2 appears only through the quadratic term at $2\omega_{z2}$, because the coefficients $h_{1n} = 0$ for n even in Equ.(2.75). By contrast, mode 1 appears at ω_{z1} with the linear term and at $2\omega_{z1}$ with the quadratic term in Equ.(2.75).

Modes 3 and 5 are also observable from the cable tension, although less than mode 1, as we can expect from the analytical form of h_{1n} ($\approx n^{-3}$). The anti-symmetric in-plane modes and all the out-of-plane modes are observable only for very large amplitudes, because they contribute to the cable tension through the quadratic terms y_n^2 and z_n^2.

3.4.3 Open-loop transfer function

Figure 3.12 shows the frequency response between the active tendon displacement u and the tension T in the cable (i.e. open-loop transfer function of the control system). We see that it is dominated by the first mode and that there is a transmission zero right before ω_{z1}. We observe that the contribution of the third vertical mode at ω_{z3} is substantially smaller, which confirms the previous
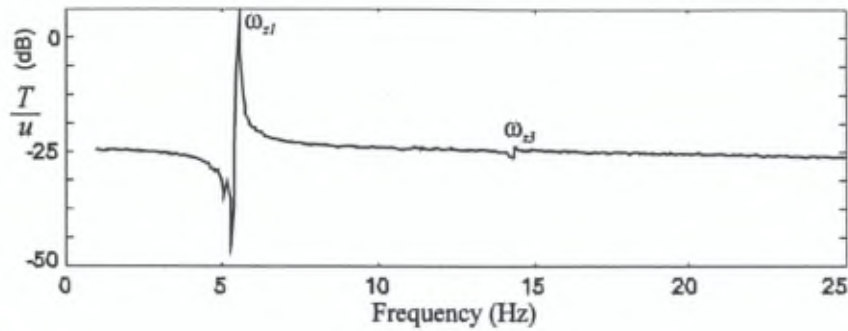
Figure 3.12: Frequency response function between the active tendon displacement u and the tension T in the cable.

remark concerning the observability and controllability of high order symmetric in-plane modes.

Figure 3.13 shows the frequency response functions obtained from numerical simulations using the nonlinear model described by Equ.(2.73) to (2.75), implemented in a specially written C++ program. Most of the features observed in the experimental frequency response functions can also be observed in the simulated ones.
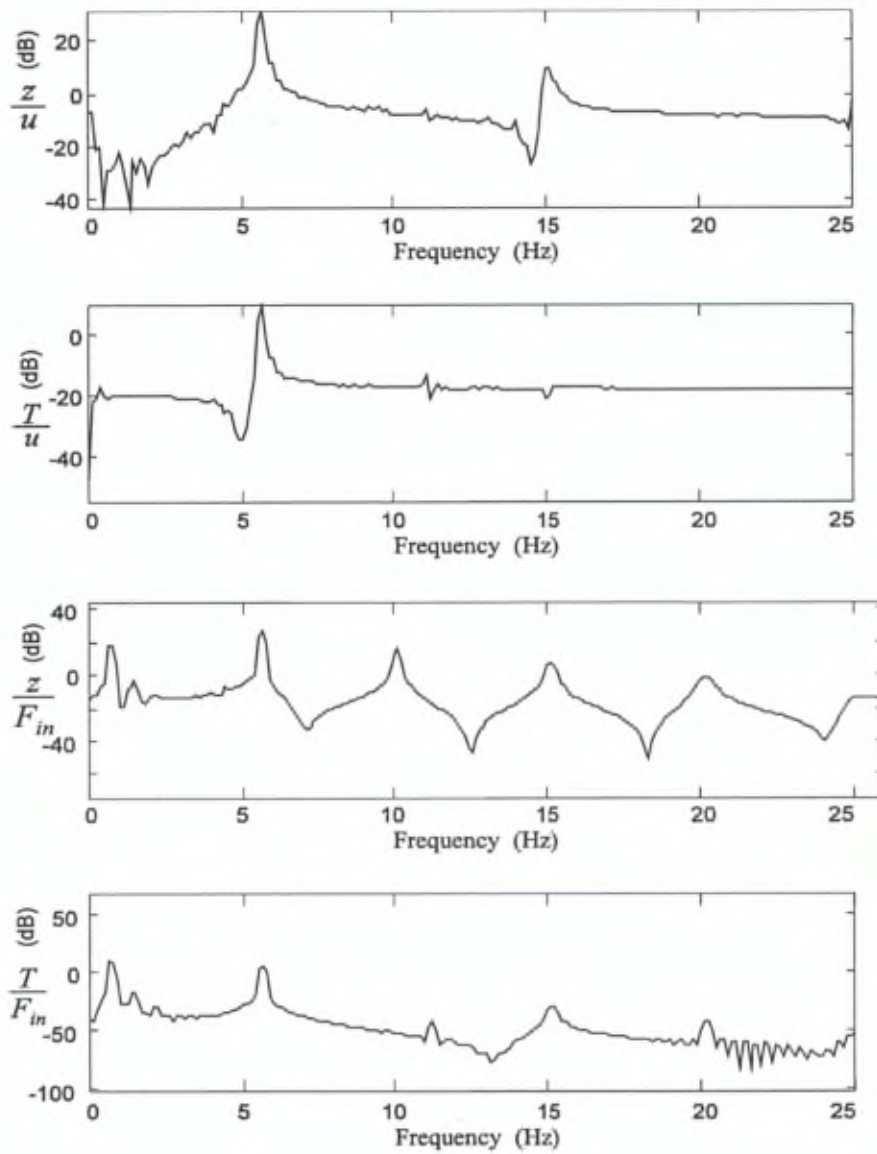
Figure 3.13: Numerical Frequency response function between
(a) the active tendon displacement u and the in-plane vibration z.
(b) the active tendon displacement u and the tension T in the cable.
(c) the shaker force F_{in} and the amplitude z of the in-plane vibration.
(d) the shaker force F_{in} and the tension T in the cable.

Chapter 4

Active damping of a cable

4.1 Introduction

Over the last decade, there has been a growing interest in the active control of string and cable vibration. The problem is difficult because of the highly nonlinear behaviour of strings and cables with sag. The control methods used to suppress the vibration of such nonlinear systems can be separated in three classes, depending on the actuator operating mode :

(i) transverse point force

(ii) transverse support motion

(iii) axial support motion (tendon control)

The first class is illustrated in Fig.4.1.a. In the theoretical study of Yamagushi et al. [71], a wave control approach is used to damp the vibration of a cable with sag. From a practical point of view, the control forces applied transversally to the cable are responsible of localized bending stresses and thus might lead to fatigue problems. Moreover, this type of control is difficult to implement; and the choice of the actuators and sensors is of considerable difficulty with respect to a good observability and controllability.

The second class is illustrated in Fig.4.1.b. In a recent work [32], Lee and Mote apply a transversal boundary control technique to control the transverse vibration of a translating string; a time optimal controller for the maximum energy dissipation of the string is determined by minimizing the energy of waves reflected from the boundary. Furthermore, transversal boundary control can be implemented not only by active control such as a direct velocity feedback, but also through a passive design using a damping mechanism as indicated in Fig.4.1.c [32, 72].

The third class (active tendon control with an axially movable support) has
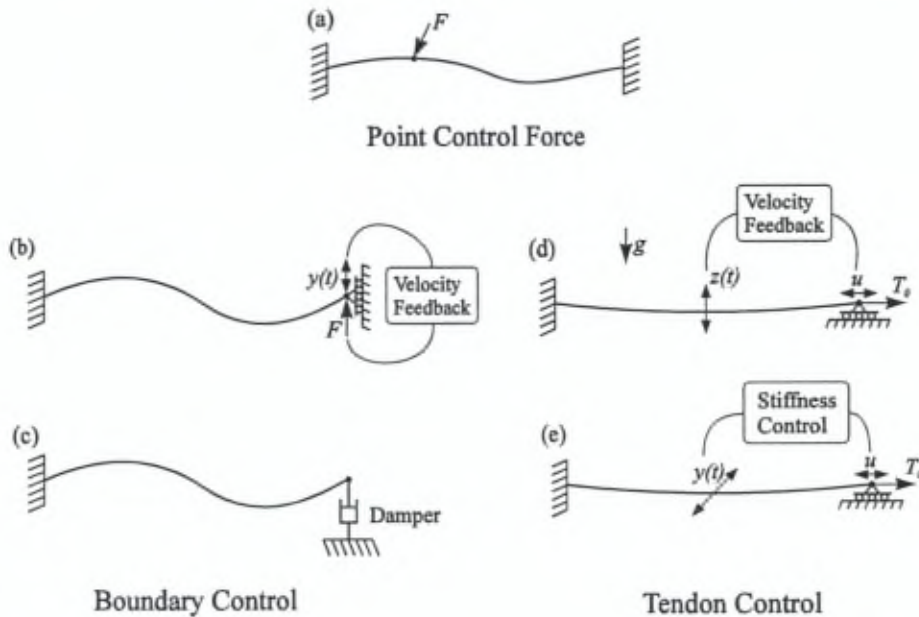
Figure 4.1: Possible control strategies for the transverse vibration of cables and strings.

been studied by Fujino and coworkers. They demonstrated [18] that the in-plane vertical cable vibration can be controlled by sag induced forces (Fig.4.1.d) and that sag induced control is very efficient for the first in-plane mode, even for very small values of the sag to span ratio ($d/l < 0.5\%$). Sag induced forces do not affect the out-of-plane vibration of the cable which behaves like a taut string. Chen [10] showed theoretically on a string that the out-of-plane vibration can also be controlled by the longitudinal motion of the support at a frequency equal to twice the frequency of the transverse vibration of the string, making a positive use of the parametric excitation. This stiffness control algorithm has been tested by Fujino and coworkers [19] on a cable-structure system (Fig.4.1.e).

All the control strategies based on a non-collocated actuator-sensor pairs for the local in-plane and out-of-plane cable modes must rely on a simplified model and, as a result, are prone to *spillover* : Control spillover arises from the control variable u exciting the higher order modes in addition to the targeted one. Observation spillover results from the contamination of the sensor signal by contributions from the higher order modes. It is well known that when both control and observation spillover exist, they can result in spillover instability [5].

This chapter will first review the existing control strategies of active tendon

control of a cable; next, an alternative control strategy based on a force sensor collocated with the active tendon is proposed. Some experiments are conducted on our laboratory mock-up and the results are compared with the predictions.

4.2   Control efficiency

An energy analysis is conducted to evaluate the control efficiency [19]. For simplicity, let us assume that the in-plane transverse vibration with active control, z_n, is harmonic with frequency $\widehat{\omega}_{zn}$ which is close to the undamped natural frequency, $\widehat{\omega}_{zn} \approx \omega_{zn}$,

$$z_n = a_{zn} \cos(\omega_{zn} t) \tag{4.1}$$

We define the energy dissipation as the integral over one cycle, $\tau_n = \omega_{zn}/2\pi$, of the product of the generalized velocity and the generalized damping force. For a linear oscillator,

$$m_{zn} \left(\ddot{z}_n + 2\xi_{zn}\omega_{zn}\dot{z}_n + \omega_{zn}^2 z_n \right) = 0 \tag{4.2}$$

The energy dissipation due to inherent damping can be written as,

$$
\begin{aligned}
E_p \left(2m_{zn}\xi_{zn}\omega_{zn}\dot{z}_n \right) &= -\int_0^{\tau_n} \left(2m_{zn}\xi_{zn}\omega_{zn}\dot{z}_n \right) \dot{z}_n dt \\
&= -2\pi m_{zn}\xi_{zn} \left(\omega_{zn}a_{zn} \right)^2
\end{aligned}
\tag{4.3}
$$

Returning to the cable system, the differential motion of the cable support $u(t)$ creates two basic effects as seen in chapter 2:

- Active sag induced force $(-\alpha_{cn}\ddot{u})$; this term is due to the presence of sag in the cable, and exists for the in-plane symmetric modes only.

- Active stiffness variation $R_n u y_n$ and $R_n u z_n$, where R_n is given by Equ.(3.6).

The energy dissipation due to the sag induced force is,

$$E_p \left(-\alpha_{cn}\ddot{u} \right) = -\int_0^{\tau_n} \left(-\alpha_{cn}\ddot{u} \right) \dot{z}_n dt = \alpha_{cn} \int_0^{\tau_n} \ddot{u}\dot{z}_n dt \tag{4.4}$$

The equivalent linear damping ξ_{zn}^{ai} is obtained by comparing Equ.(4.4) with the corresponding equation for the linear oscillator (4.3); we get

$$\xi_{zn}^{ai} = \frac{-E_p \left(-\alpha_{cn}\ddot{u} \right)}{2\pi m_{zn} \left(\omega_{zn}a_{zn} \right)^2} \tag{4.5}$$

The energy dissipation due to active stiffness control is similarly,

$$E_p \left(R_n z_n u \right) = - \int_0^{\tau_n} \left(R_n z_n u \right) \dot{z}_n dt = -R_n \int_0^{\tau_n} u z_n \dot{z}_n dt \qquad (4.6)$$

Following the same procedure, the equivalent linear damping ξ_{zn}^{as} due to active stiffness force is obtained by comparing Equ.(4.6) with Equ.(4.3); we obtain

$$\xi_{zn}^{as} = \frac{-E_p \left(R_n z_n u \right)}{2\pi m_{zn} \left(\omega_{zn} a_{zn} \right)^2} \qquad (4.7)$$

Similarly, for the out-of plane motion, the energy dissipation due to active stiffness control reads

$$E_p \left(R_n y_n u \right) = - \int_0^{\tau_n} \left(R_n y_n u \right) \dot{y}_n dt = -R_n \int_0^{\tau_n} u y_n \dot{y}_n dt \qquad (4.8)$$

which yields the equivalent linear damping

$$\xi_{yn}^{as} = \frac{-E_p \left(R_n y_n u \right)}{2\pi m_{yn} \left(\omega_{yn} a_{yn} \right)^2} \qquad (4.9)$$

4.3 Existing control strategies

4.3.1 Active sag induced inertia

The control law proposed in [18] consists of a proportional feedback of the modal velocity (assumed available) :

$$u(t) = \frac{g}{\omega_{zn}} \dot{z}_n \qquad (4.10)$$

where g is the control gain. This control acts essentially at the primary resonance. Following the procedure to estimate the control efficiency, one finds that the energy due to stiffness control vanishes; the energy dissipation due to sag induced inertia can be evaluated by introducing Equ.(4.10) in Equ.(4.4); we find easily

$$E_p \left(-\alpha_{cn} \ddot{u} \right) = -\alpha_{cn} g \pi \left(a_{zn} \omega_{zn} \right)^2 \qquad (4.11)$$

and the equivalent damping ratio, Equ.(4.5), is

$$\xi_{zn}^{ai} = g \frac{\lambda}{1 + \frac{\lambda^2}{12}} \frac{1}{\sqrt{\varepsilon_0}} \frac{1 + (-1)^{n+1}}{n\pi} \qquad (4.12)$$

where n is the order of the mode, ε_0 is the static strain in the cable, and λ^2 is the Irvine parameter, related to the static strain and the sag to span ratio d/l by Equ.(2.22).

We note that the control law is the most effective for the first symmetric in-plane mode and is a linear function of the control gain. This controller has been tested experimentally ($d/l \approx 0.5\%$ and $a_u < 80~\mu m$). In the experimental set-up of Fujino [18], a CCD camera is used to track the modal in-plane displacement, which is filtered in order to extract the modal velocity; in our experiment the same filtering process is applied to the signal of the optical sensor described in section 3.2.2. A damping ratio of about $\xi_{z1}^{ai} \approx 1~\%$ has been achieved for the first symmetric in-plane mode.

4.3.2 Active stiffness control

Chen's controller

The stiffness control was first proposed by Chen [10] to suppress the vibration of a taut string; the modal control law is based on the measurement of the transverse modal displacement y_n and velocity $\dot{y}_n$; the proposed feedback for the axial support displacement is

$$u(t) = \frac{g}{\omega_{yn}} \frac{\dot{y}_n y_n}{|y_n|} \tag{4.13}$$

This control acts essentially at the parametric resonance ($2\omega_{yn}$); if one substitutes $y_n = a_{yn} \cos(\omega_{yn} t)$, we get $g = a_u/a_{yn}$. Upon substituting this control law in Equ.(4.8), we find after some algebra

$$E_p \left(R_n y_n u \right) = -\frac{4}{3} g R_n \omega_{yn} a_{yn}^3 \tag{4.14}$$

Hence, the equivalent damping ratio ξ_{yn}^{as} due to active stiffness force [Equ.(4.9)], becomes

$$\xi_{yn}^{as} = \frac{2}{3\pi} \frac{1}{\varepsilon_0} \frac{1}{1 + \frac{\lambda^2}{12}} \frac{a_u}{l} \tag{4.15}$$

where a_u is the amplitude of the support displacement, ε_0 denotes the static strain in the cable and λ^2 is given by Equ.(2.22).
Similarly, the control law Equ.(4.13) can be applied to the the in-plane motion by sensing the vertical modal displacement and velocity coordinates z_n and $\dot{z}_n$; in this case the equivalent damping reads

$$\xi_{zn}^{as} = \frac{2}{3\pi} \frac{1}{\varepsilon_0} \frac{1}{1 + \frac{\lambda^2}{12}} \frac{1}{\kappa_n} \frac{a_u}{l} \tag{4.16}$$

with

$$\kappa_n = 1 + \frac{4\lambda^2}{(n\pi)^4} (1 + (-1)^{n+1}) = \frac{\omega_{zn}^2}{\omega_{yn}^2} \tag{4.17}$$

We note that the efficiency of this stiffness control is an increasing function of the actuator amplitude. Its application to our laboratory mock-up ($d/l \approx$ 0.5 %) shows that for small amplitudes of the support displacement ($a_u <$ 80 μm), a damping ratio of $\xi_{z1}^{as} = 0.5$ % for the first vertical cable mode is predicted by the numerical simulations and corresponds to the value predicted by Equ.(4.16). However, its practical implementation on the experimental set-up is inconvenient and leads to spillover instability.

Onoda's controller

The stiffness control law used by Onoda [45, 46] is a nonlinear saturation controller; the out-of-plane vibration is controlled by

$$u(t) = \left\{ \begin{array}{ll} a_u & \text{if} \quad y_n \dot{y}_n > 0 \\ -a_u & \text{if} \quad y_n \dot{y}_n < 0 \end{array} \right. \tag{4.18}$$

Following the same process, and after some algebra, one finds that the energy dissipation due to the stiffness control force is

$$E_p\left(R_n y_n u\right) = -2 R_n a_u a_{yn}^2 \tag{4.19}$$

and the equivalent damping ratio Equ.(4.9) reads

$$\xi_{yn}^{as} = \frac{1}{\pi} \frac{1}{\varepsilon_0} \frac{1}{1 + \frac{\lambda^2}{12}} \frac{a_u}{l} \tag{4.20}$$

As above, this result can be transposed to the vertical motion but the presence of a sag induced inertia excites other symmetric modes leading to spillover problems. A multimodal control has also been proposed by the same author, but its application to a taut string shows that spillover instability occurs [46].

Fujino's controller

The stiffness control law proposed by Fujino and coworkers is based on Chen's controller; the actuator displacement is related to the measurement of the cable mode amplitudes by a nonlinear continuous function :

$$u(t) = a_u \frac{2}{\omega_{yn}} \frac{\dot{y}_n y_n}{y_n^2 + \frac{\dot{y}_n}{\omega_{yn}}} \tag{4.21}$$

Substituting Equ.(4.21) in Equ.(4.8), we get

$$E_p\left(R_n y_n u\right) = -\frac{\pi}{2} R_n a_u a_{yn}^2 \tag{4.22}$$

Thus, the additional damping ratio for the out-of-plane mode Equ.(4.9), is

$$\xi_{yn}^{as} = \frac{1}{4} \frac{1}{\varepsilon_0} \frac{1}{1 + \frac{\lambda^2}{12}} \frac{a_u}{l} \tag{4.23}$$

Similarly, for the in-plane mode, the equivalent damping Equ.(4.7) reads

$$\xi_{zn}^{as} = \frac{1}{4}\frac{1}{\varepsilon_0}\frac{1}{1+\frac{\lambda^2}{12}}\frac{1}{\kappa_n}\frac{a_u}{l} \tag{4.24}$$

This stiffness control law does not produce any energy dissipation due to sag induced inertia so that $\xi_{zn}^{ai} = 0$. Equation (4.23) and (4.24) show that the stiffnesss control is efficient for large amplitudes of the actuator. The control algorithm has been tested in simulation using the cable model Equ.(2.73) to (2.75), and experimentally. A damping ratio below 1 % has been obtained for an amplitude $a_u = 70$ μm, which reflects both the predicted value given by Equ.(4.24) and the results obtained by simulation.
For multimodal systems, the controller is based on the reconstructed modal states z_n and $\dot{z}_n$ from the vertical displacement measurement of the cable (i.e. with the optical sensor) and it may lead to spillover instability. This instability is observed when the cable is connected to a structure.

Multimodal control

A bilinear control theory based on the direct method of Liapunov has been used to control multimodal cable vibration [64]. In principle, if all the states are available, the control algorithm guarantees a reduction of the energy in the cable system. However, it relies on the knowledge of the state vector, and when applied with an observer, the stability properties are lost.
A stiffness control algorithm based on a bilinear observer and a quadratic feedback from a single sensor to a parametric actuator can be applied to suppress the transverse vibration of a string [57]. The applicability of this stiffness control has been demonstrated on a pinned and clamped beam experiment; however spillover instability is observed in certain conditions depending on the system parameters.

4.4   Integral Force Feedback controller

4.4.1   Energy absorbing control

It is widely accepted that the active damping of linear structures is much simplified if one uses collocated actuator and sensor pairs [8]. This is because the poles and zeros alternate near the imaginary axis. For such configurations, a wide class of controllers can be developed using positivity concepts [6]. For non-linear structures, the use of collocated actuator-sensor pairs is still quite attractive, because it is possible to develop control schemes which are guaranteed to be energy absorbing, assuming perfect actuator and sensor dynamics. First, consider the configuration of Fig.4.2.a : the actuator produces a point force and the collocated sensor measures the velocity. The power flow from the

(a) Velocity feedback   (b) Force feedback
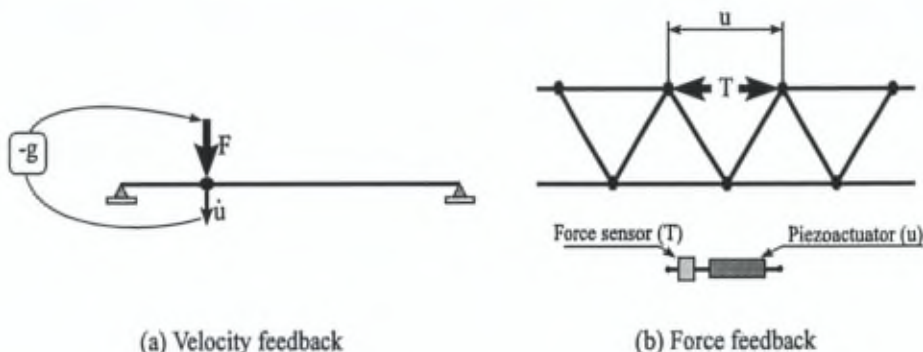
Figure 4.2: Energy absorbing control.

control system is $W = F\dot{u}$. Any control law rendering W negative will be stabilizing, because if we take the total energy E (potential + kinetics) of the vibrating structure as a Liapunov function, we have $\dot{E} = W$. $W < 0$ can be achieved by the feedback law,

$$F = -g\dot{u} \quad \Rightarrow \quad W = -g\dot{u}^2 \quad (g > 0) \tag{4.25}$$

This well known scheme is called *Direct Velocity Feedback*. A nonlinear alternative feedback law is,

$$F = -F_0 sign(\dot{u}) \quad \Rightarrow \quad W = -F_0|\dot{u}| \quad (F_0 > 0) \tag{4.26}$$

This "bang-bang" control produces a faster decay, but it can lead to chattering near the equilibrium.

Next, consider the dual situation (Fig.4.2.b) where the actuator controls the relative position u of two points inside the structure (e.g. piezoelectric linear actuator) and the sensor output is the force T in the active member (T is collocated with u). As before, $\dot{E} = W = -T\dot{u}$ and it is readily verified that the *positive Integral Force Feedback* (IFF),

$$u = g \int T dt \quad \Rightarrow \quad W = -gT^2 \quad (g > 0) \tag{4.27}$$

produces an energy absorbing control. Integral force feedback on piezoelectric actuators has already been applied successfully to the control of truss structures [56].

From the foregoing discussion, we can anticipate that the integral force feedback will be effective in damping the local in-plane mode of the cable. Moreover, this will be achieved without threat of spillover instability, provided that the actuator and sensor dynamics are good enough. Force feedback cannot be used

for damping the out-of-plane modes, because these modes are weakly observable from the force sensor. The in-plane vibration of a cable with small sag is considered in the next section.

4.4.2   Control law

The proposed control law is the Integral Force Feedback,

$$u(t) = g \int_0^t T(\tau)d\tau \tag{4.28}$$

Upon substituting the dynamical component of the tension in the cable T from Equ.(2.75) and introducing $z_n = a_{zn} \cos(\omega_{zn}t)$ in Equ.(4.4), we find, after some algebra, that the energy dissipation due to the sag induced force reads

$$E_p\left(-\alpha_{cn}\ddot{u}\right) = -\pi\alpha_{cn}\left(a_{zn}\omega_{zn}\right)^2 \frac{\frac{gh_{1n}}{\omega_{zn}}}{1 + \left(\frac{gh_u}{\omega_{zn}}\right)^2} \tag{4.29}$$

The equivalent damping ratio ξ_{zn}^{ai} given by Equ.(4.5) is

$$\xi_{zn}^{ai} = \frac{2}{(n\pi)^4}(1 + (-1)^{n+1})\lambda^2 \frac{\frac{gh_u}{\omega_{zn}}}{1 + \left(\frac{gh_u}{\omega_{zn}}\right)^2} \tag{4.30}$$

Similarly, the energy dissipation due to active stiffness control is

$$E_p\left(R_n z_n u\right) = \frac{\pi}{2}R_n a_{zn}^4 \frac{\frac{gh_{2n}}{4\omega_{zn}}}{1 + \left(\frac{gh_u}{2\omega_{zn}}\right)^2} \tag{4.31}$$

and the corresponding damping ratio reads

$$\xi_{zn}^{as} = -\frac{1}{8}(n\pi)^2 \left(1 + \frac{\lambda^2}{12}\right)\frac{1}{\varepsilon_0} \frac{\frac{gh_u}{2\omega_{zn}}}{1 + \left(\frac{gh_u}{2\omega_{zn}}\right)^2} \tag{4.32}$$

Following the same process for the out-of-plane motion we find

$$\xi_{yn}^{as} = -\frac{1}{8}(n\pi)^2 \left(1 + \frac{\lambda^2}{12}\right)\frac{1}{\varepsilon_0} \frac{\frac{gh_u}{2\omega_{yn}}}{1 + \left(\frac{gh_u}{2\omega_{yn}}\right)^2} \tag{4.33}$$

The maximum value of the sag induced damping ξ_{zn}^{ai} is obtained when $gh_u/\omega_{zn} = 1$; for this particular value, we have

$$\xi_{zn}^{ai} = \frac{\lambda^2}{(n\pi)^4}(1 + (-1)^{n+1}) \tag{4.34}$$
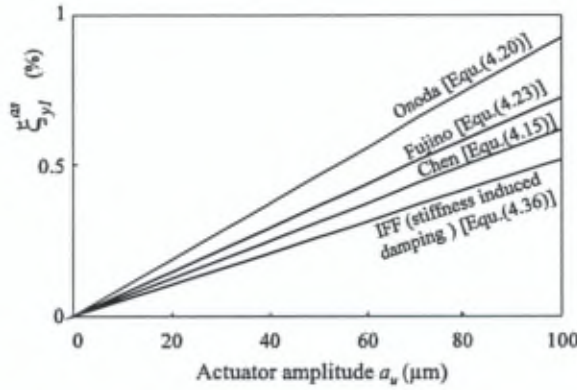
Figure 4.3: Damping ratio of the first out-of-plane mode due to stiffness control $(d/l = 0.3\%)$.

On the other hand, the maximum damping ξ_{zn}^{as} due to the stiffness control is achieved when $gh_u/\omega_{zn} = 2$; we obtain,

$$\xi_{zn}^{as} = \frac{\sqrt{2}}{8} \frac{1}{\varepsilon_0} \frac{1}{1 + \frac{\lambda^2}{12}} \frac{1}{\kappa_n} \frac{a_u}{l} \tag{4.35}$$

We note that the damping due to the sag induced inertia depends heavily on the parameter λ^2 and that it is reduced drastically as the order of the mode increases (as n^{-4}), so that in practice, only the first symmetric vertical mode is damped effectively. For small amplitudes of the actuator (here $a_u \approx 70\mu m$), the sag induced damping dominates for the symmetric in-plane modes, $\xi_{zn}^{ai} \gg \xi_{zn}^{as}$. For the out-of-plane motion the optimal damping ratio is again obtained when $gh_u/\omega_{yn} = 2$:

$$\xi_{yn}^{as} = \frac{\sqrt{2}}{8} \frac{1}{\varepsilon_0} \frac{1}{1 + \frac{\lambda^2}{12}} \frac{a_u}{l} \tag{4.36}$$

Notice that the Integral Force Feedback extracts energy from both sag induced inertia forces and stiffness control forces; this is why it works also for the transverse vibration of a string, provided however, that the actuator amplitudes are large.

Figure 4.3 compares the damping ratio ξ_{y1}^{as} obtained with the Integral Force Feedback for the first out-of-plane mode, with those obtained with the various stiffness control strategies discussed earlier.
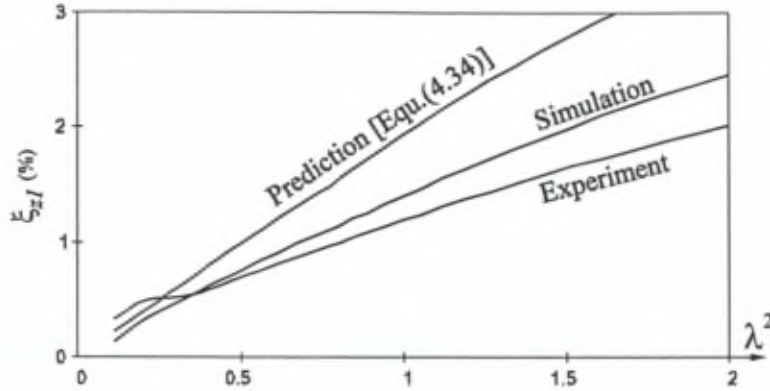
Figure 4.4: Influence of λ^2 on the maximum sag induced damping with the *Integral Force Feedback*.

4.4.3 Implementation, experimental results

In the practical implementation of the integral force feedback, because of the high-pass behaviour of the force sensor, only the dynamic component of the tension in the cable is considered; in addition to that a forgetting factor is applied to prevent saturation [54]. The integral control law

$$u = \frac{g}{s}T \tag{4.37}$$

can readily be transformed into a difference equation using the bilinear transform [16]; this leads to

$$u_{i+1} = u_i + g\frac{\Delta t}{2}(T_{i+1} + T_i) \tag{4.38}$$

where Δt is the sampling period. We easily recognize the trapezoid rule for integration. In order to avoid saturation, it is wise to slightly modify this relation according to

$$u_{i+1} = \alpha u_i + g\frac{\Delta t}{2}(T_{i+1} + T_i) \tag{4.39}$$

where α is a forgetting factor slightly lower than 1. α depends on the sampling frequency; it can either be tuned experimentally or obtained from a modified compensator

$$u = \frac{g}{s+a}T \tag{4.40}$$

where the breakpoint frequency a is small compared to the frequency of the first controlled mode of the system, in order to produce a phase shift of 90^0 at ω_{z1}.
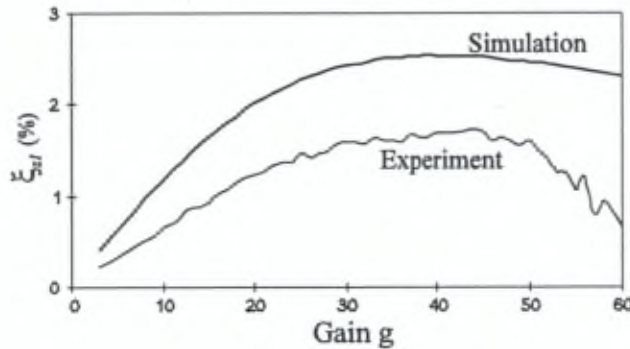
Figure 4.5: Active damping with *Integral Force Feedback* (d/l=0.5 %).

The maximum achievable damping ratio $\xi_{z1} = \xi_{z1}^{ai} + \xi_{z1}^{as} \approx \xi_{z1}^{ai}$ is plotted as a function of λ^2 in Fig.4.4; the experimental results confirm the trend of the predictions of Equ.(4.34) and the results obtained with the numerical simulation of the cable model [Equ.(2.73) to (2.75)].

Figure 4.5 compares the numerical and experimental values of ξ_{z1} as a function of the control gain. The discrepancy between the simulations and the experiments is attributed to the flexibility of the lever system; it is explained in details in chapter 6. Note that the drop of the active damping coefficient for large gains is observed experimentally. Note also that the experimental values of ξ_{z1} are at least as good as other previously published results [18] for comparable values of d/l. The present control law, however, has the advantage that it is not subject to spillover.

Figure 4.6 shows experimental results for the tension in the cable and the transverse displacement during the free response from non-zero initial conditions, with and without control. The sudden change in the cable tension when the control is switched on is due to the feedthrough component $h_u(u_b - u_a)$ in Equ.(2.75).

Various experiments have been conducted with other control laws; Figure 4.7 shows the time response obtained with a *P minus I* controller (combined with a low-pass filter with cut-off frequency near $\omega_c = 100$ Hz). Although a very large damping ratio can be achieved for the first mode ($\xi_{z1} > 10$ % !), this control law has been found destabilizing for higher modes in the experimental set-up; it is not recommended because it is violently unstable when the cable is connected to a flexible structure, as discussed in the next chapter.
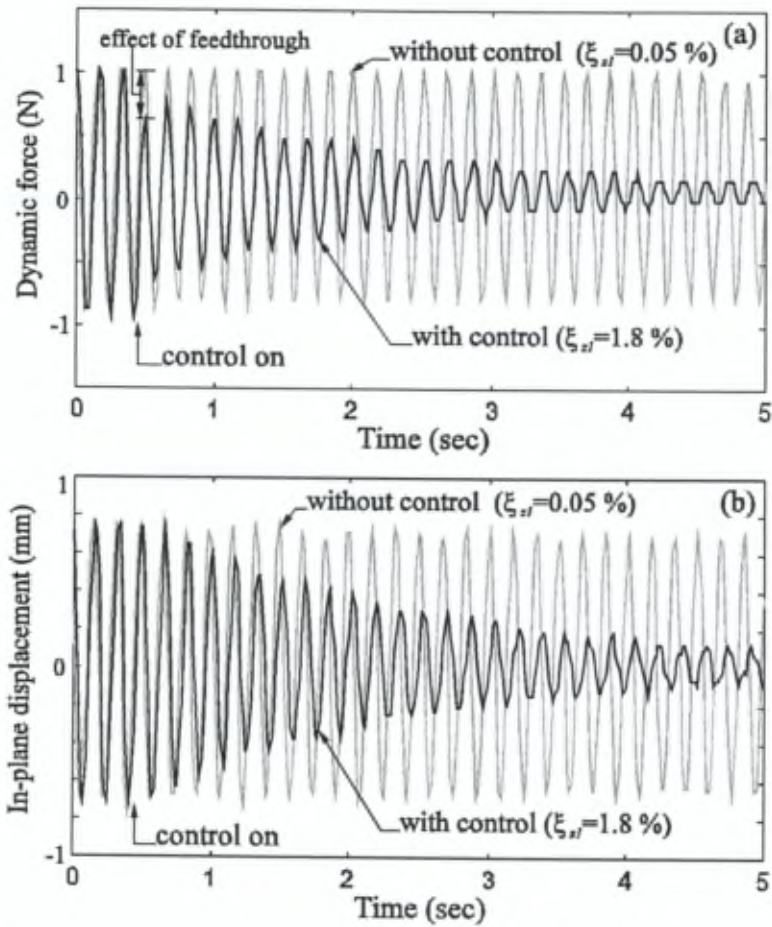
Figure 4.6: Free oscillations with *Integral Force Feedback* (d/l=0.5 %).
(a) Dynamic component of the cable tension.
(b) In-plane displacement.
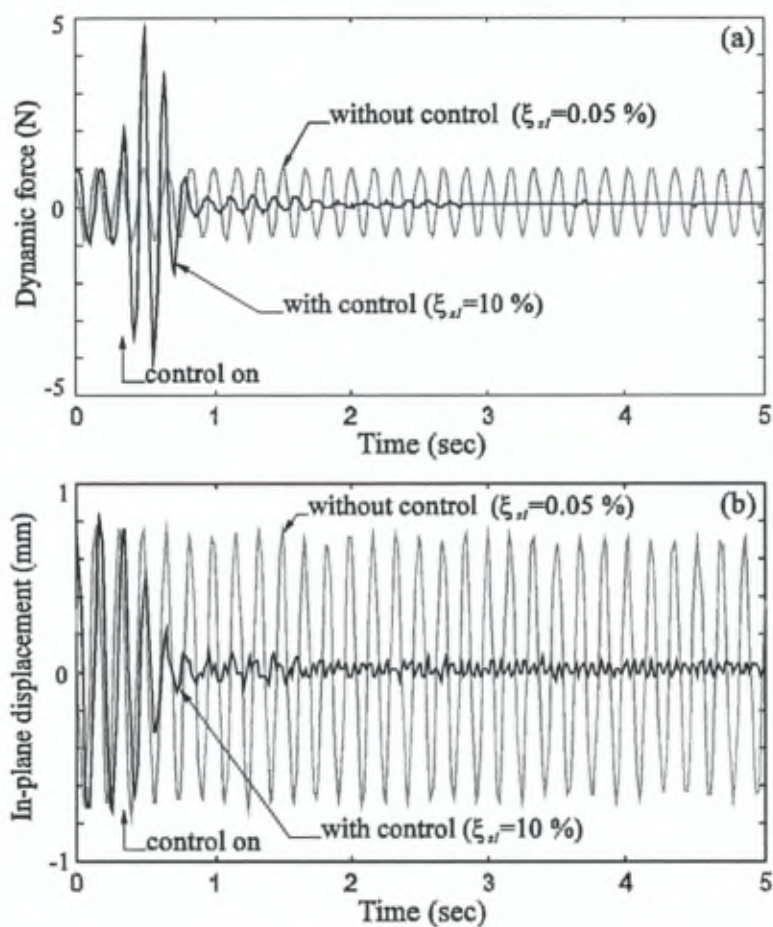
Figure 4.7: Free oscillations with *P minus I* (d/l=0.5 %).
(a) Dynamic component of the cable tension.
(b) In-plane displacement.

Chapter 5

Cable Structure Model

5.1 Introduction

Consider the cable structure of Fig.5.1, consisting of a linear structure (here a truss) with a number of nodes interconnected with cables. As an alternative to a general nonlinear finite element approach which would be extremely time consuming, especially for control system design purposes, we have developed a dedicated software which combines a finite element model of the linear structure with an analytical model of the cables in modal coordinates.
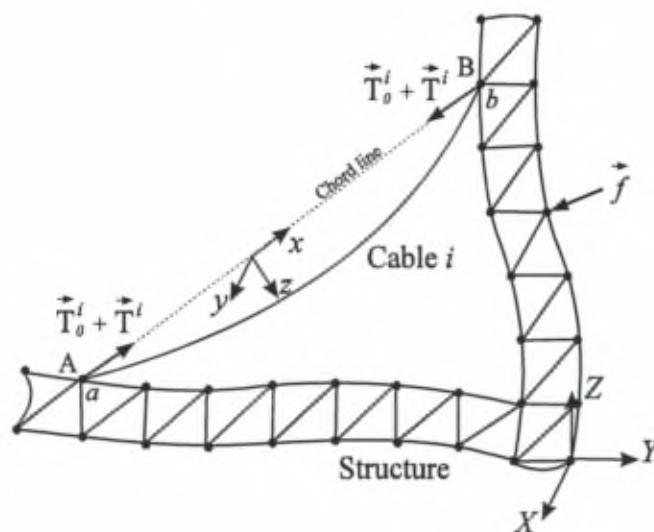
Figure 5.1: Cable structure model.

This model is an extension of that of the cable with movable supports, Equ.(2.73) to (2.75); the model of each cable is written in a local coordinate system as indicated in Fig.5.1; the local x axis is taken along the chord line while the z axis is in the gravity plane (it is arbitrary in a zero-gravity environment). The governing equations result from Lagrange's equations, using the modal amplitudes as generalized coordinates and a nonlinear strain-displacement relationship as discussed in chapter 2; their development follows and the analytical expressions of the various constants are given in appendix C.

5.2 Energy partition in the structure

The motion of the structure is expressed in the global coordinate system (XYZ) as indicated in Fig.5.1. The potential energy of the prestressed structure is

$$\mathcal{V}_s = \frac{1}{2}x \ Kx \qquad (5.1)$$

where the stiffness matrix K results from the contribution of the linear stiffness and the geometric stiffness due to the prestresses induced by the dead load and the static tension applied by the cables; x is the vector of degrees of freedom of the structure.
The kinetic energy is

$$\mathcal{T}_s = \frac{1}{2}\dot{x} \ M\dot{x} \qquad (5.2)$$

where M represents the mass matrix of the structure.

5.3 Energy partition in the cable

Consider the cable structure where each cable (i) is anchored at the structure nodes a and b as indicated in Fig.5.1; the superscript i refers to the cable number. As previously seen in chapter 2, the modal motion of each cable is written in its local coordinate system $(xyz)^i$. Each cable is provided with an active tendon placed at one end (say a in Fig.5.1); the longitudinal displacement at the anchor node a results from the contribution of the longitudinal component u_a^i induced by the structure movement and the contribution of the actuator stroke u^i; so that the longitudinal differential motion of each cable is $u_b^i - u_a^i - u^i$.
The relative displacement components of the structure nodes a and b (U_a^i, V_a^i, W_a^i) and (U_b^i, V_b^i, W_b^i) expressed in the global structure coordinates (XYZ) can be written in terms of the structure degrees of freedom as

$$\left(U_a^i, V_a^i, W_a^i\right)^T = L_a^i x \qquad (5.3)$$

$$\left(U_b^i, V_b^i, W_b^i\right)^T = L_b^i x \qquad (5.4)$$

where L_a^i and L_b^i represent the localisation matrices of the structure nodes a and b. If $\mathcal{R}^i = \left(\mathcal{R}_u^i, \mathcal{R}_v^i, \mathcal{R}_w^i \right)^T$ is the rotation matrix which transforms the structure displacements from the global to the local coordinate system, we have

$$\left(u_a^i, v_a^i, w_a^i \right)^T = \mathcal{R}^i \left(U_a^i, V_a^i, W_a^i \right)^T = \mathcal{R}^i L_a^i x \tag{5.5}$$

and

$$\left(u_b^i, v_b^i, w_b^i \right)^T = \mathcal{R}^i \left(U_b^i, V_b^i, W_b^i \right)^T = \mathcal{R}^i L_b^i x \tag{5.6}$$

5.3.1   Kinetic energy

For each cable, the kinetic energy can be expressed in terms of the structure degrees of freedom x and the actuator stroke u^i by replacing u_a^i by $u_a^i + u^i$ and by substituting Equ.(5.5) and (5.6) in Equ.(A.6); after some algebra, we get

$$\mathcal{T} = \begin{aligned} &\tfrac{1}{2}\dot{y}^{iT}\mu_c^i\dot{y}^i + \tfrac{1}{2}\dot{z}^{iT}\mu_c^i\dot{z}^i + \dot{x}^T G_y^{iT}\dot{y}^i + \dot{x}^T G_z^{iT}\dot{z}^i - \dot{x}^T G_u^{iT}\dot{z}^i \\ &+ \tfrac{1}{2}\dot{x}^T m_{cs}^i\dot{x} + \alpha_c^{iT}\dot{z}^i\dot{u}^i + \eta_s^{Ti}\dot{x}\dot{u}^i + \tfrac{1}{2}m_u^i\dot{u}^{i2} \end{aligned} \tag{5.7}$$

where $y^i = \left(y_1^i\ y_2^i \cdots y_n^i \right)^T$ and $z^i = \left(z_1^i\ z_2^i \cdots z_n^i \right)^T$ denote the vectors of out-of-plane and in-plane cable modes respectively; μ_c^i is the matrix of the modal masses. The matrices G_y^i and G_z^i refer to the interaction between the transverse motion of the cable (out-of-plane and in-plane respectively) and the structure movement; while G_u^i refers to the interaction between the in-plane cable vibration and the axial movement of the cable support induced by the structure vibration. Their analytical expressions, as well as the one of m_u^i, the vector α_s^i and the matrix m_{cs}^i are given in appendix C.

5.3.2   Potential energy

The potential energy of each cable [Equ.(A.20)] is,

$$\begin{aligned} \mathcal{V} = {}& \mathcal{V}^{*i} + \mathcal{V}^{oi} + \mathcal{V}_{ext}^i = \frac{l^i}{2E\,A}\left(T_o^i + T^i\right)^2 - \frac{l^i}{E^i A^i}T_o^i T_d^{(1)i} \\ &+ \frac{\lambda^2}{12}\frac{E_q^i}{E^i}T_0^i\left[\mathcal{R}_u^{iT}(L_b^i - L_a^i)x - u^i\right] - \frac{\gamma^i A^i l^i}{2}\mathcal{R}_w^{iT}(L_b^i + L_a^i)x \\ &+ \mathcal{V}_s^{oi} + \mathcal{V}_{ext}^i \end{aligned} \tag{5.8}$$

where T_0^i is the static component of the cable tension and T^i is the dynamical component given by [Equ.(A.14)]

$$T^i = T_q^i + T_{qs}^i + T_d^{(1)i} + T_d^{(2)i} \tag{5.9}$$

where the contributions are respectively

- the quasi-static tension due to the actuator stroke

$$T_q^i = -h_u^i u^i \qquad (5.10)$$

- the quasi-static tension due to the longitudinal differential motion of the cable supports anchored at the structure nodes a and b

$$T_{qs}^i = h_u^i(u_b^i - u_a^i) = h_u^i \mathcal{R}_u^{iT}(L_b^i - L_a^i)x \qquad (5.11)$$

- the component due to the modal motion of the cable

$$T_d^i = T_d^{(1)i} + T_d^{(2)i} = h_1^{iT}z^i + y^{iT}h_2^i y^i + z^{iT}h_2^i z^i - \frac{T_q^i + T_{qs}^i}{T_0^i}h_1^{iT}z^i \quad (5.12)$$

5.4   Governing equations

The total kinetic and potential energy of the cable structure are

$$\mathcal{T} = \mathcal{T}_s + \sum_i^{n_c} \mathcal{T}_{cable}^i$$

$$\mathcal{V} = \mathcal{V}_s + \sum_i^{n_c} \mathcal{V}_{cable}^i \qquad (5.13)$$

where n_c represents the number of cables. Upon substituting Equ.(5.2) and (5.7) into Equ.(5.13), we can neglect the kinetic energy resulting from the cable supports motion $\sum_i^{n_c}\left(\dot{x}^T m_{cs}^i \dot{x}\right) \ll \dot{x}^T M\dot{x}$. Applying the Lagrange equation to the cable structure system one finds that the equations governing the modal motion of the cables are

$$\frac{d}{dt}\left(\frac{\partial \mathcal{T}}{\partial \dot{y}}\right) + \frac{\partial \mathcal{V}}{\partial y^i} = 0$$

$$\frac{d}{dt}\left(\frac{\partial \mathcal{T}}{\partial \dot{z}}\right) + \frac{\partial \mathcal{V}}{\partial z^i} = 0 \qquad (5.14)$$

and that governing the motion of the structure reads

$$\frac{d}{dt}\left(\frac{\partial \mathcal{T}}{\partial \dot{x}}\right) + \frac{\partial \mathcal{V}}{\partial x} = 0 \qquad (5.15)$$

Substituting Equ.(5.1), (5.2), (5.7), and (5.8) in Equ.(5.13), introducing the result in Equ.(5.14) and adding some modal damping ξ_y^i and ξ_z^i, we obtain the equations governing the vector of generalized coordinates y^i and z^i of the cable,

$$\mu_c^i \left(\ddot{y}^i + 2\xi_y^i \Omega^i \dot{y}^i + \Omega^{i2} y^i \right) + S^i y^i (T_q^i + T_{qs}^i + T_d^i) + G_y^i \ddot{x} \quad = F_y^i \qquad (5.16)$$

$$\mu_c^i \left(\ddot{z}^i + 2\xi_z^i \Omega^i \dot{z}^i + \Omega^{i2} z^i \right) + S^i z^i (T_q^i + T_{qs}^i + T_d^i) + G_z^i \ddot{x}$$
$$+ \Lambda^i T_d^i - G_u^i \ddot{x} + \alpha_c^i \ddot{u}^i \quad = F_z^i \qquad (5.17)$$

Compared to the previous model of a cable Equ.(2.73) to (2.75), the equations governing the transverse motion of the cable contains two additional terms due to the seismic excitation produced by the transverse acceleration of the cable supports, $G_y^i \ddot{x}$ and $G_z^i \ddot{x}$, which was ignored in the cable model of chapter 2. The longitudinal motion of the supports is responsible of a sag induced inertia force $-G_u^i \ddot{x}$ and also contributes to the quasi-static tension T_{qs}^i [Equ.(5.11)] which is responsible of the parametric excitation terms for both the out-of-plane and the in-plane cable modes ($S^i T_{qs}^i y^i$ and $S^i T_{qs}^i z^i$ where the constant matrix S^i is defined in appendix A). The active tendon displacement contributes to the quasi-static tension T_q^i and also for the inertia force $\alpha_c^i \ddot{u}^i$ that affects only the symmetric in-plane modes of the cable.

Following the same procedure with Equ.(5.15), we obtain the equation governing the vector x of the generalized coordinates of the structure,

$$M\ddot{x} + Kx = Bf - \sum_i^{nc} \left[\begin{array}{c} Q^i(T_0^i + T_q^i + T_{qs}^i + T_d^{(2)i}) \\ +G_y^{iT} \ddot{y}^i + G_z^{iT} \ddot{z}^i - G_u^{iT} \ddot{z} + \eta_s^i \ddot{u}^i \end{array} \right] \qquad (5.18)$$

The left hand side of the structure equation is obtained from a standard finite element code; the sum in the right hand side represents the forces applied to the structure by the cables; it consists of the axial loads of the cable tension for which the linear component $T_d^{(1)i}$ has disappeared, the reaction forces due to the transverse vibration of the cable and the external forces applied to the structure f through the influence matrix B. The transformation matrix

$$Q^i = \frac{1}{1 + \frac{\lambda^{i2}}{12}} \left(\mathcal{R}_u^{iT}(L_b^i - L_a^i) \right)^T \qquad (5.19)$$

projects the cable loads from the local to the global coordinate system. The equation governing the structure is further transformed into modal coordinates to reduce the number of degrees of freedom. For this purpose, let us introduce the vector of the modal coordinates q and the matrix of the mode shapes Φ of the structure, prestressed by its dead load and the static tension of the cables T_0 :

$$x = \Phi q \qquad (5.20)$$

Substituting Equ.(5.20) into Equ.(5.18), multiplying by Φ^T, adding some modal damping ξ_s in the structure and removing the static tension T_0 from Equ.(5.18), one finds that the dynamics of the structure around its static equilibrium is governed by

$$\mu_s\left(\ddot{q} + 2\xi_s\Omega_s\dot{q} + \Omega_s^2 q\right) = \Phi^T B f - \sum_i^{nc}\left[\begin{array}{c} P^i(T_q^i + T_{qs}^i + T_d^{(2)i}) \\ +\Gamma_y^{iT}\ddot{y}^i + \Gamma_z^{iT}\ddot{z}^i - \Gamma_u^{iT}\ddot{z} + \alpha_s^i\ddot{u}^i \end{array}\right] (5.21)$$

where we have introduced the new constants defined as follows

$\mu_s = \Phi^T M \Phi$: modal mass matrix of the structure

$\Omega_s^2 = \mu_s^{-1}\Phi^T K \Phi$: modal frequency matrix of the prestressed structure. One should note that the structure is prestressed by each cable with the static tension T_0^i.

and

$$P^i = \Phi^T Q^i \qquad (5.22)$$
$$\Gamma_y^i = G_y^i\Phi \quad , \quad \Gamma_z^i = G_z^i\Phi \quad , \quad \Gamma_u^i = G_u^i\Phi \qquad (5.23)$$
$$\alpha_s^i = \Phi^T \eta_s^i \qquad (5.24)$$

Introducing the structure modal coordinates Equ.(5.20) in Equ.(5.17), the equations governing the cable dynamics can be changed into

$$\mu_c^i\left(\ddot{y}^i + 2\xi_y^i\Omega^i\dot{y}^i + \Omega^{i2}y^i\right) + S^i y^i(T_q^i + T_{qs}^i + T_d^i) + \Gamma_y^i\ddot{q} = F_y^i \qquad (5.25)$$

$$\mu_c^i\left(\ddot{z}^i + 2\xi_z^i\Omega^i\dot{z}^i + \Omega^{i2}z^i\right) + S^i z^i(T_q^i + T_{qs}^i + T_d^i) + \Gamma_z^i\ddot{q}$$
$$+\Lambda^i T_d^i - \Gamma_u^i\ddot{q} - \alpha_c^i\ddot{u}^i = F_z^i \qquad (5.26)$$

The modal matrices μ_s, Ω_s and mode shapes Φ are extracted from the finite element model of the prestressed structure where each cable are replaced by the static forces applied at the node a and b. Figure 5.2 summarizes the modelling technique of cable structures. A dedicated C++ program has been developed for the simulation of the cable structure dynamics defined by the differential equations (5.21),(5.25) and (5.26).

Standard Finite
element code

Cable Structure Dynamics
C++ Software
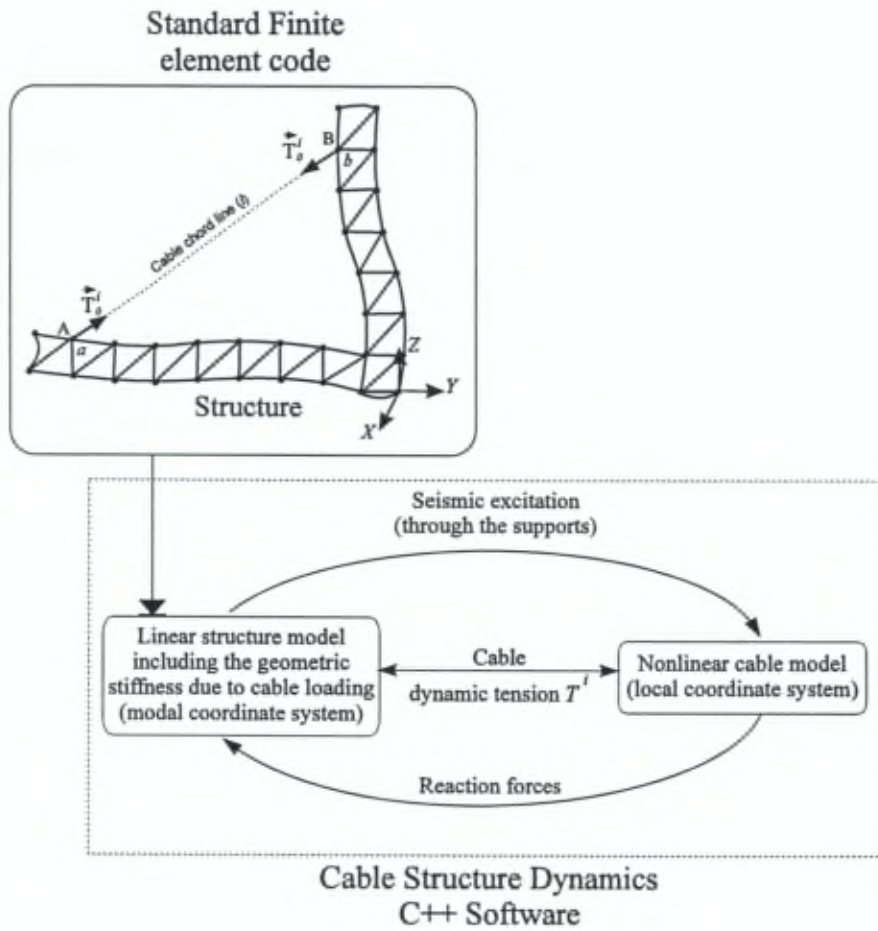
Figure 5.2: Cable structure modelling technique.

Chapter 6

Active damping of cable structures

6.1 Introduction

In chapter 4, active tendon control has been applied to suppress the transverse vibration of a cable with small sag. We have demonstrated that the Integral Force Feedback enjoys guaranteed stability properties and is effective for the first in-plane cable mode; the control algorithm has been demonstrated successfully on a laboratory test article. As we have seen in the previous chapter, when the cable is connected to a structure they interact in a nonlinear manner : the cable excites the structure through the time varying tension in the cable and through the reaction forces; conversely the structure excites the cable through linear inertia forces (seismic excitation) and quadratic coupling terms. The latter may produce a parametric excitation when the frequency of the vibrating support is twice the frequency of the transverse vibration of the cable.

The active damping of cable stayed bridges with an active tendon has been investigated by Fujino and coworkers [19, 68]; the various strategies investigated for damping the main structure and the in-plane and out-of-plane vibration of the cable are represented in Fig.6.1. They demonstrated that the vertical global mode of the bridge can be damped with a linear feedback of the girder velocity on the active tendon displacement (Fig.6.1.a) and that the in-plane (vertical) local cable vibration can be controlled efficiently by sag induced forces (Fig.6.1.b, see section 4.3.1). As we have seen in the previous chapter, the sag induced forces do not affect the out of plane local vibration of the cable, but the stiffness control discussed in chapter 4 can be applied (Fig.6.1.c). However, experimental results [19] have shown that an instability can occur when the cable structure interaction is large, especially when the structure natural frequency is close to twice that of the cable, causing the time-varying tension to resonate with the
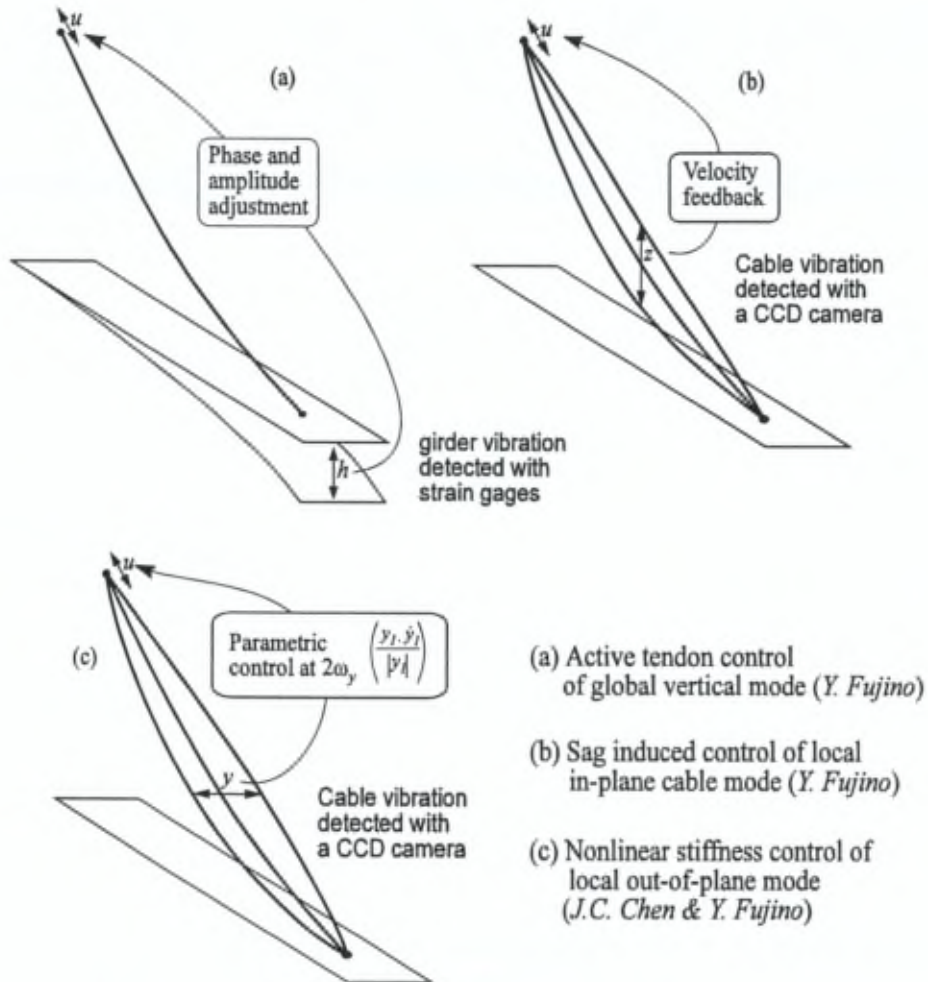
Figure 6.1: Control strategies investigated by Fujino and coworkers.

structure. Note that the above strategies use a non-collocated pair of sensor and actuator and are prone to spillover [5].

In the first part of the present chapter, the proposed control strategy is applied theoretically and experimentally to a cable structure with one degree of freedom. Next, the decentralized active tendon control strategy is demonstrated numerically on a truss with guy cables. An approximate linear theory leading to a root locus technique for the prediction of the closed-loop poles is also presented; it leads to simple results which can be directly useful in the preliminary design of active cable structures. Finally, a laboratory mock-up is used to demonstrate experimentally the decentralized control of a multimodal structure with several cables; the predictions by the linear approach and the numerical simulations of the nonlinear model (chapter 5) are compared with the experimental results.

6.2 Structure with one degree of freedom

6.2.1 Experimental set-up

In order to test the control strategy for a cable-structure system, the mock-up (Fig.3.1) has been modified in such a way that one end of the cable is connected to a spring-mass system with a tunable natural frequency (Fig.6.2). The modified experimental set-up is represented in Fig.6.3; a shaker and an accelerometer are attached to the spring-mass system to evaluate the performance of the control system.

6.2.2 Governing equations

For the mass-spring system (Fig.6.2), the equation governing the structure dynamics [Equ.(5.21)] becomes

$$M \left(\ddot{q} + 2\xi_s \omega_s \dot{q} + \omega_s^2 q \right) = f - \Gamma_u^T \ddot{z} - \alpha_s^T \ddot{u} + h_u \left(u - q \right) - T_d^{(2)} \qquad (6.1)$$

where q represents the longitudinal displacement of the mass M, $\omega_s = (K/M)^{1/2}$ is the natural frequency and f is the force applied by the shaker to the system. The transfer function between the shaker force and the accelerometer signal (Fig.6.4) shows a good agreement between the numerical simulations and the experimental results.

6.2.3 Control law

The proposed control law is the Integral Force Feedback (4.28). Returning to the equation governing the structure motion, Equ.(6.1), we note that the actuator displacement u appears in the tendon force $T_q = -h_u u$. Using the same energy analysis as for the cable alone (section 4.2), the energy dissipation due to the active tendon control reads
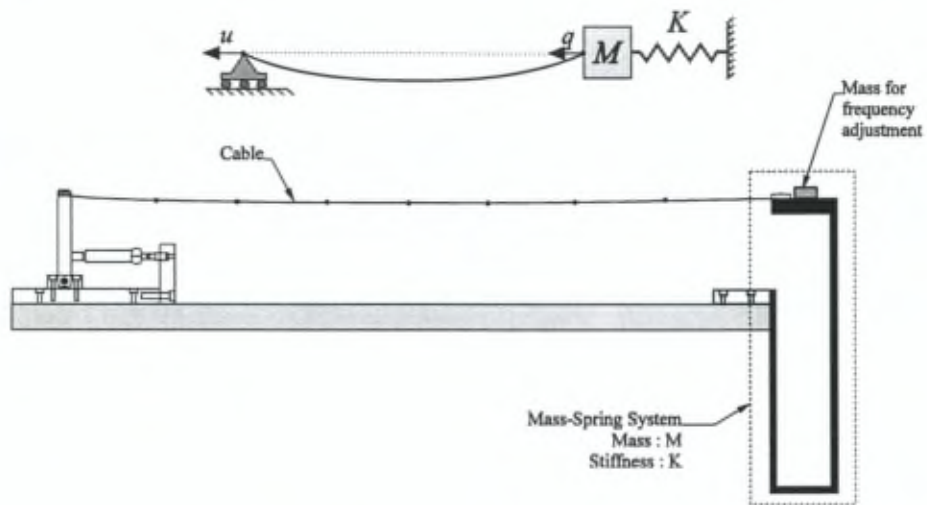
Figure 6.2: Model of the cable structure system.
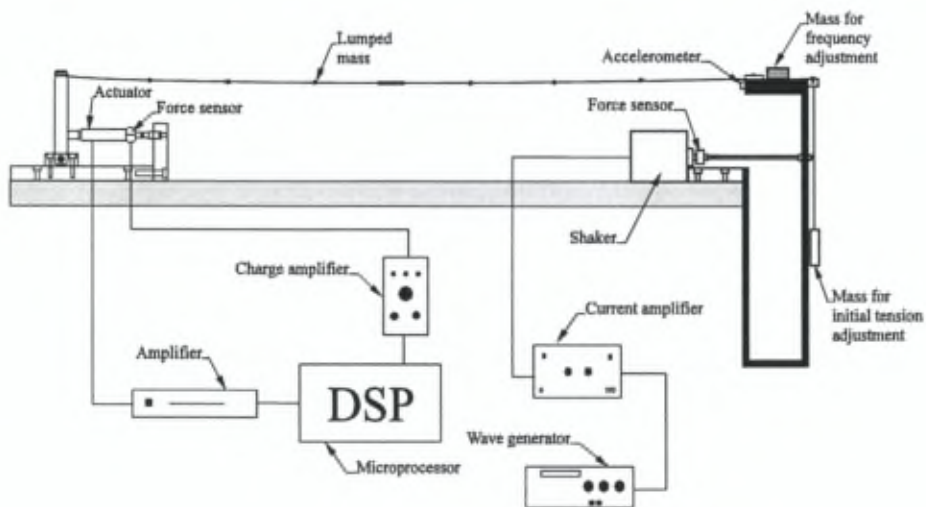
Figure 6.3: Cable structure system experimental set-up.
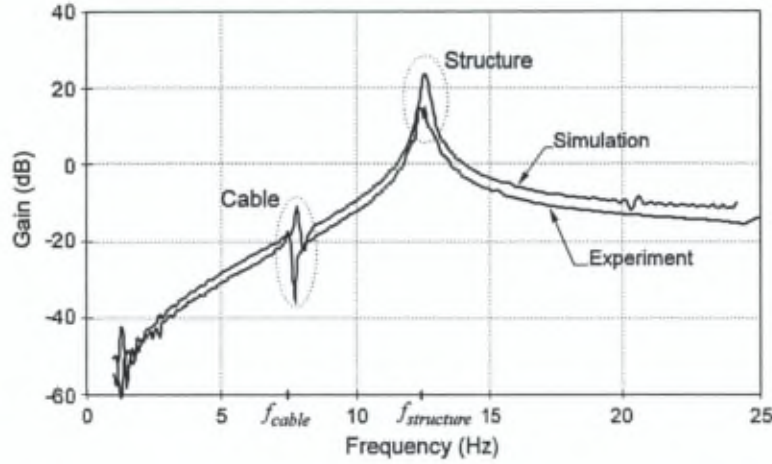
Figure 6.4: Open-loop transfer function between the force applied by the shaker and the acceleration of the mass. Comparison between experiments and simulations.

$$E_p(T_q) = -\int_0^{T_n} T_q \dot{q} dt = \pi h_u a_q^2 \frac{\frac{g h_u}{\omega_s}}{1 + \left(\frac{g h_u}{\omega_s}\right)^2} \tag{6.2}$$

where a_q represents the amplitude of the displacement of the mass M; the equivalent damping introduced by the control in the structure is

$$\xi_s^a = \frac{1}{2} \frac{h_u}{K + h_u} \frac{\frac{g h_u}{\omega_s}}{1 + \left(\frac{g h_u}{\omega_s}\right)^2} \tag{6.3}$$

The maximum damping ξ_s^a due to the active tendon control is achieved when $g h_u / \omega_s = 1$; for this value of the gain, we have

$$\xi_s^a = \frac{1}{4} \frac{h_u}{K + h_u} \tag{6.4}$$

Note that the control acts also through the inertia term $-\alpha_s^T \ddot{u}$, but the corresponding energy dissipation is negligible compared to that of $-h_u u$. Figure 6.5 shows the numerical transfer functions with and without control, when $f_{cable} = f_{z1} = 8$ Hz, $\lambda^2 = 0.15$ and $f_{structure} = f_s = 12.6$ Hz.
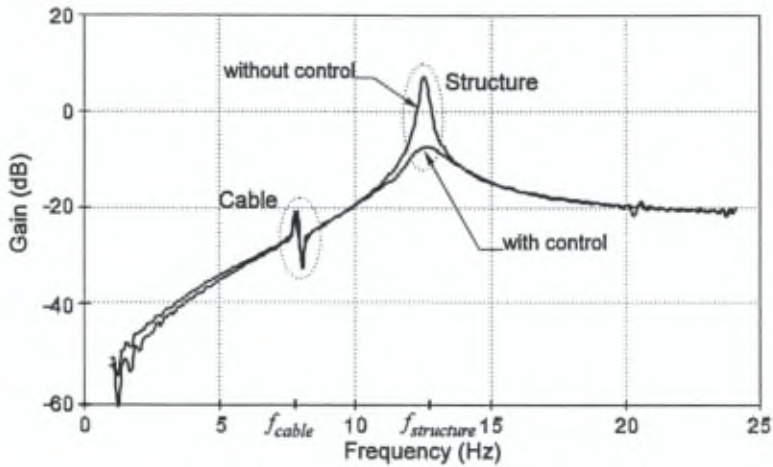
Figure 6.5: Numerical transfer function between the shaker and the accelerometer, with and without control (nonlinear simulation).
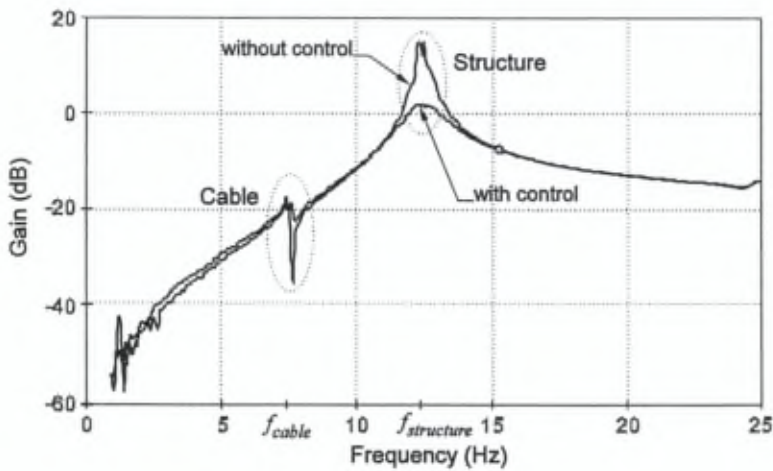
Figure 6.6: Experimental transfer function between the shaker and the accelerometer, with and without control.
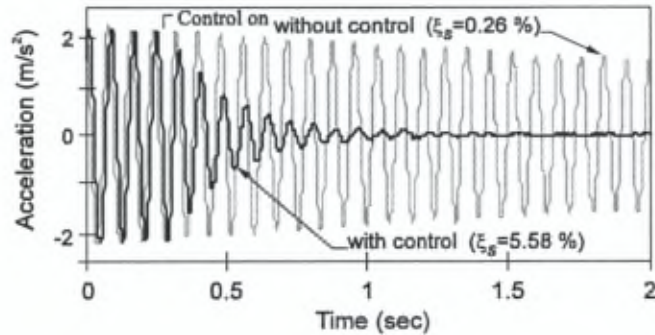
Figure 6.7: Free response of the structure, with and without control.
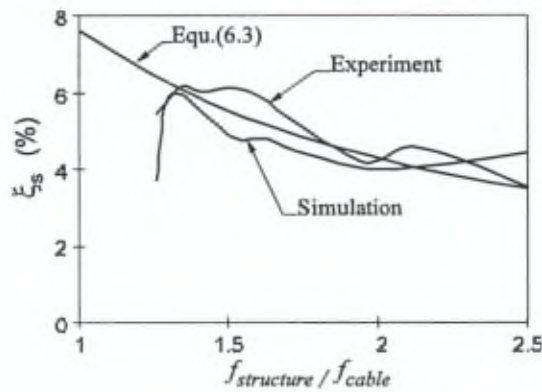
Figure 6.8: Damping ratio of the global mode.

6.2.4 Experimental results

Figure 6.6 compares the transfer functions with and without control, when $f_{cable} = 8$ Hz, $\lambda^2 = 0.15$ and $f_{structure} = 12.6$ Hz. The corresponding time-history of the transient response is shown in Fig.6.7. Figure 6.8 shows the evolution of the active damping with the ratio $f_{cable}/f_{structure}$ when the mass M of the structure is changed for fixed values of the cable sag and the control gain g. The figure includes experimental results, simulations obtained from numerical integration of Equ.(5.25), (5.26) and (6.1) and from the approximate formula Equ.(6.3). We notice that the structure remains nicely actively damped at the parametric resonance, when $f_{structure} = 2f_{cable}$.
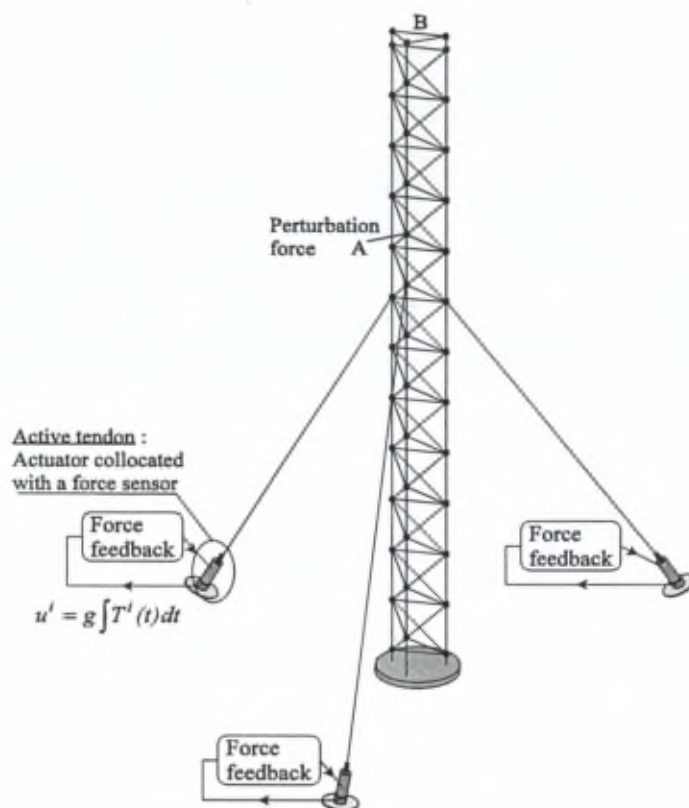
Figure 6.9: Guyed truss.

6.3 Decentralized control with several cables

6.3.1 Truss with guy cables

As an example of application, consider the 12 bay truss with three guy cables of Fig.6.9; the truss alone was already considered in [56] where its active damping was achieved with two active struts located in the first bay starting from the bottom. Here, we investigate the possibility to control the system with three guy cables of 1 mm diameter attached to the truss as indicated on the figure and provided with an active tendon at their base, at a distance of 1 m from the truss; we assume no gravity, so that the cables behave like strings. Without control, the net effect of the cables is to stiffen the truss, raising its natural frequencies; the control system affects both the natural frequencies and the damping of the modes. Figure 6.10 shows the evolution of the resonant peaks of the frequency
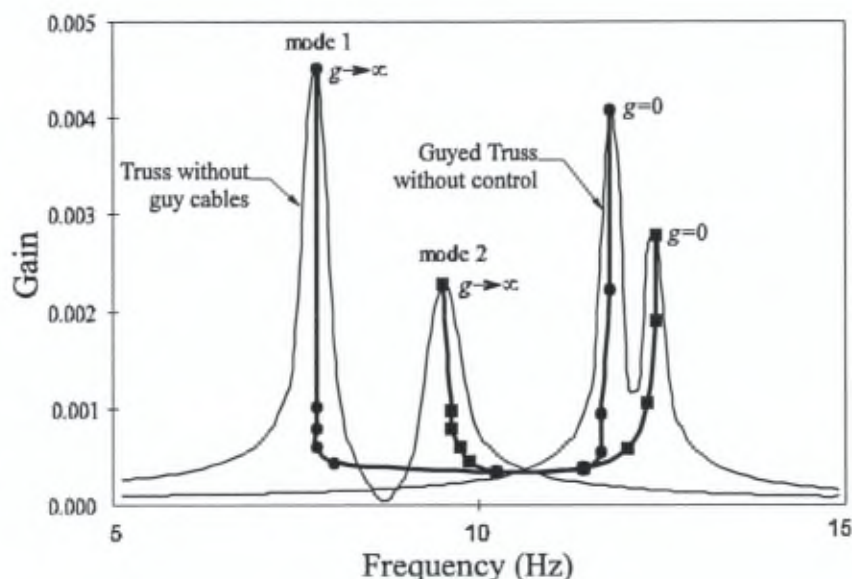
Figure 6.10: Evolution of the resonant peaks of the frequency response between A and B in Fig.6.9 when the control gain g is changed.

response between a point force applied along the truss (A in Fig.6.9) and an accelerometer placed at the top, when the gain g of the control law (4.28) is changed (the same gain is used for every active tendon). These results have been obtained by solving numerically the nonlinear model [Equ.(5.21), (5.25) and (5.26)], taking into account the physical data of the actuators, including their finite stroke. We observe that, when the gain increases, the two resonant peaks drop very quickly, then move horizontally towards the lower frequency and then start to rise again at high gains, to become identical to the resonant peaks of the truss without guy cables. This behaviour is the consequence of the well known fact that when we increase the gain, the closed-loop poles start from the open-loop poles and move towards the open-loop zeros. Since the zeros are, by definition, the frequencies of the input (the voltage at the piezo) where the output (the cable tension) vanishes, the tension in the cables becomes equal to zero and the guyed truss behaves like the free one.

6.3.2 Approximate linear theory

In a situation like the one described in the previous section, the cables are extremely light and behave essentially like strings. If we assume that the inter-action between the structure and the active cables is restricted to the tension

in the cables and if one neglects the cable dynamics, the governing equation is

$$M\ddot{x} + Kx = -BT \tag{6.5}$$

where K refers to the structure without guy cables, T is the vector of tension in the guy cables and B is the influence matrix. If we neglect the cable dynamics, the tension in the cables is given by,

$$T = K_c \left(B^T x - \delta \right) \tag{6.6}$$

where K_c is the stiffness matrix of the cables, $K_c = diag(h_u)$, $B^T x$ are the relative displacements of the extremities of the cables and δ the active displacements of the tendons. Combining Equ.(6.5) and (6.6), we get

$$M\ddot{x} + (K + BK_c B^T)x = -BK_c\delta \tag{6.7}$$

which indicates that $K + BK_c B^T$ is the stiffness matrix of the structure with guy cables. We assume that all the guy cables have the same control law with the same gain in Laplace form,

$$\delta = \frac{g}{sh_u}T \tag{6.8}$$

Combining with Equ.(6.6), we have

$$\delta = \frac{g}{s+g}B^T x \tag{6.9}$$

Laplace transforming Equ.(6.7) and substituting Equ.(6.9), we obtain the closed-loop equation

$$\left[Ms^2 + (K + BK_c B^T) - \frac{g}{s+g}BK_c B^T \right] x = 0 \tag{6.10}$$

From this equation, it is readily observed that as $g \to \infty$, the dynamics of the closed-loop system converges towards that of the structure without cables, as we observed in the numerical experiment of the previous section. Let us project Equ.(6.10) on the normal modes $x = \Phi z$ of the structure with cables, assumed normalized according to $\Phi^T M \Phi = I$. If we denote $\Omega^2 = \Phi^T(K + BK_c B^T)\Phi$, Equ.(6.10) becomes

$$\left[s^2 + \Omega^2 - \frac{g}{s+g}\Phi^T BK_c B^T \Phi \right] z = 0 \tag{6.11}$$

To derive a simple and powerful result about the way each mode evolves with g, let us assume that the mode shapes are little changed by the active cables, so that we can write

$$\Omega^2 = \Phi^T \left(K + BK_c B^T \right) \Phi = \Phi^T K \Phi + \Phi^T BK_c B^T \Phi = \omega^2 + \nu^2 \tag{6.12}$$
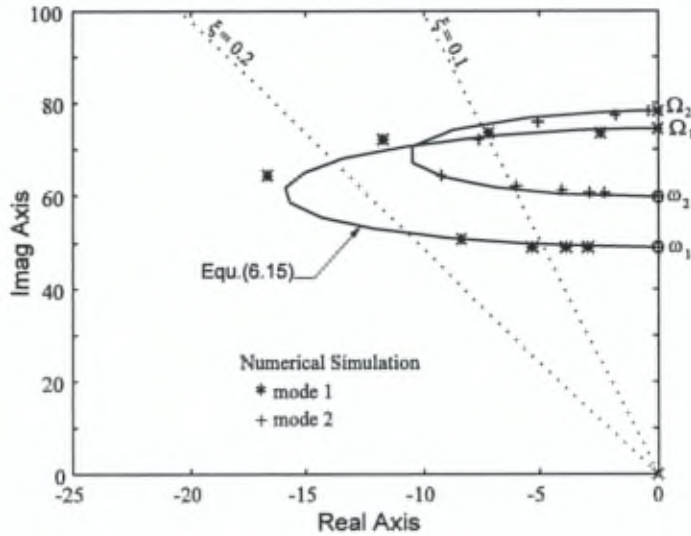
Figure 6.11: Comparison of the root locus with the numerical simulation.

where the two matrices ω^2 and ν^2 are also diagonal. This hypothesis is identical to that made to derive Jacobi's eigenvalue perturbation formula [4]. In this case, $\omega^2 = \Phi^T K \Phi$ contains the square of the natural frequencies of the structure without the active cables. Substituting Equ.(6.12) into Equ.(6.11), we obtain a set of decoupled equations; the characteristic equation for mode i is

$$s^2 + \Omega_i^2 - \frac{g}{s+g}\left(\Omega_i^2 - \omega_i^2\right) = 0 \tag{6.13}$$

or

$$s\left(s^2 + \Omega_i^2\right) + g\left(s^2 + \omega_i^2\right) = 0 \tag{6.14}$$

This equation shows that the poles go from $\pm j\Omega_i$ for $g = 0$ to $\pm j\omega_i$ for $g \to \infty$ (as we have already seen) and that, in between, they follow the root locus corresponding to the open-loop transfer function

$$G(s) = g\frac{s^2 + \omega_i^2}{s(s^2 + \Omega_i^2)} \tag{6.15}$$

where the poles and the zeros correspond to the natural frequencies of the structure with and without the active cables, respectively.

Figure 6.11 compares the prediction of the foregoing linear theory with the numerical experiment performed with the full model already reported in Fig.6.10; we see that the agreement is quite good.

According to the foregoing discussion, if a cable structure has a set of active cables which are such that the mode shapes of the structure, with and without the active cables, are not significantly different, every closed-loop pole corresponding to the decentralized integral force feedback follows the root locus defined by Equ.(6.15), where Ω_i is the natural frequency of the structure with the active cables and ω_i that of the structure without the active cables (but including the passive ones if any). The maximum value of the modal damping ξ_i can be evaluated with a perturbation method : if we substitute $s = \Omega_i[-\xi_i + j(1+\zeta_i)]$ in Equ.(6.14) and neglect the second order terms in ξ_i and ζ_i, we find easily

$$\xi_i = \frac{g(\Omega_i^2 - \omega_i^2)}{2\Omega_i(\Omega_i^2 + g^2)} \tag{6.16}$$

$$\zeta_i = -\frac{g\xi_i}{\Omega_i} \tag{6.17}$$

From Equ.(6.16), the maximum modal damping is achieved for $g^* = \Omega_i$; we find

$$\xi_i^{max} = \frac{\Omega_i^2 - \omega_i^2}{4\Omega_i^2} \tag{6.18}$$

If we assume that $\Omega_i + \omega_i \approx 2\Omega_i$, this result can be further simplified into

$$\xi_i^{max} = \frac{\Omega_i - \omega_i}{2\Omega_i} \tag{6.19}$$

Thus, the maximum modal damping is controlled by the relative spacing of the natural frequencies, with and without the active cables. This result provides a simple rationale for selecting the number, the size and the location of the active cables in the first step of the design process.

6.3.3   Experimental results

In order to validate the foregoing theoretical results of the decentralized Integral Force Feedback, a laboratory mock-up representative of a very simple scale model of a cable-stayed bridge has been constructed (Fig.6.12). The structure is designed in such a way that its behaviour is dominated by a bending mode and a torsion mode (representative of bridge deck first modes). The natural frequency can be adjusted by variable masses. The structure is supplemented by two cables connected to piezoelectric active tendons where the decentralized active damping (IFF) is applied. A shaker and an accelerometer are placed on the structure to evaluate the performances of the control system. The structure masses are chosen in such a way that without cables the frequencies of the bending and torsion modes are respectively $\omega_b = 55$ rad/sec and $\omega_t = 75$ rad/sec. When the active cables are connected to the structure, the stiffness effect increases the modal frequencies to $\Omega_b = 75$ rad/sec and $\Omega_t = 88$ rad/sec.

Decentralized Active Tendon Control
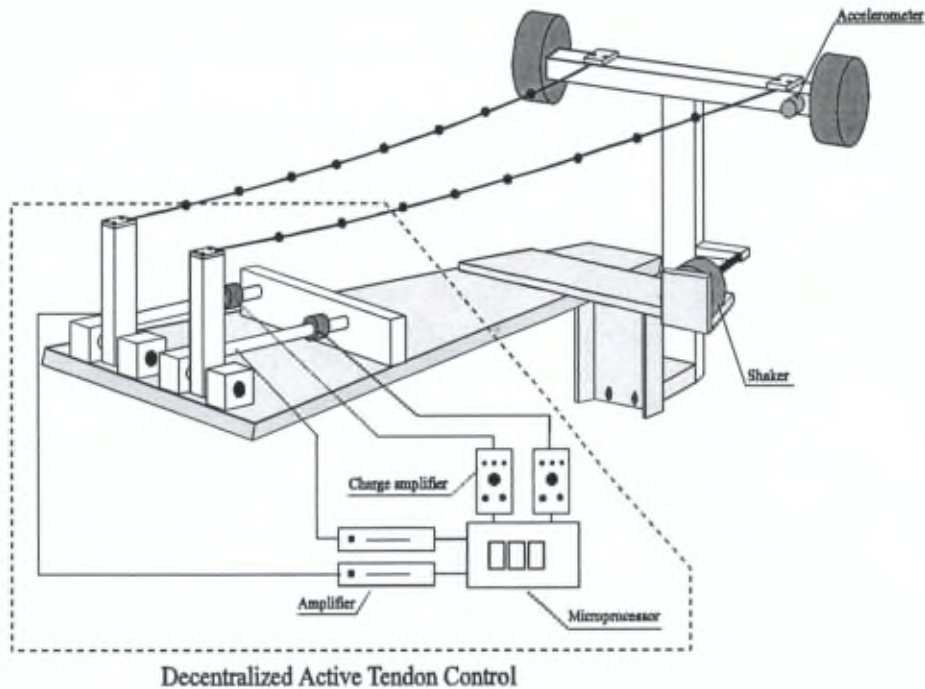
Figure 6.12: Decentralized control of structures with several cables.

The IFF control algorithm is implemented independently in each tendon (i.e. decentralized control) with the same gain g.

Figure 6.13 compares the root locus of the closed-loop poles obtained from the prediction of the linear theory, Equ.(6.15), with those obtained with a numerical simulation performed with the full nonlinear model Equ.(5.21), (5.25), (5.26), and also the experimental results. We note that, for large values of the gain g the experimental root locus converges towards a higher frequency than that of the structure alone (without active cables). This discrepancy is due to the dynamics of the lever system used to amplify the actuator stroke as explained in the next section.

Figure 6.14 shows the transfer function between the shaker force and the accelerometer, with and without the decentralized Integral Force Feedback. The corresponding free response of the structure is shown in Fig.6.15; we observe a beating due to the nearness between the bending and the torsion modes. The maximum damping ratio of 8% and 5% for the bending and the torsion mode respectively are achieved for the same gain g. In order to validate Equ.(6.19) which states that the maximum modal damping is controlled by the relative spacing of the natural frequencies, with and without active cables, the frequency
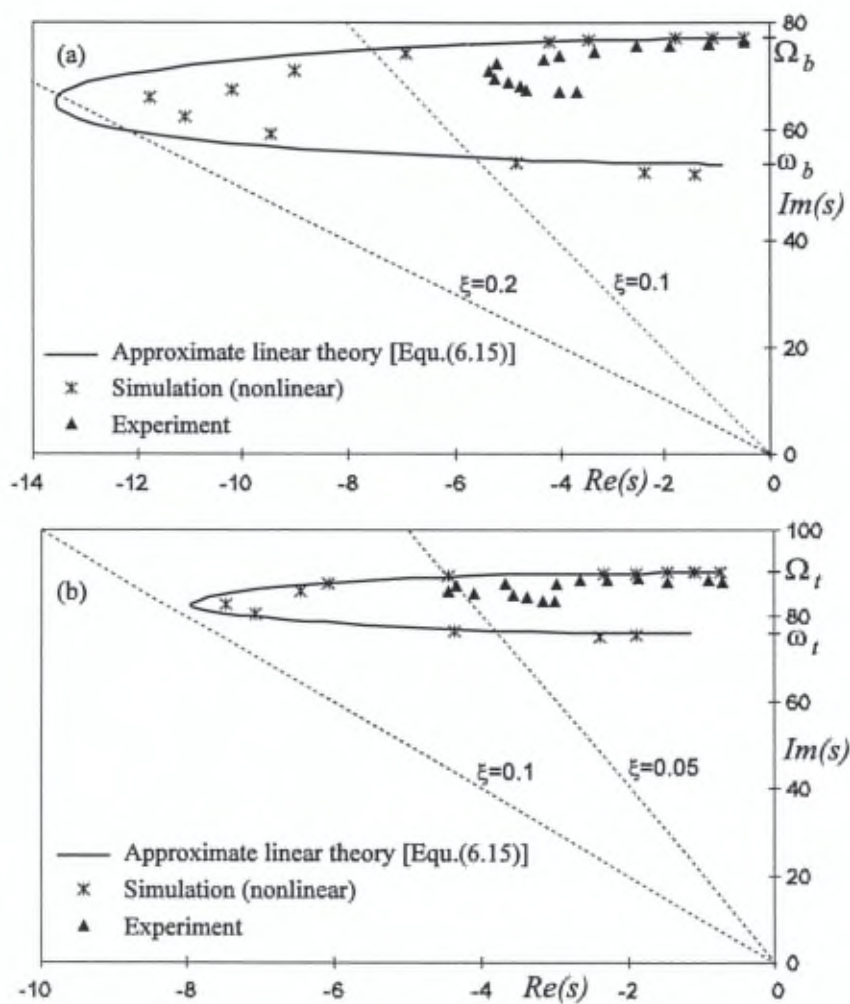
Figure 6.13: Comparison of the experimental root locus with the linear prediction and the numerical simulation : (a) bending mode (b) torsion mode.
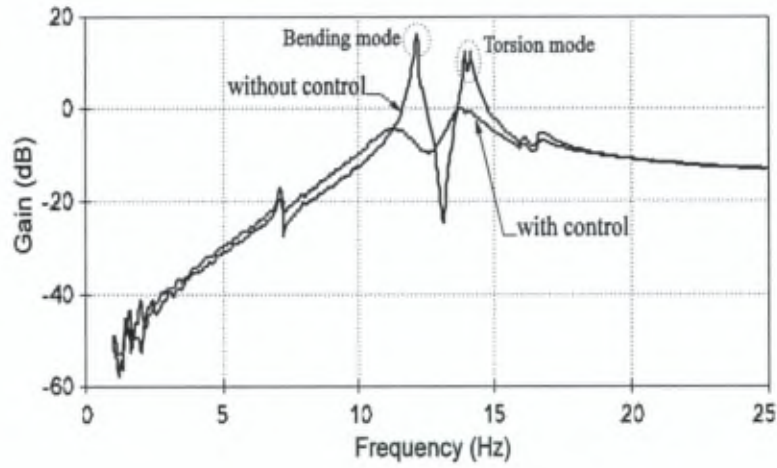
Figure 6.14: Experimental transfer function between the shaker and the accelerometer, with and without control.
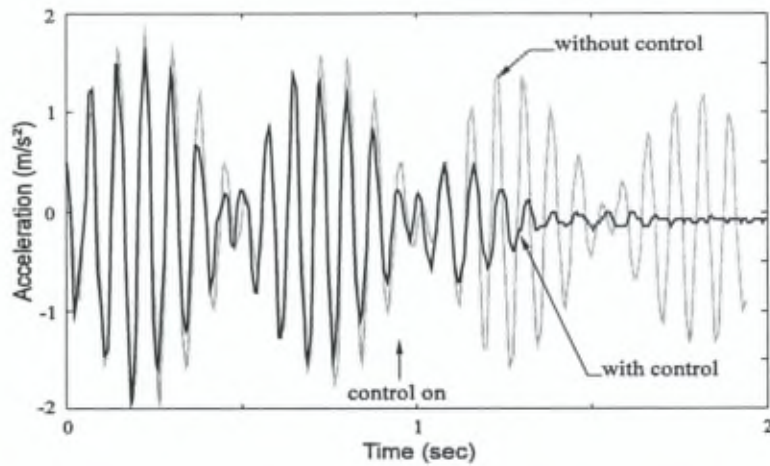
Figure 6.15: Experimental free response of the structure, with and without control.
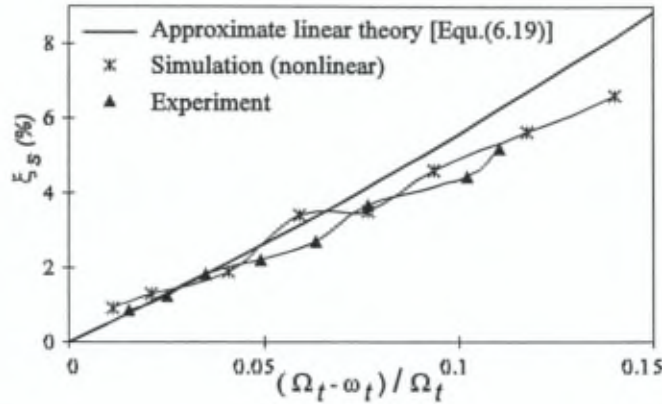
Figure 6.16: Dependance between the damping ratio and $(\Omega_t - \omega_t)/\Omega_t$ for the torsion mode.

of the torsion mode Ω_t has been varied by changing the cable anchor location on the structure, to increase the distance to the torsion axis. Figure 6.16 compares the experimental maximum damping ratio of the torsion mode with the values predicted by the approximate relation (6.19) and also with the numerical simulations of the full model; the agreement is quite good.

6.4   Influence of the lever system

Consider the linear model of the cable structure with one degree of freedom (Fig.6.2) including the model of the lever system as indicated in Fig.(6.17). The structure is described by its mass M and its stiffness K; the cable stiffness is h_u; I_θ is the moment of inertia of the lever. K_a denotes the tendon stiffness and K_θ represents the stiffness of the non ideal rotational joint.

The potential energy of this system is

$$\mathcal{V}^* = \frac{K}{2}x^2 + \frac{h_u}{2}(r\theta - x)^2 + \frac{K_a}{2}(\delta_d - b\theta)^2 + \frac{K_\theta}{2}\theta^2 \tag{6.20}$$

and the kinetic energy reads

$$\mathcal{T} = \frac{M}{2}\dot{x}^2 + \frac{I_\theta}{2}\dot{\theta}^2 \tag{6.21}$$

where x denotes the absolute displacement of the structure, and θ the small angle of the lever, induced by the small actuator stroke ($\pm 22\mu$m). Applying the Lagrange equations to the undamped system, we easily find the equations governing its dynamics; we get
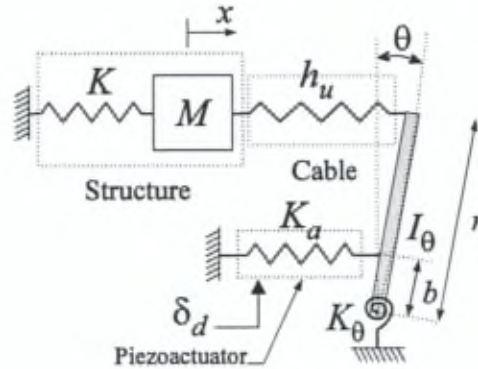
Figure 6.17: Model of the cable structure system including the lever mechanism.

$$M\ddot{x} + (K + h_u)x - rh_u\theta = 0$$
$$I_\theta\ddot{\theta} + (K_\theta + r^2 h_u + b^2 K_a)\theta - rh_u x = bK_a\delta_d \qquad (6.22)$$

The input of the system is the actuator displacement δ_d and the output is the force measured in the active tendon

$$F = K_a(\delta_d - b\theta) \qquad (6.23)$$

Figure 6.18 represents the frequency response functions between δ_d and F for several values of the stiffness K_θ, while the values of the other parameters are representative of the real system. One observes that, as the stiffness K_θ is increased from $K_\theta = 0$, the frequency of the zero moves from the natural frequency of the structure alone $\omega_s = (K/M)^{1/2}$ towards the natural frequency of the cable structure $\Omega_s = [(K + h_u)/M]^{1/2}$. This result has been verified using various lever mechanisms with different values of the stiffness K_θ. Thus, returning to the prediction of the maximum damping ratio Equ.(6.19), one concludes that the control authority decreases with the imperfections of the lever rotational joint.

6.5   Conclusion

The energy absorbing and guaranteed stability properties of the Integral Force Feedback have been proved on a cable structure system for a wide variety of operating conditions. The experimental results and the numerical simulations from the full nonlinear model are in good agreement. Moreover, in the particular case where the structure frequency is twice the cable frequency, we have verified
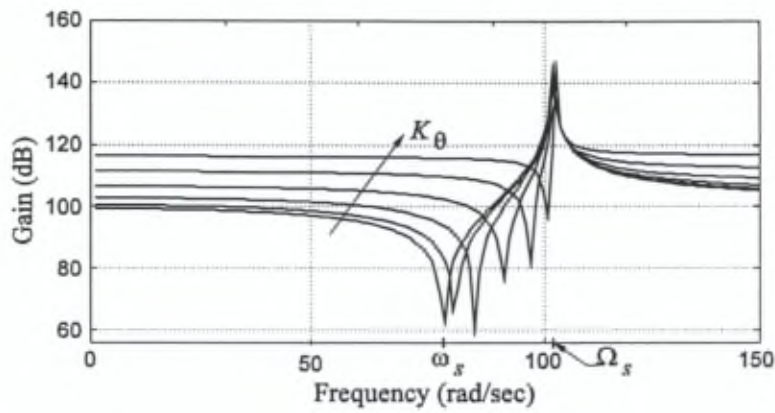
Figure 6.18: Transfer function between the force F measured in the tendon and the desired displacement δ_d of the actuator, for several values of K_θ.

that the cable structure is actively damped and that the parametric excitation of the cable does not occur. Simple and powerful results have been established, which allow one to predict the closed-loop poles with a root locus technique.

Chapter 7

Flutter control of cable-stayed bridges

7.1 Introduction

Under the excitation of strong wind gusts, a flexible suspension bridge may vibrate with large amplitudes, and instability may occur when the mean wind velocity reaches a critical level, referred to as the *critical flutter speed*. This aeroelastic mechanism termed *flutter* is attributed to a vortex type excitation which is coupled with the motion of the bridge and generates self-excited aerodynamic forces. If the wind velocity increases beyond the critical flutter speed the resulting aerodynamic force will amplify the motion and the instability of the torsion modes arises [7, 13, 21]. On several occasions some suspended bridges have suffered serious damage or even complete destruction under wind, as the Tacoma Narrows disaster of 1940 (Fig.7.1). The classical flutter theory of thin airfoils has been well verified experimentally using wind tunnel tests, but it cannot be applied directly to bridges. The extensive work of Scanlan provides experimentally valuable information on the aeroelastic behavior of many types of bridge decks [62]. In this chapter, the flutter analysis applied to the classical case of a thin airfoil is reviewed; the equations governing the motion of the airfoil are discussed and the flutter mechanism is investigated using a root locus technique. However, the theoretical aerodynamic formulation for airfoil flutter is not directly transferable to bridges, as we will see. The approach based on experimental wind tunnel tests proposed by Scanlan is sufficient to predict the flutter instability, but is not enough for the design of a control system for flutter suppression.

The second part of this chapter presents the application of the decentralized active tendon strategy to the control of the torsional flutter of cable-stayed bridges. For the experimental demonstration on a laboratory mock-up, the flut-
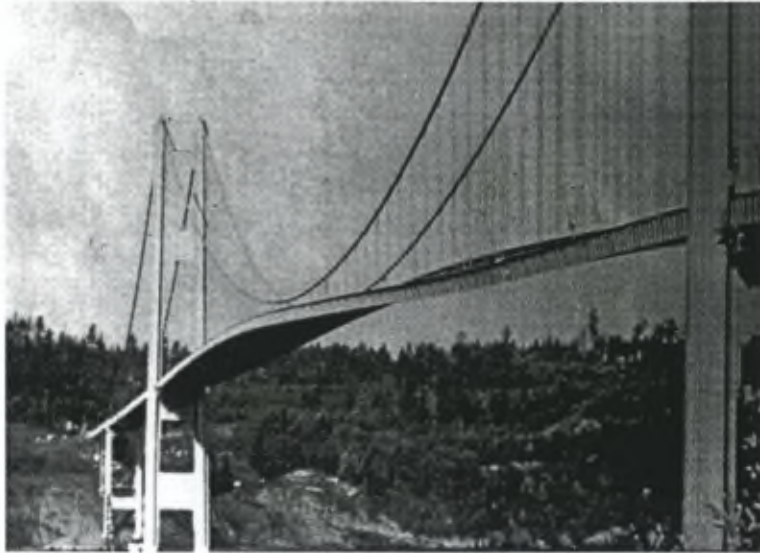
Figure 7.1: Flutter of the Tacoma Narrows bridge in 1940.

ter is mechanically simulated by a control system which becomes unstable as the gain goes beyond some critical value.

7.2 Flutter analysis of a thin flat plate

7.2.1 Aerodynamic forces and moments

Let us consider a strip of unit width of a two dimensional flat plate airfoil (Fig.7.2) having two degrees of freedom : a bending h (positive downward measured at the elastic axis) and a pitching α (positive nose-up) about the elastic axis. Let the plate be situated in a flow of incompressible fluid at speed U, and consider its unsteady motion. The angle of attack α is assumed infinitesimal. The vertical velocity called the downwash at the 3/4 chord point, due to the vertical and pitching motion, is expressed as a function of the reduced time $\tau = Ut/b$ which represents the distance travelled by the wind in semichords b; we have

$$w(\tau) = U\left[\alpha(\tau) + \frac{1}{b}h'(\tau) + \left(\frac{1}{2} - a_h\right)\alpha'(\tau)\right] \qquad (7.1)$$

The prime denotes the derivatives with respect to the reduced time τ. The first term is the downwash corresponding to the pitching angle α. The component
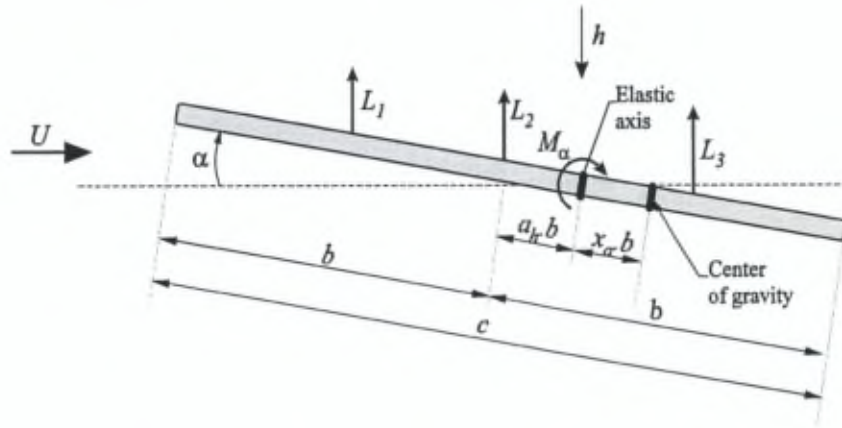
Figure 7.2: The two-dimensional flat-plate airfoil.

Uh'/b is due to translation velocity and the third one is the downwash due to the rotation velocity about the elastic axis. The unsteady aerodynamic forces acting on a thin airfoil in motion in a two-dimensional incompressible fluid was obtained by Wagner, Von Karman and others [21]. Wagner's function $\phi(\tau)$ gives the growth of circulation about the airfoil due to a sudden increase of downwash which is uniform along the airfoil. This lift is given by

$$L_1(\tau) = 2\pi\rho bU \left[w(0)\phi(\tau) + \int_0^\tau \phi(\tau-\sigma)\frac{dw}{d\sigma}d\sigma \right] \quad \text{for} \quad \tau \geq \sigma \qquad (7.2)$$

It can be shown that this force acts at 1/4 chord on the airfoil and thus is also responsible of a torque. An approximate expression of the Wagner function (Fig.7.3) is

$$\phi(\tau) = 1 - 0.165e^{-0.0455\tau} - 0.335e^{-0.3\tau} \quad \text{for} \quad \tau \geq 0 \qquad (7.3)$$

When the airfoil has a general motion, the lift and moment of the non circulatory origin must be added; they consist of the following contributions :

- A lift force with center of pressure at mid chord, equal to the apparent mass $m_a = \rho\pi b^2$ times the vertical acceleration at the mid-chord point

$$L_2 = \rho\pi U^2 \left[h'' - a_h b\alpha'' \right] \qquad (7.4)$$

- A lift force with center of pressure at 3/4 chord, of the nature of a centrifugal force, equal to the apparent mass m_a times $U^2\alpha'/b$
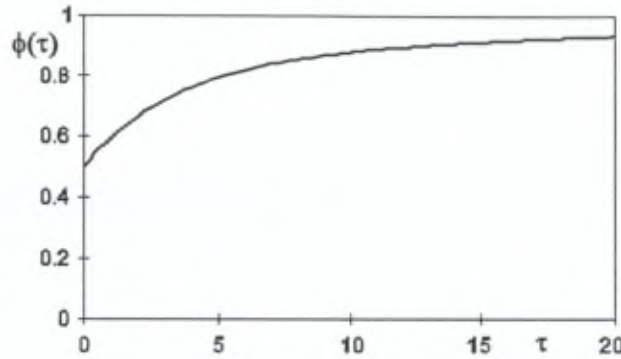
Figure 7.3: Wagner's function for an incompressible fluid.

$$L_3 = \rho \pi b U^2 \alpha' \tag{7.5}$$

- A nose down torque equal to the apparent moment of inertia $m_a b^2 / 8$ times the angular acceleration,

$$M_a = -\frac{\rho \pi b^2 U^2}{8} \alpha'' \tag{7.6}$$

Thus, the resultant lift per unit span is

$$L_h = L_1 + L_2 + L_3 \tag{7.7}$$

and the resultant moment per unit span about the elastic axis reads

$$M_\alpha = \left(\frac{1}{2} + a_h \right) b L_1 + a_h b L_2 - \left(\frac{1}{2} - a_h \right) b L_3 + M_a \tag{7.8}$$

7.2.2 Equations of motion

Let the bending and pitching displacements be resisted by a pair of springs at the elastic axis with stiffnesses K_h and K_α as indicated in Fig.7.4. The equations governing the vertical and rotational motion of the flat-plate airfoil are as follows,

$$m \left(\ddot{h} + 2\xi_h \omega_h \dot{h} + \omega_h^2 h \right) + S\ddot{\alpha} = -L_h(t) + p(t)$$
$$I_\alpha \left(\ddot{\alpha} + 2\xi_\alpha \omega_\alpha \dot{\alpha} + \omega_\alpha^2 \alpha \right) + S\ddot{h} = M_\alpha(t) + q(t) \tag{7.9}$$

where m denotes the total mass of the plate per unit span, I_α is the mass moment of inertia and $S = mbx_a$ is the static moment, both taken about the elastic
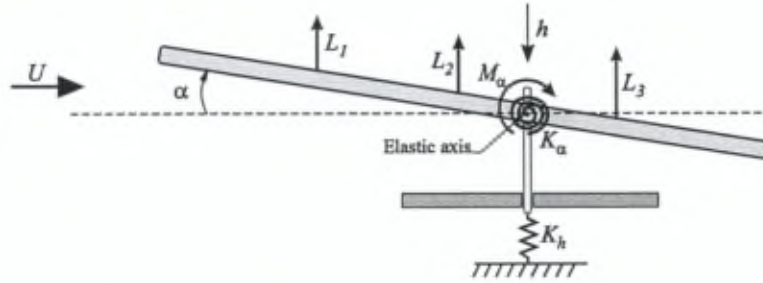
Figure 7.4: Unsteady motion of a flat-plate airfoil.

axis. $\omega_h = (K_h/m)^{1/2}$, $\omega_\alpha = (K_\alpha/I_\alpha)^{1/2}$ are the natural frequencies in bending and torsion, respectively, and ξ_h and ξ_α denote the structural damping ratios. $L_h(t)$ and $M_\alpha(t)$ are the resultant lift and moment and $p(t)$ and $q(t)$ denote the external applied force and moment. The distance bx_a appearing in the static moment is that between the elastic axis and the center of mass, positive when the center of mass is behind the elastic axis. We note that the bending and torsion are coupled by the inertia terms $S\ddot\alpha$, $S\ddot h$ and the aerodynamic forces L_h and M_α. Introducing the reduced time τ in Equ.(7.9) we have

$$m\left(h'' + 2\xi_h\omega_h^* h' + \omega_h^{*2}h\right) + S\alpha'' = \left(\frac{b}{U}\right)^2 \left[-L_h(\tau) + p(\tau)\right]$$

$$I_\alpha\left(\alpha'' + 2\xi_\alpha\omega_\alpha^* \alpha' + \omega_\alpha^{*2}\alpha\right) + Sh'' = \left(\frac{b}{U}\right)^2 \left[M_\alpha(\tau) + q(\tau)\right] \quad (7.10)$$

where $\omega_h^* = b\omega_h/U$ and $\omega_\alpha^* = b\omega_\alpha/U$ represent the reduced frequency of the bending and torsion respectively.

7.2.3 Stability of the oscillating airfoil

The method of Laplace transform can be applied to study the stability of the oscillating airfoil. Upon substituting Equ.(7.7) and (7.8) into Equ.(7.10) and Laplace transforming, assuming that $h(0) = \dot h(0) = \alpha(0) = \dot\alpha(0) = 0$, we obtain

$$\left(\begin{array}{cc} G_{11}(s) & G_{12}(s) \\ G_{21}(s) & G_{22}(s) \end{array}\right)\left(\begin{array}{c} H(s) \\ A(s) \end{array}\right) = \left(\begin{array}{c} P(s) \\ Q(s) \end{array}\right) \quad (7.11)$$

where $H(s)$, $A(s)$, $P(s)$ and $Q(s)$ are the Laplace transforms of $h(t)$, $\alpha(t)$, $p(t)$ and $q(t)$, respectively, and

$$G_{11}(s) = \left[m + m_a + 2\pi \rho b U \Phi(s) \right] s^2 + 2m\xi_h \omega_h s + m\omega_h^2$$

$$G_{12}(s) = \left[S - a_h b m_a + 2\pi \rho b^2 U \left(\tfrac{1}{2} - a_h \right) \Phi(s) \right] s^2 + \left[m_a U + 2\pi \rho b U^2 \Phi(s) \right] s$$

$$G_{21}(s) = \left[S - a_h b m_a + 2\pi \rho b^2 U \left(\tfrac{1}{2} + a_h \right) \Phi(s) \right] s^2$$

$$G_{22}(s) = \begin{aligned} &\left[I_\alpha + m_a \left(a_h b \right)^2 + m_a \tfrac{b^2}{8} - 2\pi \rho b^3 U \left(\tfrac{1}{4} - a_h^2 \right) \Phi(s) \right] s^2 \\ &+ \left[2 I_\alpha \xi_\alpha \omega_\alpha - 2\pi \rho b^2 U^2 \left(\tfrac{1}{2} + a_h \right) \Phi(s) + m_a \left(\tfrac{1}{2} - a_h \right) b U \right] s \\ &+ I_\alpha \omega_\alpha^2 \end{aligned}$$

$$(7.12)$$

It can be shown [21] that the Laplace transform $\Phi(s)$ of the Wagner function $\phi(\tau)$ can be expressed in terms of the Theodorsen function $C(k)$ by replacing the reduced frequency $k = \omega b / U$ by $-js$ and multiplying by the Laplace transform of the step function $(1/s)$:

$$\Phi(s) = \int_0^\infty \phi(\tau) e^{-s\tau} d\tau = \frac{C(-js)}{s} = \frac{F(-js) + jG(-js)}{s} \qquad (7.13)$$

In classical aeroelasticity, the tabulated values of the real and imaginary parts (F and G) of the Theodorsen function $C(k)$ are used to determine the critical flutter speed. A root locus technique is more appropriate because it allows to evaluate the damping of the bending and the torsion modes when the velocity of the flow varies. A polynomial form of $\Phi(s)$ can be derived from Equ.(7.3),

$$\Phi(s) = \frac{1}{s} - \frac{0.165}{s + 0.0455} - \frac{0.335}{s + 0.3} \qquad (7.14)$$

The stability of the system can be assessed by tracking the evolution of the poles when the flow velocity U varies. They are the solution of the characteristic equation :

$$\Delta(s) = \begin{vmatrix} G_{11} & G_{12} \\ G_{21} & G_{22} \end{vmatrix} = 0 \qquad (7.15)$$

The critical flutter speed is that for which one branch of the root locus enters the right half plane. To illustrate the approach, consider the flat-plate airfoil with the following characteristics [21],

$$b = 0.291 \text{ (m)}, \ m = 3.261 \text{ (kg/m)}, \ S = 0.09489 \text{ (kg)}, \ a_h = -0.2$$

$$I_\alpha = 0.069 \text{ (kgm)}, \ \omega_\alpha = 75.39 \text{ (rad/s)}, \ \omega_h = \omega_\alpha / 5.$$
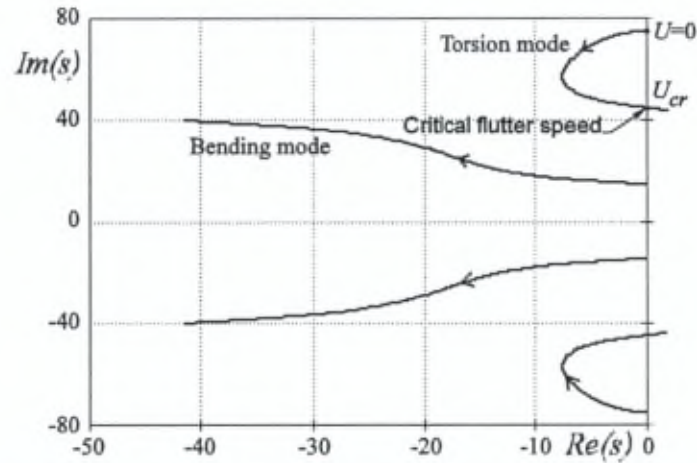
Figure 7.5: Root locus of the airfoil system when the flow velocity U varies.
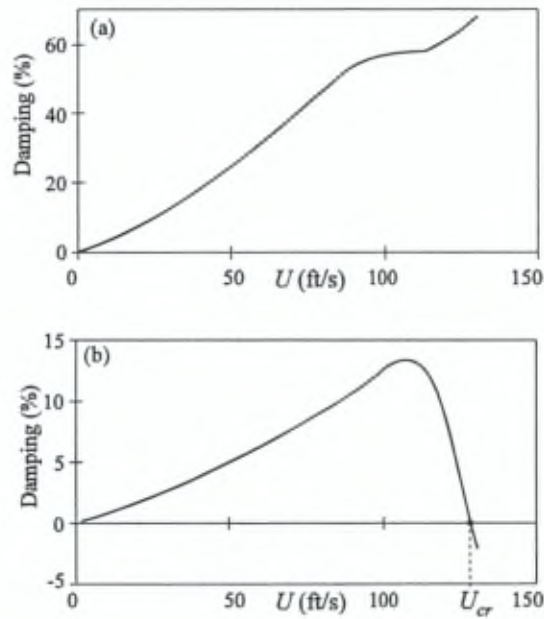
Figure 7.6: Damping ratio as a function of the flow speed U :
(a) bending mode (b) torsion mode.

Figure 7.5 shows the root locus of the bending and torsion poles as a function of the flow speed U; Fig.7.6 represents, the corresponding damping ratio of each mode. We see that, when the velocity of the flow gradually increases the rate of damping of the torsion mode first increases; if U increases further, a point is reached at which the damping rapidly decreases. At the critical flutter speed, the locus of the torsion mode crosses the imaginary axis which corresponds to a zero damping ratio. Beyond this critical value, the instability of the torsional mode occurs. The flutter theory applied to thin airfoils [21] shows that flutter instability will occur only if a coupling between the bending and the torsion mode exists. These analytical results are in good agreement with the experiments performed in wind tunnels [62]. Numerous studies [13, 61, 62] have, however, pointed out the dissimilarity between airfoil and bridge deck flutter mechanisms.

7.3   Unsteady aerodynamics of a bridge deck

It is a common practice to study the flutter susceptibility of a suspended bridge deck by creating a reduced-scale, geometrically faithful model of a typical section of the deck and suspending it from springs for wind tunnel testing [62]. For the harmonic oscillations of a bridge deck cross-section, Scanlan has postulated the following linear form of the resulting lift and moment :

$$
L_h = \frac{1}{2}\rho U^2 B \left[K H_1^*(K)\frac{\dot{h}}{U} + K H_2^*(K)\frac{B\dot{\alpha}}{U} + K^2 H_3^*(K)\alpha \right]
$$

$$
M_\alpha = \frac{1}{2}\rho U^2 B^2 \left[K A_1^*(K)\frac{\dot{h}}{U} + K A_2^*(K)\frac{B\dot{\alpha}}{U} + K^2 A_3^*(K)\alpha \right]
$$

(7.16)

The nondimensional coefficients H_i^* and A_i^*, termed "flutter derivatives", are to be determined experimentally. These flutter coefficients are, as in classical flutter, expected to be functions of the reduced frequency $K = B\omega/U$ where ω is the circular frequency of the oscillations and $B = 2b$ is the full deck width. To demonstrate the link of the present formulation to the airfoil flutter theory, it has been shown [62] that the set of H_i^*, A_i^*, when written for the classical case of a thin airfoil, has the following analytical expressions,

$$
\begin{aligned}
kH_1^*(k) &= -\pi F(k) \\
kH_2^*(k) &= -\tfrac{\pi}{4}\left[1 + F(k) + \tfrac{2}{k}G(k)\right] \\
k^2 H_3^*(k) &= -\tfrac{\pi}{2}\left[F(k) - \tfrac{k}{2}G(k)\right]
\end{aligned}
$$

(7.17)

and
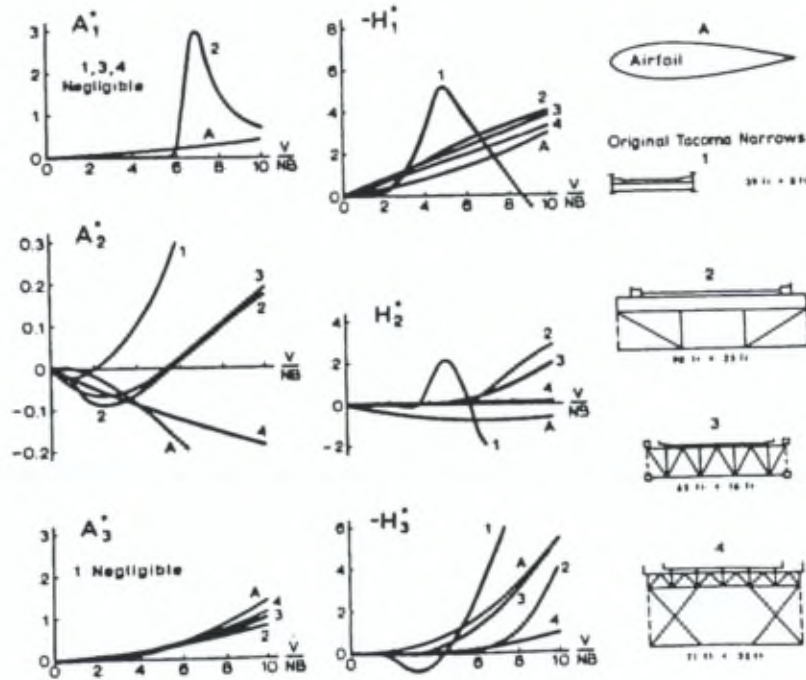
Figure 7.7: Aerodynamic derivatives for airfoil and various bridge deck sections (after Scanlan).

$$kA_1^*(k) = \tfrac{\pi}{4}F(k)$$
$$kA_2^*(k) = -\tfrac{\pi}{16}\left[1 - F(k) - \tfrac{2}{k}G(k)\right] \qquad (7.18)$$
$$k^2 A_3^*(k) = \tfrac{\pi}{8}\left[F(k) - \tfrac{k}{2}G(k)\right]$$

where F and G are respectively, the real and imaginary parts of the Theodorsen function $C(k)$, with $k = K/2$. It may be observed that, for the airfoil, the damping derivatives kH_1^* and kA_2^* remain negative for all values of k, which means that for individual motion h or α, the wind contributes positively to the damping in the deck, and thus no instability can be observed without coupling. By contrast to the case of the thin airfoil, all the values H_i^* and A_i^* for the bridge decks must be obtained from experiments. Figure 7.7 shows the values of the flutter derivatives for an airfoil, the original Tacoma Narrows deck, and three truss-stiffened bridge decks. Overall, the most important difference between airfoil and bridge deck results is revealed by the coefficient A_2^*, which, while differing among bridges, differs always more drastically with A_2^* for the airfoil.
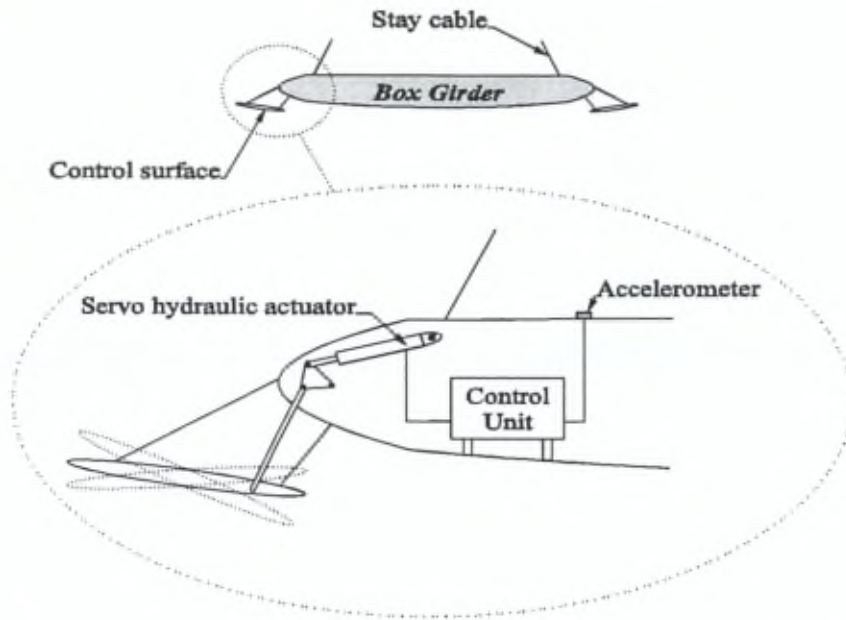
Figure 7.8: Active control surface system in streamlined bridge girder.

The single most outstanding effect of A_2^* is its sign reversal for the large majority of bridges, revealing a single-degree of freedom torsional instability, an effect not possible for an unstalled airfoil. As is well known, airfoil flutter will develop if a coupling occurs between the bending (h) and torsion (α) motions (because H_1^* and A_2^* are wholly negative). Such coupling is also possible for certain bridges, especially those with streamlined decks, but it is not necessary to create flutter.

7.4   Flutter control

By contrast to thin airfoils, most suspended bridges flutter in torsion and it appears that the key issue for flutter prevention in bridge design is the increase of their torsional stiffness. This traditional method to increase the flutter speed usually yields an expensive design. Research and development activities still focus on box girder concepts which alleviate the aeroelastic problems. The use of high damping structural material is also recommended whenever possible.

All passive techniques will eventually meet limitations when it comes to very large bridges with main spans exceeding 1000 m. An alternative approach, more promising and economical may be the application of active control devices. The active control device shown in Fig.7.8 is based on the idea of constantly monitor-

ing movements of the deck and use the control surface movements to generate a stabilizing aerodynamic force (lift) counteracting any tendency of a self-excited oscillation [28, 30].

Another way of increasing the critical flutter speed is the deployment of eccentric masses. If placed inside the bridge girder, eccentric masses moving in the transverse direction constitute a possible means of improving the stability of long span bridges. This concept requires a control system to monitor wind condition and to control the mass position. Another possible solution for cable-stayed bridges is the application of active tendon control, which has been theoretically investigated by Yang [73, 74]. He demonstrated that the flutter speed can be raised with a linear feedback of the girder velocity on the active tendon force; a decentralized control scheme is used; the sensors are placed at the anchorage of each active cable in order to sense the vibration of the bridge deck. However, this control scheme based on the use of non-collocated actuator/sensor pairs is prone to spillover instability.

7.5 A laboratory demonstration of flutter control

Our proposed decentralized active tendon control strategy based on a force sensor collocated with the actuator can be applied to the control of torsion flutter. The laboratory test structure used for this purpose is shown in Fig.7.9. The torsion flutter is simulated by a control system based on an electrodynamic shaker and two accelerometers placed on the structure and combined together in order to obtain a signal proportional to the angular acceleration of the torsion coordinate $\ddot{\alpha}$; a compensator based on a state feedback plus observer has been designed to relocate the torsion mode in the right half (unstable) plane (location corresponding to $g^* = 1$ in Fig.7.12).

The experimental frequency response function between the shaker input v and the angular acceleration $\ddot{\alpha}$ is represented in Fig.7.10.b. Assuming a perfect actuator dynamics, the analytical model of the cable structure can be identified to the linear second order system shown in Fig.7.10.a. The governing equations of this system are

$$\frac{d}{dt}\begin{pmatrix} \dot{\alpha} \\ \alpha \end{pmatrix} = \begin{pmatrix} -2\xi_t\Omega_t & -\Omega_t^2 \\ 1 & 0 \end{pmatrix}\begin{pmatrix} \dot{\alpha} \\ \alpha \end{pmatrix} + \begin{pmatrix} k \\ 0 \end{pmatrix}v = Ax + Bv$$

$$y = \ddot{\alpha} = \begin{pmatrix} -2\xi_t\Omega_t & -\Omega_t^2 \end{pmatrix}\begin{pmatrix} \dot{\alpha} \\ \alpha \end{pmatrix} + kv = Cx + Dv \qquad (7.19)$$

where Ω_t and ξ_t represent the natural frequency and the inherent damping ratio of the torsion mode; $x = (\dot{\alpha}\ \alpha)^T$ denotes the state vector; v and y are the input and the output of the system respectively.
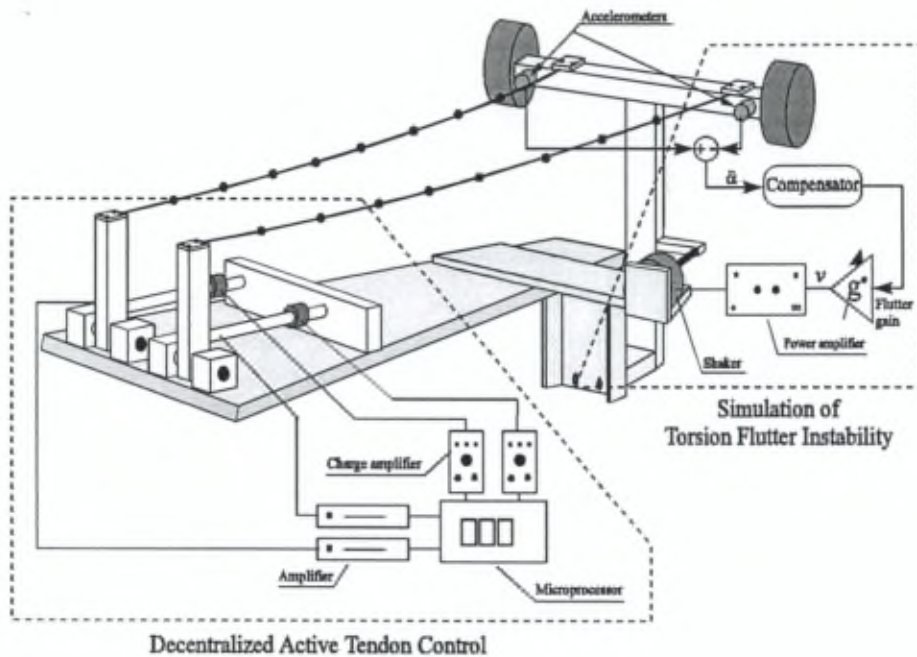
Figure 7.9: Test structure experiment for the flutter control.

A state feedback regulator is used to relocate the torsion poles in the unstable region of the complex plane; the control law is

$$v = -g^* G x = -g^* G \left(\dot{\alpha} \quad \alpha \right)^T \tag{7.20}$$

where the gain vector G is selected in such a way that the torsion mode is relocated in the right half (unstable) plane for $g^* = 1$; the scalar gain g^* is added to the gain vector G in order to simulate the wind speed in the flutter mechanism : For $g^* = 0$, the closed-loop system is identical to the open-loop structure (no wind), while for $g^* = 1$, the closed-loop system is in simulated unstable (flutter) condition.

Since the above state feedback requires the knowledge of the state vector $x = \left(\dot{\alpha} \quad \alpha \right)^T$, there must be an additional step of state reconstruction. For this purpose, and starting from the identified model (Fig.7.10), an observer has been designed in order to estimate the torsion states $\hat{\alpha}$ and $\dot{\hat{\alpha}}$ (angle and velocity respectively). The state space equations of the observer are

$$\frac{d\hat{x}}{dt} = (A - LC)\,\hat{x} + (B - LD)\,v + Ly \tag{7.21}$$
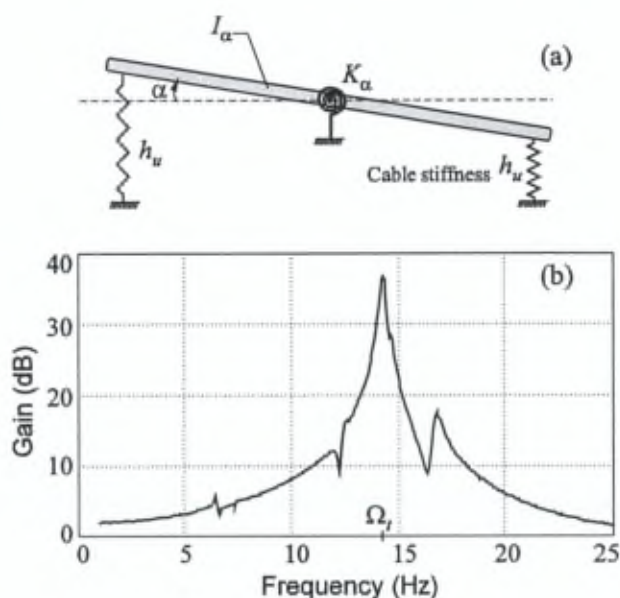
Figure 7.10: Cable structure torsion mode : (a) linear model (b) experimental transfer function between the shaker input v and the angular acceleration $\ddot{\alpha}$.

where the gain matrix L is chosen in such a way that the observer poles (given by the eigenvalues of the matrix $A - LC$) are stable and faster than the regulator poles [54]. Thus, the equations of the compensator are obtained by combining the state feedback regulator Equ.(7.20) and the state observer Equ.(7.21); Fig.7.11 represents a block diagram of the compensator which simulates the flutter mechanism. When the gain g^* is varied from 0 to 1, the torsion poles move from the stable open-loop poles to the unstable ones, and the simulated flutter condition is achieved when g^* is such that the poles cross the imaginary axis (critical flutter gain).

In order to demonstrate the efficiency of the decentralized control with respect to the flutter mechanism, the compensator has been tested on the test structure (Fig.7.9). Figure 7.12 shows the evolution of the torsion poles in the complex plane as a function of g^*, with and without active tendon control; we see that the critical flutter gain g^* is increased considerably by the active tendon control. Figure 7.13 shows the damping ratio of the torsion mode as a function of g^*, with and without active damping.
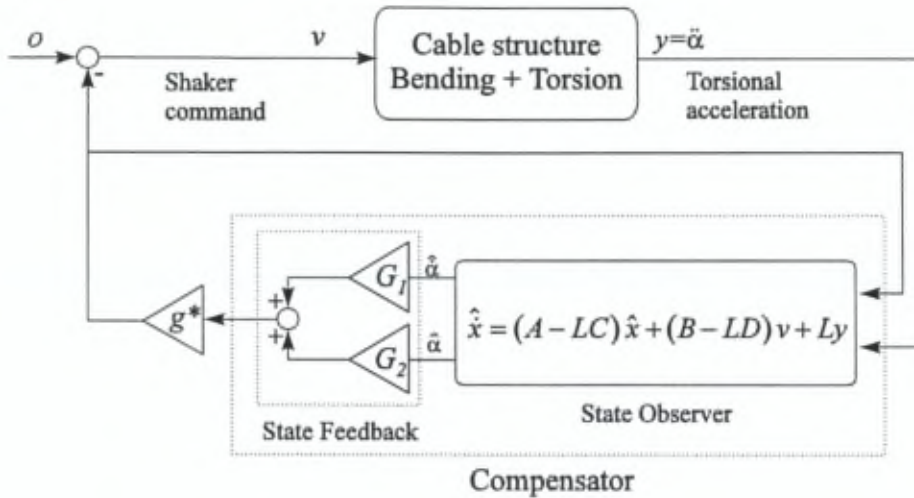
Figure 7.11: Block diagram of the compensator : state feedback plus observer.
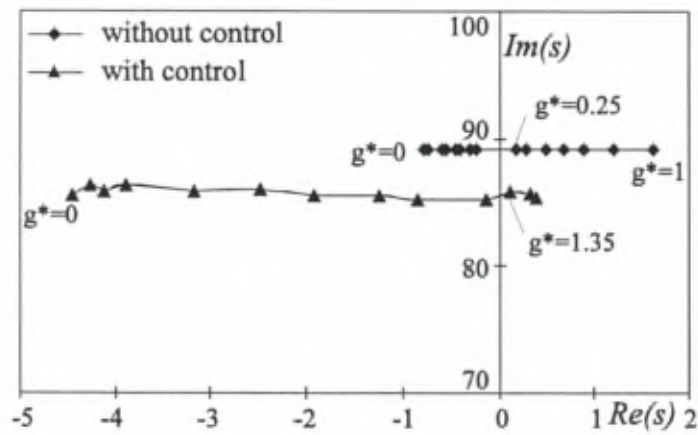
Figure 7.12: Root locus of the torsion mode as a function of the flutter gain g^*.
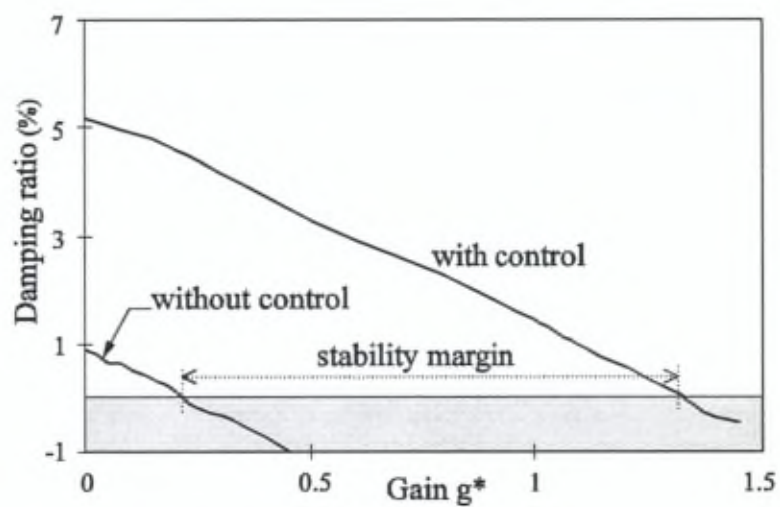
Figure 7.13: Effective damping of the torsion mode as a function of g^*.

Chapter 8

Conclusion

8.1 Main achievements of this study

We have presented a control strategy for the active damping of cable-stayed structures. The control methodology is based on the use of an active tendon consisting of a force sensor collocated with an actuator which controls the displacement of the cable anchor point. The proposed control law called *Integral Force Feedback* enjoys guaranteed stability properties, even for nonlinear systems.

The efficiency and the robustness of the control algorithm have been demonstrated on several laboratory mock-ups, including a cable alone, a cable structure and a simple scale model of a cable-stayed bridge. The control efficiency has been confirmed on the cable as well as on the structure, even at the parametric resonance. The Integral Force Feedback has been applied successfully to the decentralized control of a structure with several active cables.

We have established simple and powerful criteria useful for the design of active cable-stayed structures; they allow one to predict the closed-loop behaviour of the system and to choose the number and the localisation of the active tendons. The torsion flutter has been mechanically simulated on a laboratory test article with a specially designed control system using a shaker and an accelerometer. It has been demonstrated that the flutter speed is considerably increased when the proposed decentralized control strategy is applied.

We have also developed a modelling technique of cable-stayed structures which is very efficient and can be used for control system design purposes. The model combines a finite element model of the prestressed structure and the nonlinear analytical dynamics of the stay cables in modal coordinates.
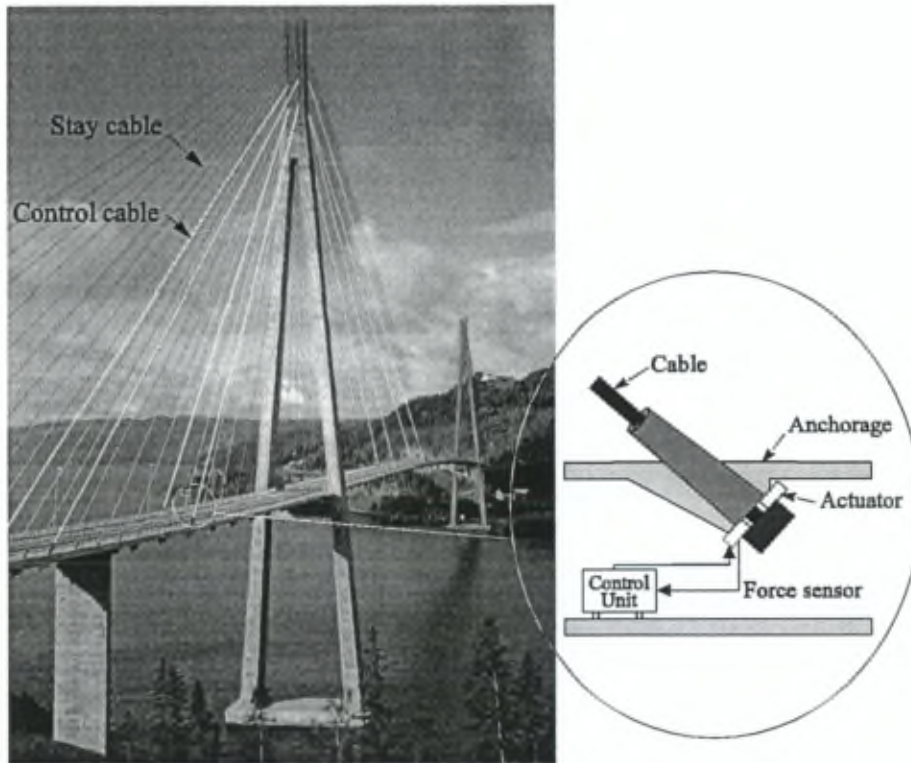
Figure 8.1: Conceptual design of the active tendon control of a cable-stayed bridge.

8.2 Future works

The proposed control strategy can be extended to the active damping of tension trusses, guyed mast and towers and all other cable-stayed structures. For instance, the active damping of large space structures has long been recognized as a major issue for various reasons. On the other hand, it is quite likely that minimum weight future large space structures will consist of large trusses connected by tension cables. In this context, the damping strategy may consist in providing the tension cables with an active tendon in order to control the cable structure system; the damping efficiency should be appreciable because of the large stiffening effect of the stay cables.

The practical application of active tendon control to cable-stayed bridges relies on placing an actuator at one end of the cable and controlling its motion; Fig.8.1 shows the conceptual design of an active tendon control device. One

should note that the required maximum displacement of the actuator would not exceed 0.01% of the cable span and the dynamical control force in the tendon would not be greater than 0.5% of the static tension. Our scale mock-up used piezoelectric actuators, but other types of actuators must be considered for full scale applications : most likely hydraulic, or maybe giant magnetostrictive actuators.

Starting from this study, a consortium was formed in the frame work of the EEC BRITE-EURAM III program and an industrial project entitled "ACE : Active Control in Civil Engineering" started in May 1997. In addition to the Active Structures Laboratory (ULB) the consortium includes Bouygues S.A. (FR, coordinator), Defense Research Agency (GB), Magnetostrictive Technology Systems Limited (GB), Mannesman Rexroth GmbH (DE), Institut fur Werkzeugmaschinen und Fluidtechnik TUD (DE), Johs Holt AS (NW), VSL S.A. (FR) and Ecole Centrale de Lyon (FR). The main objectives of the project are :

- to develop an active vibration control system for cable-supported structures.

- to improve an appropriate software package for the dynamic analysis of cable-stayed structures especially suited for control design purposes.

- to develop the appropriate actuators.

- to validate the active control concept with larger scale mock-ups including, one scaled cable-stayed bridge (approximate length 30 m) and one scaled guyed tower (the main difference between these two cable structures comes from the level of the static tension in the stay cables).

In parallel to this industrial project, the future research program of the Active Structures Laboratory will include the aeroelastic modelling of cable-stayed bridges for flutter prediction and the development of a prototype gyrostabilizer for flutter control.

Appendix A

Governing equations of the cable motion

A.1 Quasi-static motion

Integrating the second equation of (2.47) and introducing the boundary conditions Equ.(2.48), we obtain

$$\frac{\partial^2 v^q}{\partial x^2} = 0 \quad \Rightarrow \quad v^q(x,t) = v_a + (v_b - v_a)\frac{x}{l} \tag{A.1}$$

Expanding the first and third equations (2.47), we find,

$$\frac{\partial^2 w^q}{\partial x^2} = -\frac{\sigma^q}{\sigma^s}\frac{d^2 w^s}{dx^2} \tag{A.2}$$

The integration of Equ.(A.2) with the boundary conditions (2.48) yields,

$$w^q(x,t) = w_a + (w_b - w_a)\frac{x}{l} - \frac{\sigma^q}{\sigma^s}w^s(x) \tag{A.3}$$

Substituting Equ.(2.50) into (2.49) and integrating the strain-displacement relation, we get

$$u^q(x,t) = \frac{\sigma^q}{E}x - \frac{w_b - w_a}{l}w^s(x) + \frac{\sigma^q}{\sigma^s}\int \left(\frac{dw^s}{dx}\right)^2 dx + C \tag{A.4}$$

The constant of integration C is obtained using the boundary condition of the axial component Equ.(2.48) at one anchor. Besides, according to the definition of the equivalent modulus, Equ.(2.38), the quasi-static stress σ^q is related to the support axial displacements by

$$\sigma^q = E_q\frac{u_b - u_a}{l} \tag{A.5}$$

where E_q represents the effective modulus defined by Equ.(2.38). Finally, the set of equations (A.1),(A.3) and (A.4) governs the quasi-static motion of a small sag cable with movable anchors Equ.(2.52).

A.2 Energy partition in the cable vibration

A.2.1 Kinetic energy

Substituting Equ.(2.58), (2.52) and (2.55) in the expression of the kinetic energy Equ.(2.60) we obtain after some algebra (e.g. using a symbolic calculation software),

$$
\begin{aligned}
\mathcal{T} \;=\;& \tfrac{1}{2}\rho A l\Bigg\{ \Big(\frac{1}{1+\frac{\lambda^2}{12}}\Big)^2\Big(\frac{1}{3}+\frac{\lambda^2}{20}+\frac{\lambda^4}{504}+\frac{\lambda^2}{120}\frac{E}{\sigma^s}\Big)(\dot u_b-\dot u_a)^2 \\[4pt]
& \dot u_b\dot u_a+\tfrac{1}{3}\,(\dot v_b-\dot v_a)^2+\dot v_b\dot v_a+\tfrac{1}{3}\,(\dot w_b-\dot w_a)^2+\dot w_b\dot w_a \\[4pt]
& -\frac{1}{12}\frac{\lambda}{1+\frac{\lambda^2}{12}}\sqrt{\frac{\sigma^s}{E}}\left[1+\frac{\lambda^2}{12}+\frac{E}{\sigma^s}\right](\dot w_b-\dot w_a)(\dot u_b-\dot u_a) \\[4pt]
& +\frac{\lambda^2}{120}\frac{\sigma^s}{E}(\dot w_b-\dot w_a)^2 \\[4pt]
& -\frac{1}{6}\frac{\lambda}{1+\frac{\lambda^2}{12}}\sqrt{\frac{E}{\sigma^s}}(\dot u_b-\dot u_a)\dot w_a-\frac{\lambda}{6}\sqrt{\frac{\sigma^s}{E}}(\dot w_b-\dot w_a)\dot u_a \\[4pt]
& +\sum_k\left[\frac{2}{k\pi}\,\big(\dot v_a+(-1)^{k+1}\dot v_b\big)\dot y_k+\frac{2}{k\pi}\,\big(\dot w_a+(-1)^{k+1}\dot w_b\big)\dot z_k\right. \\[4pt]
& \left.-2\frac{\gamma l}{\sigma^s}\frac{(1+(-1)^{k+1})}{k\pi}\frac{1}{(k\pi)^2}\frac{E_q}{\sigma^s}(\dot u_b-\dot u_a)\dot z_k+\tfrac{1}{2}\dot y_k^2+\tfrac{1}{2}\dot z_k^2\right]\Bigg\}
\end{aligned}
$$

$$\text{(A.6)}$$

If there is no transverse motion [Equ.(2.72)] and if we neglect the second order terms ($\dot u_a^2$, $\dot u_b^2$) the expression of the kinetic energy is simplified into

$$
\mathcal{T}=\tfrac{1}{2}\rho A l\sum\left[\tfrac{1}{2}\dot y^2+\tfrac{1}{2}\dot z^2\right]-2\frac{E}{(k\pi)^3}\frac{\gamma l}{\sigma}^2\big(1+(-1)^{+1}\big)(\dot u\;-\dot u\;)\dot z \qquad \text{(A.7)}
$$

Defining the vectors of out-of-plane and in-plane cable mode amplitudes

$$
\begin{aligned}
y &= \big(\; y_1 \quad y_2 \quad \cdots \quad y_n \;\big)^T \\
z &= \big(\; z_1 \quad z_2 \quad \cdots \quad z_n \;\big)^T
\end{aligned}
\qquad \text{(A.8)}
$$

the kinetic energy Equ.(A.7) becomes,

$$\mathcal{T} = \frac{1}{2}\dot{y} \ \mu \ \dot{y} + \frac{1}{2}\dot{z} \ \mu \ \dot{z} - \alpha \ (\dot{u} \ - \dot{u} \ )\dot{z} \tag{A.9}$$

where the modal mass matrix μ_c and the vector α_c are given by Equ.(A.35) and (A.40).

A.2.2 Strain

The axial strain in the cable involves a static component ε_0, a quasi-static contribution ε_q and a dynamic one ε_d. The static strain in the cable is

$$\varepsilon_0 = \frac{\sigma^s}{E} \tag{A.10}$$

The quasi-static contribution reads

$$\varepsilon_q = \frac{E_q}{E}\frac{u_b - u_a}{l} \tag{A.11}$$

and the dynamic strain is composed of a linear component $\varepsilon_d^{(1)}$ and a nonlinear one $\varepsilon_d^{(2)}$. Substituting the third equation (2.52) and Equ.(2.55) in the expression governing the linear component of the dynamical strain, Equ.(2.63), and integrating along the cable span we find

$$\begin{aligned}
\varepsilon_d^{(1)}(t) &= \frac{1}{l}\int_0^l \varepsilon_d^{(1)}(x,t)dx = \frac{1}{l}\int_0^l \frac{dw^s}{dx}\frac{\partial w^d}{\partial x}dx \\
&= \sum_k z_k \int_0^l \frac{d^2 w^s}{dx^2}\psi_k(x)dx \\
&= \sum_k \frac{\gamma}{\sigma^s}\frac{\left(1 + (-1)^{k+1}\right)}{k\pi}z_k
\end{aligned} \tag{A.12}$$

Similarly, the nonlinear contribution of the dynamic strain is obtained by substituting Equ.(2.55) into the integrated form of Equ.(2.64),

$$\begin{aligned}
\varepsilon_d^{(2)}(t) &= \frac{1}{l}\int_0^l \varepsilon_d^{(2)}(x,t)dx = \frac{1}{2l}\int_0^l \left[2\frac{\partial w^q}{\partial x}\frac{\partial w^d}{\partial x} + \left(\frac{\partial v^d}{\partial x}\right)^2 + \left(\frac{\partial w^d}{\partial x}\right)^2\right] dx \\
&= \frac{1}{2l}\sum_k y_k^2 \int_0^l \left(\frac{d\phi_k}{dx}\right)^2 dx + z_k^2 \int_0^l \left(\frac{d\psi_k}{dx}\right)^2 dx \\
&\quad - \sum_k \frac{\sigma^q}{\sigma^s}\frac{\gamma}{\sigma^s}\frac{\left(1 + (-1)^{k+1}\right)}{k\pi}z_k
\end{aligned} \tag{A.13}$$

A.2.3   Tension

The components of the variable part of cable tension, expressed in terms of the cable strain Equ.(2.67) reads

$$T = T_q + T_d^{(1)} + T_d^{(2)} \tag{A.14}$$

with

- the quasi-static tension T_q :

$$T_q = EA\varepsilon_q = \frac{E_q A}{l}(u_b - u_a) \tag{A.15}$$

- the linear component of the dynamical tension T_d due to the cable sag :

$$T_d^{(1)} = EA\varepsilon_d^{(1)} = h_1^T z \tag{A.16}$$

- the nonlinear component of the dynamical tension T_d due to the cable stretching and the axial displacement of the cable supports :

$$T_d^{(2)} = EA\varepsilon_d^{(2)} = \frac{1}{2}y^T h_2 y + \frac{1}{2}z^T h_2 z - \frac{T_q}{T_0}T_d^{(1)} \tag{A.17}$$

where the vector h_1 and the matrix h_2 are given by Equ.(A.33) and (A.34).

A.2.4   Potential energy

The Potential energy due to elastic elongation Equ.(2.69) can be expressed in terms of tension as follows

$$\mathcal{V}^* = \frac{l}{2EA}\left(T_0 + T\right)^2 \tag{A.18}$$

The analytical expression of the gravitational potential energy can be obtained by substituting the third equation (2.52) and Equ.(2.55) into Equ.(2.70); after integration along the cable span, we obtain

$$\mathcal{V}^o = \frac{\lambda^2}{12}\frac{E_q}{E}T_0(u_b - u_a) - \frac{l}{EA}T_0 T_d^{(1)} + \mathcal{V}_s^o \tag{A.19}$$

where $\mathcal{V}_s^o$ denotes the constant, purely static term, which will disappear from the Lagrange equations.

The total potential energy is finally

$$
\begin{aligned}
\mathcal{V}_c &= \mathcal{V}^* + \mathcal{V}^o + \mathcal{V}_{ext} \\
&= \frac{l}{2EA}\left(T_0 + T\right)^2 - \frac{l}{EA}T_0 T_d^{(1)} \\
&\quad + \frac{\lambda^2}{12}\frac{E_q}{E}T_0(u_b - u_a) + \mathcal{V}_s^o + \mathcal{V}_{ext}
\end{aligned} \tag{A.20}
$$

A.2.5   Lagrange equations

Using the expression of the kinetic energy Equ.(A.9) and potential energy Equ.(A.20),we have

$$
\begin{aligned}
\frac{\partial T_c}{\partial \dot{y}} &= \mu_c \dot{y} \\
\frac{\partial T_c}{\partial \dot{z}} &= \mu_c \dot{z} - \alpha_c (\dot{u}_b - \dot{u}_a) \\
\frac{\partial \mathcal{V}_c}{\partial y} &= \frac{l}{EA}(T_0 + T)\frac{\partial T}{\partial y} + \frac{\partial \mathcal{V}_{ext}}{\partial y} \\
\frac{\partial \mathcal{V}_c}{\partial z} &= \frac{l}{EA}(T_0 + T)\frac{\partial T}{\partial z} - \frac{l}{EA}T_0\frac{\partial T_d^{(1)}}{\partial z} + \frac{\partial \mathcal{V}_{ext}}{\partial z} \\
\frac{\partial \mathcal{V}_{ext}}{\partial y} &= -F_y \\
\frac{\partial \mathcal{V}_{ext}}{\partial z} &= -F_z
\end{aligned}
\tag{A.21}
$$

and from Equ.(A.16), (A.17) and (A.14), we obtain,

$$
\begin{aligned}
\frac{\partial T}{\partial y} &= \frac{\partial T_d^{(2)}}{\partial y} = 2h_2 y \\
\frac{\partial T}{\partial z} &= \frac{\partial T_d}{\partial z} = \frac{\partial T_d^{(1)}}{\partial z} + \frac{\partial T_d^{(2)}}{\partial z} \\
\frac{\partial T_d^{(1)}}{\partial z} &= h_1 \quad \text{and} \quad \frac{\partial T_d^{(2)}}{\partial z} = 2h_2 z - \frac{T_q}{T_0}\frac{\partial T_d^{(1)}}{\partial z}
\end{aligned}
\tag{A.22}
$$

Substituting the previous equations in the Lagrange equations (2.59), we get the equation governing the out-of-plane motion,

$$
\begin{aligned}
&\frac{d}{dt}\left(\frac{\partial T_c}{\partial \dot{y}}\right) + \frac{\partial \mathcal{V}_c}{\partial y} \\
&= \frac{d}{dt}(\mu_c \dot{y}) + \frac{l}{EA}(T_0 + T)\frac{\partial T_d^{(2)}}{\partial y} - F_y = 0
\end{aligned}
\tag{A.23}
$$

and the in-plane motion,

$$
\frac{d}{dt}\left(\frac{\partial T_c}{\partial \dot{z}}\right) + \frac{\partial \mathcal{V}_c}{\partial z} = \frac{d}{dt}(\mu_c \dot{z} - \alpha_c(\dot{u}_b - \dot{u}_a))
\tag{A.24}
$$

$$
+ \frac{l}{EA}(T_0 + T)\left\{\left(1 - \frac{T_q}{T_0}\right)\frac{\partial T_d^{(1)}}{\partial z} + 2h_2 z\right\} - \frac{l}{EA}T_0\frac{\partial T_d^{(1)}}{\partial z} - F_z
$$

or

$$\mu_c \ddot{z} - \alpha_c(\ddot{u}_b - \ddot{u}_a)$$
$$+\frac{l}{EA}\left\{(T_0 + T)\,2h_2 z + \left[T\left(1 - \frac{T_q}{T_0}\right) - T_q\right]h_1\right\} - F_z = 0 \quad \text{(A.25)}$$

Assuming that the quasi-static tension and the linear component $T_d^{(1)}$ are negligible compared to the static tension ($1 - \frac{T_q}{T_0} \approx 1$ and $1 - \frac{T_d^{(1)}}{T_0} \approx 1$), using Equ.(A.22), the previous equations (A.23) and (A.25), are reduced to,

$$\mu_c \ddot{y} + \frac{2l}{EA}\left(T_0 + T\right)h_2 y = F_y \quad \text{(A.26)}$$

$$\mu_c \ddot{z} + \frac{2l}{EA}(T_0 + T)h_2 z + \frac{l}{EA}T_d h_1 - \alpha_c(\ddot{u}_b - \ddot{u}_a) = F_z \quad \text{(A.27)}$$

Introducing the contribution of the axial tension Equ.(2.67), the frequency matrix $\Omega = diag(\omega_i)$ [see Equ.(A.36)] and the vectors S, and Λ given by Equ.(A.39) and (A.32), the previous equations can be written alternatively as

$$\mu_c\left(\ddot{y} + \Omega^2 y\right) + Sy(T_q + T_d) = F_y \quad \text{(A.28)}$$

$$\mu_c\left(\ddot{z} + \Omega^2 z\right) + Sz(T_q + T_d) + \Lambda T_d - \alpha_c(\ddot{u}_b - \ddot{u}_a) = F_z \quad \text{(A.29)}$$

Adding some modal damping we have

$$\mu_c\left(\ddot{y} + 2\xi_y\Omega\dot{y} + \Omega^2 y\right) + Sy(T_q + T_d) = F_y \quad \text{(A.30)}$$

$$\mu_c\left(\ddot{z} + 2\xi_z\Omega\dot{z} + \Omega^2 z\right) + Sz(T_q + T_d) + \Lambda T_d - \alpha_c(\ddot{u}_b - \ddot{u}_a) = F_z \quad \text{(A.31)}$$

where the modal damping matrices ξ_y, ξ_z are given by Equ.(A.37) and (A.38).

A.3   Summary of the cable parameters

This section summarizes the analytical form of the various coefficients which appear in the dynamic equations of the cable, with the following notations

l : cable span

A : cable cross section

ρ : specific mass

E : Young's modulus

σ^s : static stress (or the static tension $T_0 = A\sigma^s$)

θ : cable inclination angle

$\gamma = \rho g \cos \theta$: distributed cable weight along z

$\lambda^2 = \left(\frac{\gamma l}{\sigma^s}\right)^2 \frac{E}{\sigma^s}$: Irvine parameter

With the foregoing notations, the constant vectors and matrices appearing in the cable dynamic equations read

$$\Lambda = \begin{pmatrix} \frac{2\gamma l}{\pi \sigma^s} & 0 & \cdots & \frac{\gamma l}{\sigma^s}\frac{(1+(-1)^{n+1})}{n\pi} \end{pmatrix}^T \tag{A.32}$$

$$h_1 = \frac{EA}{l}\Lambda = \begin{pmatrix} EA\frac{2\gamma}{\pi\sigma^s} & 0 & \cdots & EA\frac{\gamma}{\sigma^s}\frac{(1+(-1)^{n+1})}{n\pi} \end{pmatrix}^T \tag{A.33}$$

$$h_2 = \begin{pmatrix} EA\left(\frac{\pi}{2l}\right)^2 & 0 & \cdots & 0 \\ 0 & EA\left(\frac{\pi}{l}\right)^2 & \cdots & 0 \\ \vdots & \cdots & \ddots & \vdots \\ 0 & 0 & \cdots & EA\left(\frac{n\pi}{2l}\right)^2 \end{pmatrix} \tag{A.34}$$

$$\mu_c = \frac{1}{2}\rho A l I_n \tag{A.35}$$

where I_n is the identity matrix of order n.

$$\Omega^2 = \frac{\sigma^s l}{E}\mu_c^{-1}h_2 = \begin{pmatrix} \frac{\sigma^s}{\rho}\left(\frac{\pi}{l}\right)^2 & 0 & \cdots & 0 \\ 0 & \frac{\sigma^s}{\rho}\left(\frac{2\pi}{l}\right)^2 & \cdots & 0 \\ \vdots & \cdots & \ddots & \vdots \\ 0 & 0 & \cdots & \frac{\sigma^s}{\rho}\left(\frac{n\pi}{l}\right)^2 \end{pmatrix} \tag{A.36}$$

$$\xi_y = diag\left(\xi_{y_i}\right) \tag{A.37}$$

$$\xi_z = diag\left(\xi_{z_i}\right) \tag{A.38}$$

$$S = \frac{2l}{EA}h_2 = \begin{pmatrix} \frac{\pi^2}{2l} & 0 & \cdots & 0 \\ 0 & \frac{(2\pi)^2}{2l} & \cdots & 0 \\ \vdots & \cdots & \ddots & \vdots \\ 0 & 0 & \cdots & \frac{(n\pi)^2}{2l} \end{pmatrix} \tag{A.39}$$

$$\alpha_c = h_u\left(\Omega^2\right)^{-1}\Lambda = \begin{pmatrix} \rho A l \frac{E_s}{\sigma^s}\frac{\gamma l}{\sigma^s}\frac{2}{\pi^3} & 0 & \cdots & \rho A l \frac{E_s}{\sigma^s}\frac{\gamma l}{\sigma^s}\frac{(1+(-1)^{n+1})}{(n\pi)^3} \end{pmatrix}^T \tag{A.40}$$

Appendix B

Cable dynamic nonlinearities

B.1 The multiple scales method

Consider the second order differential equation,

$$\frac{d^2x}{dt^2} = f(x, \dot{x}, t) \tag{B.1}$$

where f is a nonlinear function of the states x, $\dot{x}$ and time t.

The main idea of the method of multiple scales is to consider the expansion representing the response to be a function of multiple independent variables T_n, or scales, instead of a single variable t. The independent variables are defined as,

$$T_n = \epsilon^n t \quad \text{for} \quad n = 1, 2, \cdots \tag{B.2}$$

It follows that the derivatives with respect to t become,

$$\frac{d}{dt} = \frac{dT_0}{dt}\frac{\partial}{\partial T_0} + \frac{dT_1}{dt}\frac{\partial}{\partial T_1} + \cdots = D_0 + \epsilon D_1 + \cdots$$

$$\frac{d^2}{dt^2} = D_0^2 + 2\epsilon D_0 D_1 + \epsilon^2 \left(D_1^2 + 2D_0 D_2\right) + \cdots \tag{B.3}$$

with $D_i = \frac{\partial}{\partial T_i}$ for $i = 1, 2, \cdots$.

One assumes that the solution of (B.1) can be represented by the expansion

$$
\begin{aligned}
x(t, \epsilon) &= x_0(T_0, T_1, T_2, \cdots) + \epsilon x_1(T_0, T_1, T_2, \cdots) \\
&\quad + \epsilon^2 x_2(T_0, T_1, T_2, \cdots) + \cdots + O(\epsilon^N)
\end{aligned} \tag{B.4}
$$

108

where $\epsilon \ll 1$. The linear differential equations governing each function $x_i(T_0, T_1, T_2)$ are obtained from the substitution of Equ.(B.4) in Equ.(B.1).

In the next section, the method of multiple scales is used to establish a second order approximation ($N = 3$) of the frequency response of the Duffing equation around the primary resonance. Subsequently, the frequency response and the stability of the parametrically excited Duffing equation will be considered.

B.1.1 Primary resonance with quadratic and cubic non-linearities

Consider the Duffing equation (3.7) with a harmonic excitation F_{un}. If we let $z_n = \epsilon \cos(\omega_{zn}t)$ in Equ.(3.7), the cubic nonlinearity generates a third order term in ϵ. To analyze the frequency response we need to order the damping, the excitation and the cubic nonlinearity, so that they interact at the same level of approximation. Therefore, if we let $z_n = \epsilon x$, we need to order the damping term $2\xi_{zn}\omega_{zn}\dot{z}_n$ as $2\epsilon^2 \widehat{\xi}_{zn}\omega_{zn}\dot{z}_n$ and the excitation term F_{un} as $\epsilon^3 \widehat{F}_{un}$ so that the governing equation (3.7) becomes

$$\ddot{x} + \omega_{zn}^2 x = \epsilon^2 \frac{\widehat{F}_{un}}{\mu_{cn}} - 2\epsilon^2 \widehat{\xi}_{zn}\omega_{zn}\dot{x} - \epsilon\beta_n x^2 - \epsilon^2 \nu_n x^3 \tag{B.5}$$

where $\xi_{zn} = \epsilon^2 \widehat{\xi}_{zn}$ and $F_{un} = \epsilon^3 \widehat{F}_{un}$. Let us introduce a detuning parameter η, which quantitatively describes the nearness of the frequency of the excitation Ω to the primary resonance frequency ω_{zn} as,

$$\Omega = \omega_{zn} + \epsilon^2 \eta \tag{B.6}$$

where $\Omega - \omega_{zn}$ is assumed to be of the same order as the excitation [i.e. $O(\epsilon^2)$] for consistency. Substituting Equ.(B.4) and (B.6) into Equ.(B.5) and equating the coefficients of ϵ^0, ϵ and ϵ^2, we obtain

$$
\begin{aligned}
D_0^2 x_0 + \omega_{zn}^2 x_0 &= 0 \\
D_0^2 x_1 + \omega_{zn}^2 x_1 &= -2D_0 D_1 x_0 - \beta_n x_0^2 \\
D_0^2 x_2 + \omega_{zn}^2 x_2 &= -(D_1^2 + 2D_0 D_2)x_0 - 2\widehat{\xi}_{zn}\omega_{zn} D_0 x_0 - \nu_n x_0^3 \\
&\quad -2D_0 D_1 x_1 - 2\beta_n x_0 x_1 \\
&\quad + \frac{\alpha_{cn}\widehat{a}_u \Omega^2}{\mu_{cn}} \cos(\omega_{zn} T_0 + \eta T_2)
\end{aligned}
\tag{B.7}
$$

where $a_u = \epsilon^2 \widehat{a}_u$. The general solution of Equ.(B.7) can be expressed in the form,

$$x_0 = A(T_1, T_2)e^{i\omega_{zn}T_0} + \bar{A}(T_1, T_2)e^{-i\omega_{zn}T_0} \tag{B.8}$$

where $A(T_1, T_2)$ is an undetermined function at this point and $\bar{A}$ denotes its complex conjugate. The governing equations for A are obtained by requiring x_2 and x_1 to be periodic in T_0. Substituting the expression of x_0 into the second equation of Equ.(B.5), we obtain

$$D_0^2 x_1 + \omega_{zn}^2 x_1 = -2i\omega_{zn} D_1 A e^{i\omega_{zn} T_0} - \beta_n \left(A^2 e^{2i\omega_{zn} T_0} + A\bar{A} \right) + cc \qquad \text{(B.9)}$$

where cc denotes the complex conjugate of the preceding terms. Any particular solution of Equ.(B.9) has a periodic solution in T_0 if the secular terms (non periodic) containing the factor $T_0 e^{i\omega_{zn} T_0}$ vanish. We find that this condition is reduced to

$$D_1 A = 0 \quad \Rightarrow \quad A = A(T_2) \qquad \text{(B.10)}$$

Hence, the solution of Equ.(B.9) reads,

$$x_1 = \frac{\beta_n}{3\omega_{zn}^2} \left(-6A\bar{A} + A^2 e^{2i\omega_{zn} T_0} + \bar{A}^2 e^{-2i\omega_{zn} T_0} \right) \qquad \text{(B.11)}$$

Substituting the solution of x_1 in the third equation of Equ.(B.7), we obtain the differential equation governing the state x_2 as follows,

$$
\begin{aligned}
D_0^2 x_2 + \omega_{zn}^2 x_2 = \;&{-}\bigg\{ 2i\omega_{zn}(D_2 A + \widehat{\xi}_{zn}\omega_{zn} A) + \left(3\nu_n - \frac{10}{3}\frac{\beta_n^2}{\omega_{zn}^2} \right) A^2\bar{A} \\
&{-} \frac{\alpha_{cn}\widehat{a}_u \Omega^2}{2\mu_{cn}} e^{i\eta T_0} \bigg\} e^{i\omega_{zn} T_0} + cc + NST
\end{aligned}
\qquad \text{(B.12)}
$$

where cc denotes the complex conjugate of the preceding terms and NST stands for terms proportional to $e^{3i\omega_{zn} T_0}$. Therefore, any particular solution of Equ.(B.12) contains secular terms $T_0 e^{i\omega_{zn} T_0}$, unless

$$2i\omega_{zn}(A' + \widehat{\xi}_{zn}\omega_{zn} A) + \left(3\nu_n - \frac{10}{3}\frac{\beta_n^2}{\omega_{zn}^2} \right) A^2\bar{A} - \frac{\alpha_{cn}\widehat{a}_u \Omega^2}{2\mu_{cn}} e^{i\eta T_0} = 0 \qquad \text{(B.13)}$$

where the prime denotes the derivative with respect to the variable T_2. Equation (B.13) governing the unknown complex function $A(T_2)$ can be solved using a polar form

$$A = \frac{1}{2} a e^{ib} \qquad \text{(B.14)}$$

where a and b are real functions of T_2. Hence, substituting Equ.(B.14) in Equ.(B.13) and separating the result into real and imaginary parts, we find

$$a' = -\widehat{\xi}_{zn}\omega_{zn}a + \frac{\alpha_{cn}\widehat{a}_u\Omega^2}{2\mu_{cn}\omega_{zn}}\sin\gamma$$

$$a(\eta - \gamma') = \left(\frac{3}{8}\nu_n - \frac{5}{12}\frac{\beta_n^2}{\omega_{zn}^2}\right)\frac{a^3}{\omega_{zn}} - \frac{\alpha_{cn}\widehat{a}_u\Omega^2}{2\mu_{cn}\omega_{zn}}\cos\gamma \qquad (B.15)$$

where $\gamma = \eta T_2 - b$ represents the phase angle of the response.

The steady-state response ($a' = \gamma' = 0$) corresponds to the singular points (a_0, γ_0) of the system governed by Equ.(B.15) according to,

$$\widehat{\xi}_{zn}\omega_{zn}a_0 = \frac{\alpha_{cn}\widehat{a}_u\Omega^2}{2\mu_{cn}\omega_{zn}}\sin\gamma_0$$

$$a_0\eta = \left(\frac{3}{8}\nu_n - \frac{5}{12}\frac{\beta_n^2}{\omega_{zn}^2}\right)\frac{a_0^3}{\omega_{zn}} - \frac{\alpha_{cn}\widehat{a}_u\Omega^2}{2\mu_{cn}\omega_{zn}}\cos\gamma_0 \qquad (B.16)$$

After the elimination of γ_0 from Equ.(B.16), we obtain the second order approximation of the frequency response equation governing the amplitude of motion a_0 as a function of η and the amplitude a_u of the excitation in the vicinity of the primary resonance ω_{zn} :

$$\left[\frac{\eta}{\omega_{zn}} - \left(\frac{3}{8}\nu_n - \frac{5}{12}\frac{\beta_n^2}{\omega_{zn}^2}\right)\frac{a_0^2}{\omega_{zn}^2}\right]^2 = \left(\frac{\alpha_{cn}\widehat{a}_u\Omega^2}{2\mu_{cn}a_0\omega_{zn}^2}\right)^2 - \widehat{\xi}_{zn}^2 \qquad (B.17)$$

which leads to Equ.(3.9) recalling that $\Omega - \omega_{zn} = \epsilon^2\eta$.

B.1.2 Parametric resonance

Approximate frequency response

We seek to establish the frequency response of the parametrically excited Duffing equation (3.10). As previously seen, with the method of multiple scales, we need to order the damping and the parametric excitation term in such a way that they interact at the same level of approximation. Therefore, if we let $z_n = \epsilon x$, we need to order the damping term $2\xi_{zn}\omega_{zn}\dot{z}_n$ as $2\epsilon^2\widehat{\xi}_{zn}\omega_{zn}\dot{z}_n$ and the parametric excitation term $R_n u z_n$ as $\epsilon^2 R_n\widehat{u}z_n$ so that the governing equation (3.10) becomes

$$\ddot{x} + \omega_{zn}^2 x = -2\epsilon^2\widehat{\xi}_{zn}\omega_{zn}\dot{x} - \epsilon\beta_n x^2 - \epsilon^2\nu_n x^3 - \epsilon^2 R_n x\widehat{u} \qquad (B.18)$$

Since we seek a second order approximation of the frequency response function in the vicinity of the parametric resonance $2\omega_{zn}$, we introduce a detuning parameter η related to the excitation frequency by

$$\Omega = 2\omega_{zn} + \epsilon^2\eta \qquad (B.19)$$

where $\Omega - 2\omega_{zn}$ is assumed to be of the same order as the parametric excitation [i.e. $O(\epsilon^2)$] for consistency. Substituting Equ.(B.4) into Equ.(B.18), and equating the coefficients of ϵ^0, ϵ and ϵ^2, we get

$$
\begin{aligned}
D_0^2 x_0 + \omega_{zn}^2 x_0 &= 0 \\
D_0^2 x_1 + \omega_{zn}^2 x_1 &= -2D_0 D_1 x_0 - \beta_n x_0^2 \\
D_0^2 x_2 + \omega_{zn}^2 x_2 &= -(D_1^2 + 2D_0 D_2)x_0 - 2\widehat{\xi}_{zn}\omega_{zn} D_0 x_0 - \nu_n x_0^3 \\
&\quad -2D_0 D_1 x_1 - 2\beta_n x_0 x_1 \\
&\quad -R_n \widehat{a}_u x_0 \cos(2\omega_{zn} T_0 + \eta T_2)
\end{aligned}
\tag{B.20}
$$

where $a_u = \epsilon^2 \widehat{a}_u$. The solutions of the first and the second equation (B.20) have already been established in the previous section. Hence, substituting the equations governing the states x_0, Equ.(B.8), and x_1, Equ.(B.11), in the third equation (B.20), we obtain

$$
D_0^2 x_2 + \omega_{zn}^2 x_2 = -\left\{ \quad 2i\omega_{zn}(D_2 A + \widehat{\xi}_{zn}\omega_{zn}A) + \left(3\nu_n - \frac{10}{3}\frac{\beta_n^2}{\omega_{zn}^2}\right)A^2\bar{A} \right.
$$
$$
\left. + \frac{R_n \widehat{a}_u}{2}\bar{A}e^{i\eta T_0} \right\} e^{i\omega_{zn} T_0} + cc + NST
\tag{B.21}
$$

where cc represents the complex conjugate of the preceding terms and NST denotes the non secular terms periodic in $3T_0$. The elimination of the secular terms $T_0 e^{i\omega_{zn} T_0}$ from Equ.(B.21) yields

$$
2i\omega_{zn}(A' + \widehat{\xi}_{zn}\omega_{zn}A) + \left(3\nu_n - \frac{10}{3}\frac{\beta_n^2}{\omega_{zn}^2}\right)A^2\bar{A} + \frac{R_n \widehat{a}_u}{2}\bar{A}e^{i\eta T_0} = 0
\tag{B.22}
$$

Substituting the polar form Equ.(B.14) of the unknown function $A(T_2)$ in Equ.(B.22) and extracting the real and imaginary parts, we obtain

$$
a' = -\widehat{\xi}_{zn}\omega_{zn}a + \frac{R_n \widehat{a}_u}{4\omega_{zn}}a \sin\gamma
$$
$$
\omega_{zn}(\eta - \gamma') = \left(\frac{3}{4}\nu_n - \frac{5}{6}\frac{\beta_n^2}{\omega_{zn}^2}\right)a^2 + \frac{R_n \widehat{a}_u}{2}\cos\gamma
\tag{B.23}
$$

where $\gamma = \eta T_2 - 2b$ is the phase angle of the response. Hence, the singular points of Equ.(B.23) are governed by

$$
\widehat{\xi}_{zn} = -\frac{R_n \widehat{a}_u}{4\omega_{zn}^2}\sin\gamma_0
$$
$$
\eta = \left(\frac{3}{4}\nu_n - \frac{5}{6}\frac{\beta_n^2}{\omega_{zn}^2}\right)\frac{a_0^2}{\omega_{zn}} + \frac{R_n \widehat{a}_u}{2\omega_{zn}}\cos\gamma_0
\tag{B.24}
$$

Thus, the elimination of γ_0 from Equ.(B.24) leads to the frequency response equation of the parametric excited duffing equation around the parametric resonance $2\omega_{zn}$ according to

$$\left[\frac{\eta}{\omega_{zn}} - \left(\frac{3}{4}\nu_n - \frac{5}{6}\frac{\beta_n^2}{\omega_{zn}^2}\right)\frac{a_0^2}{\omega_{zn}^2}\right]^2 = \left(\frac{R_n\widehat{a}_u}{2\omega_{zn}^2}\right)^2 - 4\widehat{\xi}_{zn}^2 \qquad (B.25)$$

or Equ.(3.11), keeping in mind that $\Omega - 2\omega_{zn} = \epsilon^2\eta$.

Stability

Analysing the stability of the steady state response equation is precisely the problem of determining the behaviour of the solution near one of the singular points (a_0, γ_0). The stability of the singular points depends on the real part of the eigenvalues of the jacobian matrix of the nonlinear second order differential system defined by Equ.(B.23), which in this case reads

$$\lambda = \omega_{zn}\left[-\widehat{\xi}_{zn}^2 \pm \sqrt{\widehat{\xi}_{zn}^2 + \left(\frac{3}{4}\nu_n - \frac{5}{6}\frac{\beta_n^2}{\omega_{zn}^2}\right)\frac{a_0^2}{\omega_{zn}^2}\frac{R_n\widehat{a}_u}{2\omega_{zn}^2}\cos\gamma_0}\right] \qquad (B.26)$$

If the real part of at least one of the roots is positive definite, the corresponding steady-state solution is unstable. The solution is stable if

$$\cos\gamma_0 < 0 \qquad (B.27)$$

The second equation (B.24) shows that

$$\cos\gamma_0 = \frac{2\omega_{zn}}{R_n\widehat{a}_u}\left[\eta - \left(\frac{3}{4}\nu_n - \frac{5}{6}\frac{\beta_n^2}{\omega_{zn}^2}\right)\frac{a_0^2}{\omega_{zn}}\right] \qquad (B.28)$$

and the stability condition is changed into

$$\eta < \left(\frac{3}{4}\nu_n - \frac{5}{6}\frac{\beta_n^2}{\omega_{zn}^2}\right)\frac{a_0^2}{\omega_{zn}} \qquad (B.29)$$

We note from the steady state response Equ.(B.25) that, when there are two solutions, the stability condition Equ.(B.29) is not satisfied for the solution having the smaller amplitude (the lower branch in dashed curve as shown in Fig.3.9) and thus it is unstable; while the stability condition is satisfied for the solution having larger amplitudes (i.e. the upper branch).

Appendix C

Cable structure constants

Substituting Equ.(5.5) and (5.6) in Equ.(A.6), one easily finds that the constants appearing in the expression of the kinetic energy are as follows

$$N = \begin{pmatrix} \frac{2}{\pi} & \frac{1}{\pi} & \cdots & \frac{2}{n\pi} \end{pmatrix}^T \tag{C.1}$$

$$J = \begin{pmatrix} 1 & 0 & \cdots & 0 \\ 0 & -1 & \cdots & 0 \\ \vdots & \cdots & \ddots & \vdots \\ 0 & 0 & \cdots & (-1)^{n+1} \end{pmatrix} \tag{C.2}$$

$$G_y^i = \mu_c^i N \mathcal{R}_v^{iT} L_a^i + J \mu_c^i N \mathcal{R}_v^{iT} L_b^i \tag{C.3}$$

$$G_z^i = \mu_c^i N \mathcal{R}_w^{iT} L_a^i + J \mu_c^i N \mathcal{R}_w^{iT} L_b^i \tag{C.4}$$

$$G_u^i = \alpha_c^i \mathcal{R}_u^{iT} \left(L_b^i - L_a^i \right) \tag{C.5}$$

$$m_u^i = \frac{1}{2} \rho A l \left(\frac{1}{1 + \frac{\lambda^2}{12}} \right)^2 \left(\frac{1}{3} + \frac{\lambda^2}{20} + \frac{\lambda^4}{504} + \frac{\lambda^2}{120} \frac{E}{\sigma^s} \right) \tag{C.6}$$

$$\eta_s^i = \frac{1}{2} \rho A l \left[\begin{array}{c} \left(\mathcal{R}_u^{iT} L_b^i \right)^T + \frac{1}{6} \frac{\lambda}{1 + \frac{\lambda^2}{12}} \sqrt{\frac{E}{\sigma^s}} \left(\mathcal{R}_w^{iT} L_a^i \right)^T \\ \frac{1}{12} \frac{\lambda}{1 + \frac{\lambda^2}{12}} \sqrt{\frac{\sigma^s}{E}} \left(1 + \frac{\lambda^2}{12} + \frac{E}{\sigma^s} \right) \left(\mathcal{R}_w^{iT} (L_b^i - L_a^i) \right)^T \end{array} \right] \\ - 2 m_u^i \mathcal{R}_u^{iT} \left(L_b^i - L_a^i \right)^T \tag{C.7}$$

$$m_{cs}^i = \frac{1}{2}\rho Al \begin{bmatrix} (\mathcal{R}_u^{iT} L_b^i)^T \mathcal{R}_u^{iT} L_a^i + (\mathcal{R}_v^{iT} L_b^i)^T \mathcal{R}_v^{iT} L_a^i + (\mathcal{R}_w^{iT} L_b^i)^T \mathcal{R}_w^{iT} L_a^i \\ + \frac{1}{3}\left((\mathcal{R}_v^{iT}(L_b^i - L_a^i))^T \mathcal{R}_v^{iT}(L_b^i - L_a^i) \right) \\ + \left(\frac{1}{3} + \frac{\lambda^2}{120}\frac{\sigma^*}{E}\right) \left(\mathcal{R}_w^{iT}(L_b^i - L_a^i)\right)^T \mathcal{R}_w^{iT}(L_b^i - L_a^i) \\ - \frac{1}{6}\frac{\lambda}{1+\frac{\lambda^2}{12}}\sqrt{\frac{E}{\sigma^*}} \left(\mathcal{R}_w^{iT} L_a^i\right)^T \mathcal{R}_u^{iT}(L_b^i - L_a^i) \\ - \frac{\lambda}{6}\sqrt{\frac{E}{\sigma^*}} \left(\mathcal{R}_w^{iT}(L_b^i - L_a^i)\right)^T \mathcal{R}_u^{iT} L_a^i \\ + m_u^i \mathcal{R}_u^{iT}\left(L_b^i - L_a^i\right) \end{bmatrix} \tag{C.8}$$

Using the expression of the potential energy Equ.(5.8), we easily find

$$\frac{\partial \mathcal{V}}{\partial x} = \sum_i^{nc} \begin{bmatrix} \frac{l^i}{E^i A^i}(T_0^i + T_q^i + T_{qs}^i + T_d^{(2)i})\frac{\partial T_{qs}^i}{\partial x} \\ + \frac{\lambda^2}{12}\frac{E_d^i}{E^i}T_0^i \left(\mathcal{R}_u^{iT}(L_b^i - L_a^i)\right)^T \\ - \frac{\gamma^i A^i l^i}{2}\left(\mathcal{R}_w^{iT}(L_b^i + L_a^i)\right)^T \end{bmatrix} \tag{C.9}$$

$$\frac{\partial T_{qs}^i}{\partial x} = h_u^i \left(\mathcal{R}_u^{iT}(L_b^i - L_a^i)\right)^T \tag{C.10}$$

Note that the last static term in the sum can be neglected.

Bibliography

[1] A.M. Abdel-Ghaffar and M.A. Khalifa, "Importance of cable vibration in dynamics of cable-stayed bridges", *ASCE, J. of Engineering Mechanics*, Vol. 117, No. 11, pp. 251–259, November 1991.

[2] Y. Achkire and A. Preumont, "Optical measurement of cable and string vibration", *Proceedings of 2nd Int. Conf. on Vibration Measurements by Laser Techniques*, pp. 539–549, September 1992.

[3] Y. Achkire and A. Preumont, "Active tendon control of cable-stayed bridges", *Earthquake Engineering and Structural Dynamics*, Vol. 25, No. 6, pp. 585–597, June 1996.

[4] J.N. Aubrun, "Theory of the control of structures by low-authority controllers", *Journal of Guidance and Control*, Vol. 3, No. 5, pp. 444–451, 1980.

[5] M.J. Balas, "Active control of flexible systems", *J. of Optim. theory appl.*, Vol. 25, No. 3, pp. 415–436, 1978.

[6] R.J. Benhabib, R.P. Iwens and R.L. Jackson, "Stability of large space structures control systems using positivity concepts", *AIAA, J. of Guidance*, Vol. 4, No. 5, pp. 487–553, Sept-Oct 1981.

[7] R.L Bisplinghoff and H. Ashley, *Principles of Aeroelasticity*. Dover Publications Inc., New York, 1975.

[8] R.H. Cannon and D.E. Rosenthal, "Experiment in control of flexible structures with noncolocated sensors and actuators", *AIAA, J. of Guidance*, Vol. 7, No. 5, pp. 546–553, Sept-Oct 1984.

[9] G.S Chen., B.J. Lurie and B.K Wada, "Experimental studies of adaptive structure for precision performance", In AIAA, editor, *30th AIAA /ASME/ASCE/AHS Structures, Structural Dynamics, and Materials*, pp. 1462–1472, Washington D.C., 1989.

[10] J.C. Chen, "Response of large space structures with stiffness control", *AIAA, J. Spacecraft*, Vol. 21, No. 5, pp. 463–467, Sept-Oct 1984.

[11] A. Pinto da Costa, "Excitãçao paramétrica de tirantes de pontes", Master's thesis, Instituto Superior Técnico, Universidade Técnica de Lisboa, April 1993.

[12] A.G. Davenport, "The dynamics of cables in wind", *Proceedings of Int. Symp. on Cable Dynamics*, volume 2, pp. 1–12, Liège, Belgium, October 1995.

[13] E.H. Dowell, H.C. Curtis, R.H. Scanlan and F. Sisto, *A Modern course in Aeroelasticity*. Kluwer Academic Publishers, 1989.

[14] N.N. Dung, T. Miyata and H. Yamada, "A method for flutter control in the long span bridge", *Proceedings of Third Int. Conf. on Motion and Vibration Control*, volume 2, pp. 47–52, Chiba, Japan, September 1996.

[15] J.L. Fanson, C.H. Blackwood and C.C. Chu, "Active member control of a precision structure", *Proceedings of 30th AIAA/ASME/ASCE/AHS Structures, Structural Dynamics and Materials*, pp. 1480–1494, Washington D.C., 1989.

[16] G.F. Franklin and J.D. Powell, *Digital Control of Dynamic Systems*. Addison-Wesley, second edition, 1980.

[17] G.F. Franklin, J.D. Powell and A. Emami-Naeini, *Feedback Control of Dynamic Systems*. Addison-Wesley, third edition, 1994.

[18] Y. Fujino and T. Susumpow, "An experimental study on active control of planar cable vibration by axial support motion", *Earthquake Engineering and Structural Dynamics*, Vol. 23, pp. 1283–1297, 1994.

[19] Y. Fujino, P. Warnitchai and B.M. Pacheco, "Active stiffness control of cable vibration", *ASME, J. of Applied Mechanics*, Vol. 60, pp. 948–953, December 1993.

[20] Y. Fujino, P. Warnitchai and B.M. Pacheco, "An experimental and analytical study of autoparametric resonance in a 3dof model of cable-stayed-beam", *J. of Nonlinear Dynamics*, Vol. 4, pp. 111–138, 1993.

[21] Y.C. Fung, *An Introduction to the Theory of Aeroelasticity*. Dover Publications Inc., New York, 1969.

[22] M. Géradin and D. Rixen, *Théorie des vibrations*. Masson, 1993.

[23] H.M. Irvine, "Energy relations for a suspended cable", *[Q. J] Mech. appl. Math.*, Vol. 33, 1980.

[24] H.M. Irvine, *Cable structures.* M.I.T. press, 1981.

[25] H.M. Irvine, "On the free vibrations of a suspended cable with frictional end restraint", *ASME, J. of Applied Mechanics*, Vol. 57, pp. 419–422, June 1990.

[26] H.M. Irvine and T.K. Caughey, "The linear theory of free vibrations of a suspended cable", *Proceedings of Royal Society London*, volume 341 of *A*, pp. 299–315, 1974.

[27] H.M. Irvine and J.H. Griffin, "On the dynamic response of a suspended cable", *Earthquake Engineering and structural Dynamics*, Vol. 4, pp. 389–402, 1976.

[28] H. Kobayashi and Y. Nitta, "Active flutter control of suspension bridge by control surfaces", *Proceedings of Third Int. Conf. on Motion and Vibration Control*, volume 2, pp. 42–46, Chiba, Japan, September 1996.

[29] Y. Kubo, H. Maeda, A. Watanabe, K. Kato and S. Hoshino, "Aerodynamic behavior of newly proposed cable system for cable-stayed bridges", *Proceedings of Int. Symp. on Cable Dynamics*, volume 1, pp. 453–468, Liège, Belgium, October 1995.

[30] A. Larsen, "Bridge engineering and aerodynamics", *Proceedings of 1st Int. Symp. on Aerodynamics of Large Bridges*, pp. 3–21, Copenhagen, February 1992.

[31] C.L. Lee and N.C. Perkins, "Experimental investigation of isolated and simultaneous internal resonances in suspended cables", *J. of Vibration and Acoustics*, Vol. 117, pp. 385–391, October 1995.

[32] S. Lee and C.D. Mote, "Vibration control of an axially moving string by boundary control", *ASME, J. of Applied Mechanics*, Vol. 118, pp. 66–74, March 1996.

[33] J.L. Lilien and O. Chabart, "High voltage overhead lines; three mechanisms to avoid bundle galloping", *Proceedings of Int. Symp. on Cable Dynamics*, volume 1, pp. 381–390, Liège, Belgium, October 1995.

[34] J.L. Lilien and A. Pinto da Costa, "Vibration amplitudes caused by parametric excitation of cable-stayed bridges", *J. of Sound and Vibration*, Vol. 174, No. 1, pp. 69–90, January 1994.

[35] L.E. Lindholm and I.K. Edwards, "Analog position-sensing photodetectors", *Photonics Spectra*, Novembre 1991.

[36] A. Luongo, G. Rega and F. Verstroni, "Monofrequent oscillations of a nonlinear model of a suspended cable", *J. of Sound and Vibration*, Vol. 82, pp. 247–259, 1982.

[37] A. Luongo, G. Rega and F. Verstroni, "Planar non-linear free vibrations of an elastic cable", *Int. J. Non-Linear Mechanics*, Vol. 19, No. 1, pp. 39–52, 1984.

[38] J. Mitsugi, T. Yasaka and K. Miura, "Shape control of the tension truss antenna", *AIAA Journal*, Vol. 28, No. 2, pp. 316–322, 1990.

[39] K. Miura and Y. Miyasaki, "Concept of the tension truss antenna", *AIAA Journal*, Vol. 28, No. 6, pp. 1098–1104, 1990.

[40] T. Miyata, H. Yamada, T. Hojo and S. Yamasaki, "On aerodynamically stable pe-stay-cables with decreased drag force by introduction of newly developped lumped surface roughness", *Proceedings of Int. Symp. on Cable Dynamics*, volume 1, pp. 481–488, Liège, Belgium, October 1995.

[41] A.H. Nayfeh and D.T. Mook, *Nonlinear Oscillations*. John Wiley and Sons, 1979.

[42] S.A. Nayfeh, A.H. Nayfeh and D.T. Mook, "Nonlinear response of a taut string to longitudinal and transverse end excitation", *J. of Sound and Vibration*, Vol. 1, pp. 307–334, 1995.

[43] A. Nazmy and A.M. Abdel-Ghaffar, "Three dimensional non-linear static analyses of cable-stayed bridges", *Computers and Structures*, Vol. 34, pp. 257–271, 1990.

[44] J. Onoda, T. Endo, H. Tamaoki and N. Watanabe, "Vibration suppression by variable-stiffness members", *AIAA Journal*, Vol. 29, No. 6, pp. 977–983, June 1991.

[45] J. Onoda and K. Minesugi, "Alternative control logic for type-ii variable-stiffness system", *AIAA Journal*, Vol. 34, No. 1, pp. 207–209, 1995.

[46] J. Onoda, T. Sano and K. Kamiyama, "Active, passive, and semiactive vibration suppression by stiffness variation", *AIAA Journal*, Vol. 30, No. 12, pp. 977–983, December 1992.

[47] O. O'Reilly and P.J. Holmes, "Non-linear, non-planar and non-periodic vibrations of a string", *J. of Sound and Vibration*, Vol. 153, No. 3, pp. 413–435, 1992.

[48] B.M. Pacheco and Y. Fujino, "Keeping cables calm", *Civil Engineering*, October 1993.

[49] N.C. Perkins, "Discussion of dynamic stability of cables subjected to an axial periodic load", *J. of Sound and Vibration*, Vol. 156, No. 2, pp. 361–365, 1992.

[50] N.C. Perkins, "Modal interactions in the non-linear response of elastic ca-
bles under parametric/external excitation", *Int. J. of Non-Linear Mechan-
ics*, Vol. 27, No. 2, pp. 233–250, 1992.

[51] F.P. Perngjin and A.H. Nayfeh, "Fully nonlinear model of cables", *AIAA
Journal*, Vol. 30, No. 12, pp. 2993–2996, 1992.

[52] G. Peterson and L.E. Lindholm, "Position sensing light detectors with high
linearity", *IEEE J. of Solid-state Circuit*, Vol. 13, No. 3, pp. 392–399, June
1978.

[53] A. Preumont, "Spillover alleviation for nonlinear active control of vibra-
tion", *AIAA J. of Guidance*, Vol. 11, No. 2, pp. 124–130, March-April
1988.

[54] A. Preumont, *Vibration Control of Active Structures : An Introduction*.
Kluwer Academic Publishers, 1997.

[55] A. Preumont and Y. Achkire, "Active damping of structures with guy
cables", *AIAA, J. of Guidance, Control, and Dynamics*, Vol. 20, No. 2,
pp. 320–326, March-April 1997.

[56] A. Preumont, J.P. Dufour and Ch. Malekian, "Active damping by a local
force feedback with piezoelectric actuators", *AIAA J. of Guidance*, Vol. 15,
No. 2, pp. 390–395, March-April 1992.

[57] C.D. Rahn and C.D. Mote, "Parametric control of flexible systems", *J. of
Vibration and Acoustics*, Vol. 116, pp. 379–385, July 1994.

[58] C.D. Rahn and C.D. Mote, "Axial force stabilization of transverse vibration
in pinned and clamped beams", *ASME, J. of Dynamic Systems Measure-
ment and Control*, Vol. 118, pp. 379–380, June 1996.

[59] C.D. Rahn and C.D. Mote, "Parametric control of conservative mechanical
systems", *ASME, J. of Dynamic Systems Measurement and Control*, Vol.
118, pp. 309–314, June 1996.

[60] C.C. Rupp, "A tether tension control law for tethered subsatellites deployed
along the local vertical", *NASA TMX-64963*, September 1975.

[61] R.H. Scanlan, J.G. Béliveau and K.S. Budlong, "Indicial aerodynamic func-
tions for bridge decks", *ASCE, J. Eng. Mech. div.*, Vol. 100, No. EM4, pp.
657–673, August 1974.

[62] R.H. Scanlan and J.J. Tomko, "Airfoil and bridge deck flutter derivatives",
ASCE, J. Eng. Mech. div., Vol. 97, No. EM6, pp. 1717–1737, December
1971.

[63] T. Susumpow and Y. Fujino, "Active control of cable and cable-structure system", *Proceedings of 1st Int. Conf. on Motion and Vibration Control*, volume 1, pp. 170–175, September 1992.

[64] T. Susumpow and Y. Fujino, "Active control of multimodal cable vibrations by axial support motion", *ASCE, J. of Engineering Mechanics*, Vol. 121, September 1995.

[65] G. Tagata, "A parametrically driven harmonic analysis of a non-linear stretched string with time-varying length", *J. of Sound and Vibration*, Vol. 87, No. 3, pp. 493–511, 1983.

[66] G. Tagata, "Wave synthesis in a non-linear stretched string with time varying length or tension", *J. of Sound and Vibration*, Vol. 129, No. 2, pp. 215–235, 1989.

[67] R. Walther, B. Houriet, W. Isler and P. Moia, *Ponts Haubanés*. Presses Polytechniques Romandes, Lausanne, 1985.

[68] P. Warnitchai, Y. Fujino, B.M. Pacheco and R. Agret, "An experimental study on active tendon control of cable-stayed bridges", *Earthquake Engineering and Structural Dynamics*, Vol. 22, No. 2, pp. 93–11, 1993.

[69] H. Yamaguchi, "Modal damping of suspended cables", *Proceedings of Damping ' 89*, pp. GBC1–13, West Palm Beach, FL, 1989.

[70] H. Yamaguchi, "Control of cable vibrations with secondary cables", *Proceedings of Int. Symp. on Cable Dynamics*, volume 1, pp. 445–452, Liège, Belgium, October 1995.

[71] H. Yamaguchi and N.N. Dung, "Active wave control of sagged-cable vibration", *Proceedings of 1st Int. Conf. on Motion and Vibration Control*, volume 1, pp. 134–139, Yokohama, Japan, September 1992.

[72] H. Yamaguchi and Y. Fujino, "Modal damping of flexural oscillation in suspended cables", *Earthquake Engineering and Structural Dynamics*, Vol. 4, No. 2, pp. 413–421, October 1987.

[73] J.N. Yang and F. Giannopoulos, "Active control and stability of cable-stayed bridge", *ASCE, J. Eng. Mech. div.*, Vol. 105, pp. 677–694, August 1979.

[74] J.N. Yang and F. Giannopoulos, "Active control of two-cable-stayed bridge", *ASCE, J. Eng. Mech. div.*, Vol. 105, No. EM5, pp. 795–809, October 1979.

[75] T. Yoshimura, M.G. Savage and H. Tanaka, "Wind-induced vibrations of bridge stay-cables", *Proceedings of Int. Symp. on Cable Dynamics*, volume 1, pp. 437–444, Liège, Belgium, October 1995.